

AD-A101 669

OHIO STATE UNIV COLUMBUS ELECTROSCIENCE LAB
A SYNERGISTIC INVESTIGATION OF THE INFRARED WATER VAPOR CONTINUUM-ETC(U)
APR 81 R J NORDSTORM, M E THOMAS, E K DAMON DAAG29-77-C-0010
UNCLASSIFIED ESL-784701-7 ARO-14702.5-65 NL

F/6 4/1

1 OF 2
AD A
031669

OSU

The Ohio State University

LEVEL II
A SYNERGISTIC INVESTIGATION OF
THE INFRARED WATER VAPOR
CONTINUUM

R.J. Nordstrom, M.E. Thomas,
E.K. Damon, and R.K. Long

(12)



The Ohio State University

ElectroScience Laboratory

Department of Electrical Engineering
Columbus, Ohio 43212

Final Report 784701-7

Contract No. DAAG29-77-C-0010

Period: April 1, 1977 ~ September 30, 1980

April 1981

ADA101669

Approved for Public Release: Distribution Unlimited

DTIC FILE COPY

Department of the Army
U.S. Army Research Office
P.O. Box 1211
Research Triangle Park, North Carolina 27709

81 7 21 038

The view, opinions, and/or findings contained in this report
are those of the author(s) and should not be construed as
an official Department of the Army position, policy, or decision,
unless so designated by other documentation.

AF

Final draft.

1 Apr 77-1 - / 34

Unclassified
SECURITY CLASSIFICATION OF THIS PAGE (When Data Entered)

DD FORM 1473 EDITION OF 1 NOV 65 IS OBSOLETE
1 JAN 73

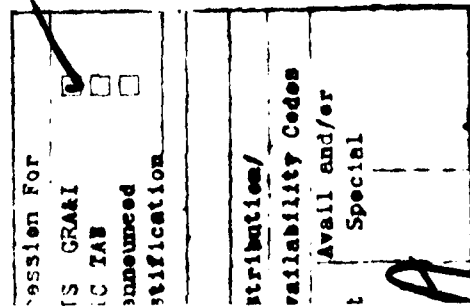
Unclassified

~~SECURITY CLASSIFICATION OF THIS PAGE (When Data Entered)~~

402251

TABLE OF CONTENTS

	<u>Page</u>
LIST OF TABLES	iv
LIST OF FIGURES	v
 I. INTRODUCTION	1
II. THE WATER VAPOR CONTINUUM	3
Pressure Dependence	6
Temperature Dependence	20
A Case for Water Dimer Absorption	26
The Water Vapor Continuum in the Region of 4 μm	30
 REFERENCES	34
III. THE N_2 -BROADENED WATER VAPOR ABSORPTION LINE SHAPE AND INFRARED CONTINUUM ABSORPTION	36
Part I: Theoretical Development	36
INTRODUCTION	36
The Hamiltonian	41
THE TRANSITION RATE	49
THE CORRELATION FUNCTION	55
The Lorentz Line Shape	56
Collision Dynamics	57
Interruption Broadening	64
Statistical Broadening	68
The p-function	74
 REFERENCES	78
Part II: Implementation of the Line Shape	80
INTRODUCTION	80
HISTORICAL PERSPECTIVE	81
THE LINE PROFILE	83
COMPARISON WITH EXPERIMENT	90
CONCLUSIONS	99
REFERENCES	100
IV. FOURIER TRANSFORM SPECTRA OF H_2O SAMPLES	102



LIST OF TABLES

<u>Table</u>	
SECTION II	
1 LEAST SQUARE FITS OF THE ABSORPTION COEFFICIENTS FROM SEVERAL DATA SETS TO THE FORM $k = a + b P_{H_2O}$	19
2 COEFFICIENTS FOR EQUATION (18) DETERMINED FROM A LEAST SQUARE FIT OF BURCH'S DATA AT SEVERAL FREQUENCIES	23
3 COMPARISON OF VALUES OF T_o IN EQUATION (18) DETERMINED FROM SEVERAL WORKERS	25
SECTION III - Part I	
1 CHARACTERISTICS OF COLLISION DYNAMICS	59
2	76
SECTION III - Part II	
1 THE FAR WING PARAMETERS	92
SECTION IV	
1 EXPERIMENTAL CONDITIONS FOR PURE H_2O SPECTRA (PATH LENGTH = 821 METERS)	103
2 EXPERIMENTAL CONDITIONS FOR NITROGEN BROADENED H_2O SPECTRA (PATH LENGTH = 821 METERS)	103

LIST OF FIGURES

Figure	
SECTION II	
1 Plot of absorption coefficient $k'(v)$ at $v = 844.2 \text{ cm}^{-1}$ as defined in Equation (4) as a function of water vapor pressure for a sample of pure water vapor at $T = 387 \text{ K}$.	9
2 Comparison of the results of McCoy, et al., and the results of Mills and Long for absorption of the P(20) laser line of CO_2 by pure water vapor samples.	14
3 Data reproduced from Reference [20] which show the fraction of total transmittance as a function of precipitable water in a 3 km path.	15
4 a. Plots of absorption coefficient $k(v)$ as defined by Equation (2) as a function of $P_{\text{H}_2\text{O}}^2$ for two independent digitizations of the data in Figure 3.	17
b. Same as 4(a) above.	17
5 Accumulation of data from several sources on the frequency dependence of the self-broadening coefficient near 296 K in the $8 \mu\text{m}$ to $12 \mu\text{m}$ atmospheric transmission window.	18
6 The self-broadening coefficient $C_s^0(v)$ at several temperatures.	21
7 The temperature dependence of the self-broadening coefficient $C_s^0(v)$ at three frequencies.	22
8 Comparison of experimental values of $C_s^0(v)$ at 296 K with calculated values assuming the continuum absorption is due to the extreme wings of simple Lorentz lines, or of full Lorentz lines.	27
9 Spectral plots of $C_s^0(v)$ between 2400 cm^{-1} and 2820 cm^{-1} for pure H_2O at four temperatures.	32
10 Semi-logarithmic plots of $C_s^0(v)$ versus $1/T$ for four different frequencies.	33
SECTION III - Part I	
1 Far wing absorption by CO_2 molecules.	39

<u>Figure</u>	<u>Page</u>
2 Interaction geometry.	45
3 Comparison among the intermolecular potential, the correlation function, and the spectral line shape.	57
4 Possible collision trajectories.	58
5 Langevin function.	63
6 $p(v)$ versus Δv .	75
SECTION III - Part II	
1 Pressure dependence of water vapor continuum absorption.	82
2 Room temperature modelling of water vapor pressure dependence.	93
3 Experimental results in the 8 to 14 μm region.	95
4 Comparison of experimental and theoretical frequency ₁ dependence of the absorption coefficient from 2470 cm^{-1} to 2870 cm^{-1} .	96
5 Comparison of experimental and theoretical temperature dependence of C_s at 944.1945 cm^{-1} .	98
SECTION IV	
1 a. HgCdTe Pure H_2O $970-980 \text{ cm}^{-1}$.	104
b. Same as 1(a) above.	104
2 a. InSb Pure H_2O .	107
b. Same as 2(a) above.	108
3 a. HgCdTe $970-980 \text{ cm}^{-1}$ Pressure-broadened.	109
b. Same as 3(a) above.	110
4 a. InSb $2250-2260 \text{ cm}^{-1}$ Pressure-broadened.	111
b. Same as 4(a) above.	112

SECTION I INTRODUCTION

This final report summarizes the results which have been obtained under ARO Contract DAAG 29-77-C-0010. The purpose of this research has been the investigation of the infrared water vapor continuum. Although a great deal of data existed prior to this research effort, a careful analysis of the continuum absorption data had not been performed. Empirical interpretations of experimental data provided convenient recipes for calculating continuum absorption values in specific spectral regions and under certain conditions of pressure, water vapor content, and temperature. However, predictions of continuum absorption in uninvestigated spectral regions or for physical conditions outside the body of existing experimental data were not possible.

Data which have been collected under this research program include room temperature and elevated temperature transmittance values of water vapor samples broadened with nitrogen and with air (80% N₂, 20% O₂). A line tunable, frequency-stabilized CO₂ laser was used as the radiation source for long-path absorption cell measurements and for nonresonant spectrophotometer measurements. Also, high-resolution Fourier transform spectroscopy was employed to record pure and pressure-broadened water vapor spectra under a variety of conditions. These spectra are discussed later in this report and will ultimately be made available as an atlas of H₂O absorption lines.

We believe that the infrared water vapor continuum is caused entirely by the wings of strong absorption lines of the H₂O molecule. The strongest absorption lines of the water molecule are located between

200 cm^{-1} and 400 cm^{-1} . The wings of these absorption lines contribute significantly to the continuum absorption even in the 8-14 μm atmosphere transmittance window, but have little effect in the 3.5-4.2 μm spectral region.

A detailed theory of the spectral line shape for pure and pressure-broadened H_2O molecules has been formulated. The resulting non-Lorentzian line shape predicts the negative temperature dependence observed in the 20 μm region.

Section II of this report contains a review of the early work concerning water vapor continuum absorption. Section III summarizes the theoretical developments which led to the formulation of the spectral line shape for H_2O molecules. Section IV discusses the Fourier transform spectra which were collected. These spectra should prove useful to those interested in locating the weak H_2O absorption lines within the atmospheric transmittance windows.

SECTION II

THE WATER VAPOR CONTINUUM

The transmission of infrared radiation through the atmosphere continues to be a subject of considerable interest. Knowledge of the various attenuation processes due to both molecular absorption and aerosol scattering is important to many different scientific disciplines. In meteorologic studies concerning the energy budget for the surface of the earth, for example, contributions from radiation transmitted through the atmosphere to the surface, as well as energy radiated away from the surface, must be known. The transmission functions which describe these processes are dependent on molecular constituents, particularly H_2O and CO_2 , and also on the aerosol concentrations in the atmosphere.

Infrared transmission studies are also needed to determine optimal spectral regions for infrared imaging systems and the evaluation of infrared sensor performance under various atmospheric conditions. Imaging and sensor systems must prove reliable in the field under all possible circumstances.

Another area in which precise information on the attenuation mechanisms is needed is the study of the propagation of infrared laser radiation. The transmission of laser radiation through the atmosphere has many applications. When considering long path lengths through the atmosphere for projects such as communications, laser ranging, or energy transfer, even small attenuations per meter can become serious.

Early workers in infrared transmission studies recorded the spectral transmittance of the atmosphere to infrared solar radiation. S.P. Langley [1,2] published several infrared solar spectra. From his work,

he concluded that there was practically complete transmission at $10.7\mu\text{m}$.

A. Adel [3,4] repeated much of Langley's work and extended the solar spectrum to $24\mu\text{m}$. While at The Ohio State University, M.V. Migeotte [5,6] investigated the infrared solar spectrum from $2\mu\text{m}$ to $12\mu\text{m}$. This work was continued in the early 1950's by J.H. Shaw and co-workers [7].

The emphasis of this early work was on the identification of atmospheric gases and the accurate determination of absorption features. Many high-resolution maps of the solar spectrum were published which collectively cover the region from $1\mu\text{m}$ to $350\mu\text{m}$.

In 1938, W.M. Elsasser [8] suggested the existence of a water vapor continuum absorption in the $8\mu\text{m}$ to $12\mu\text{m}$ region which he attributed to extreme wings of very strong absorption lines outside this region. Yates and Taylor [9] made measurements over horizontal paths using low resolution (10 cm^{-1}) spectroscopy and found greater attenuation than expected from selective absorption alone. The existence of continuum absorption near $10\mu\text{m}$ has also been confirmed in solar spectra by A. Adel [10], R. Anthony [11], and W.T. Roach and R.M. Goody [12]. In the early 1960's, K.J. Bignell and co-workers [13] studied continuum absorption in the $10\mu\text{m}$ region at 1 to 2 cm^{-1} resolution using the sun as a source, and in the $20\mu\text{m}$ region using horizontal atmospheric paths and a Nernst source. They guessed that the temperature dependence of the continuum absorption would be negligibly small. Therefore, their data are reported without indication of the temperature. In a later paper, however, Bignell [14] reported a strong negative dependence of the continuum absorption coefficient on the temperature, and also reported contributions to this absorption coefficient from a self-broadening term and a foreign

broadening term.

D.E. Burch [15] has made laboratory studies of the water vapor continuum in the 8 μm to 12 μm region and also in the 4 μm region [16]. In the 8 μm to 12 μm region he, too, found that the continuum absorption coefficient decreased rapidly with temperature. Furthermore, he found that the calculated values for the continuum absorption coefficient based on the Lorentz line shape for the strong water vapor lines were lower than the experimentally measured absorption coefficients at all wavelengths in the 8 μm to 12 μm region.

P. Varanasi, S. Chou, and S.S. Penner [17] have suggested that the continuum absorption in this region is due to absorption by water dimer molecules. The absorption coefficient from this mechanism should increase with pressure in the same way as absorption due to the extreme wings of strong lines. The basis for the dimer hypothesis is the strong temperature dependence which is exhibited by the continuum absorption.

CO_2 laser measurements of the 8 μm to 12 μm water vapor continuum have been made at this laboratory by J.H. McCoy, D.B. Rensch, and R.K. Long [18]. Recent measurements have been made by F.S. Mills, R.K. Long, and E.K. Damon [19]. These measurements involved the use of a multiple-traversal absorption cell to achieve path lengths of 1 km. Samples of pure water vapor, as well as water vapor-air mixtures, were studied at several output frequencies of the CO_2 laser. At $\lambda = 10.59 \mu\text{m}$, McCoy found that the self-broadening contribution to the continuum absorption coefficient was about 200 times stronger than the contribution due to foreign gas broadening [18].

Studies of the absorption of CO_2 laser radiation in the atmosphere are also being performed in the Soviet Union. Absorption coefficients

for the continuum absorption at the centers of the P(12) to P(26) laser lines in the 10.4 μm band of CO_2 have been studied by I.I. Ippolitov [20] and by V.N. Aref'ev, et al., [21]. A complete review of the influence of molecular absorption on the propagation of CO_2 laser radiation in the atmosphere is given by T.G. Adiks, V.N. Aref'ev, and V.I. Dianov-Klokov [22].

Laboratory measurements of the infrared continuum can be divided into two groups, depending on whether a laser or blackbody radiation source is used. The advantage of the laser measurement is that more accurate transmittance values are obtainable due to the high power, and excellent frequency and amplitude stability. The major disadvantage is that the radiation is available at only a few fixed frequencies. Information on the continuum absorption at a particular frequency could be obscured by a dominating local absorption line. Local and continuum absorption have different partial pressure dependencies, so that this may be used as a test for local effects.

Broadband spectroscopic laboratory measurements depend on comparing two transmittance spectra. The first spectrum is recorded with the absorption cell evacuated. The second spectrum is recorded with the water vapor sample in the cell, and determination of the 100% transmittance curve is sometimes difficult.

Pressure Dependence

The 8 μm to 12 μm atmospheric transmission window plays an important role in the energy budget of the surface of the earth, and in the heat balance of the atmosphere since the spectral radiance of a blackbody near 296K is a maximum in this region. Infrared imaging and sensor

systems also make extensive use of this spectral region. Attenuation of radiation by continuum absorption in this region, therefore, is important.

A comprehensive study of the water vapor continuum will provide the necessary data for systems design and should also provide an impetus for further theoretical understanding of the mechanism of continuum absorption.

A more recent report on the water vapor continuum in the $8 \mu\text{m}$ to $12 \mu\text{m}$ region is by R.E. Roberts, L.M. Biberman, and J.E.A. Selby [23]. They have accumulated much of the previously published data, including laser measurements from this laboratory, and also unpublished spectroscopic data by D.E. Burch, in an attempt to evaluate the accuracy of the LOWTRAN continuum model of J.E.A. Selby and R.A. McClatchey [24].

The amount of radiant energy at frequency ν transmitted through an absorber of length L (in cm) can be expressed as

$$T(\nu) = \exp(-k(\nu)L) \quad (1)$$

where $k(\nu)$ is the absorption coefficient (in cm^{-1}) at frequency ν . This absorption coefficient is a combination of the attenuation due to molecular absorption and radiation loss due to aerosol scattering. In this discussion, however, it is assumed that the contribution from aerosols is small. From Equation (1), the absorption coefficient can be written

$$k(\nu) = \frac{-1}{L} \ln T(\nu) . \quad (2)$$

Before this topic is developed in great detail, it is important to compare this starting point with methods used by other workers. Burch

[15] used a different starting point by writing

$$T(v) = \exp(-k'(v)u) \quad (3)$$

as his first equation. Here $k'(v)$ is the absorption coefficient in $(\text{molecule} \cdot \text{cm}^{-2})^{-1}$. We have included the prime to distinguish this coefficient from Equation (2). The quantity u is the absorber thickness expressed in $\text{molecules} \cdot \text{cm}^{-2}$. Burch then writes

$$k'(v) = \frac{-1}{u} \ln T(v) = C_s^0(v) P_{H_2O} + C_N^0(v) P_N \quad (4)$$

for the continuum absorption coefficient. This expression is based on the assumption that the absorption is due to the extreme wings of collision-broadened lines. In Equation (4), $C_s^0(v)$ and $C_N^0(v)$ are $k'(v)$ from self-broadening and foreign gas broadening (usually nitrogen) mechanisms. Burch demonstrated the linear dependence of the continuum absorption coefficient $k'(v)$ on the water vapor pressure for a pure sample of H_2O ($P_N = 0$) by plotting $\frac{-1}{u} \ln T(v)$ versus P_{H_2O} for data taken at $v = 844.2 \text{ cm}^{-1}$ at a temperature of 387 K. This plot is shown in Figure 1.

Although this linear dependence as expressed by Burch was based upon the assumption that the continuum absorption is caused by extreme wings of strong lines, Figure 1 does not necessarily substantiate this mechanism. Varanassi, et al., [17] have proposed that continuum absorption could be due to absorption by the water dimer $(H_2O)_2$. The absorption coefficient as expressed in Equation (4) caused by absorption by dimer molecules would also be linear in the water vapor pressure [25]. This statement is analyzed in more detail later in the section on water

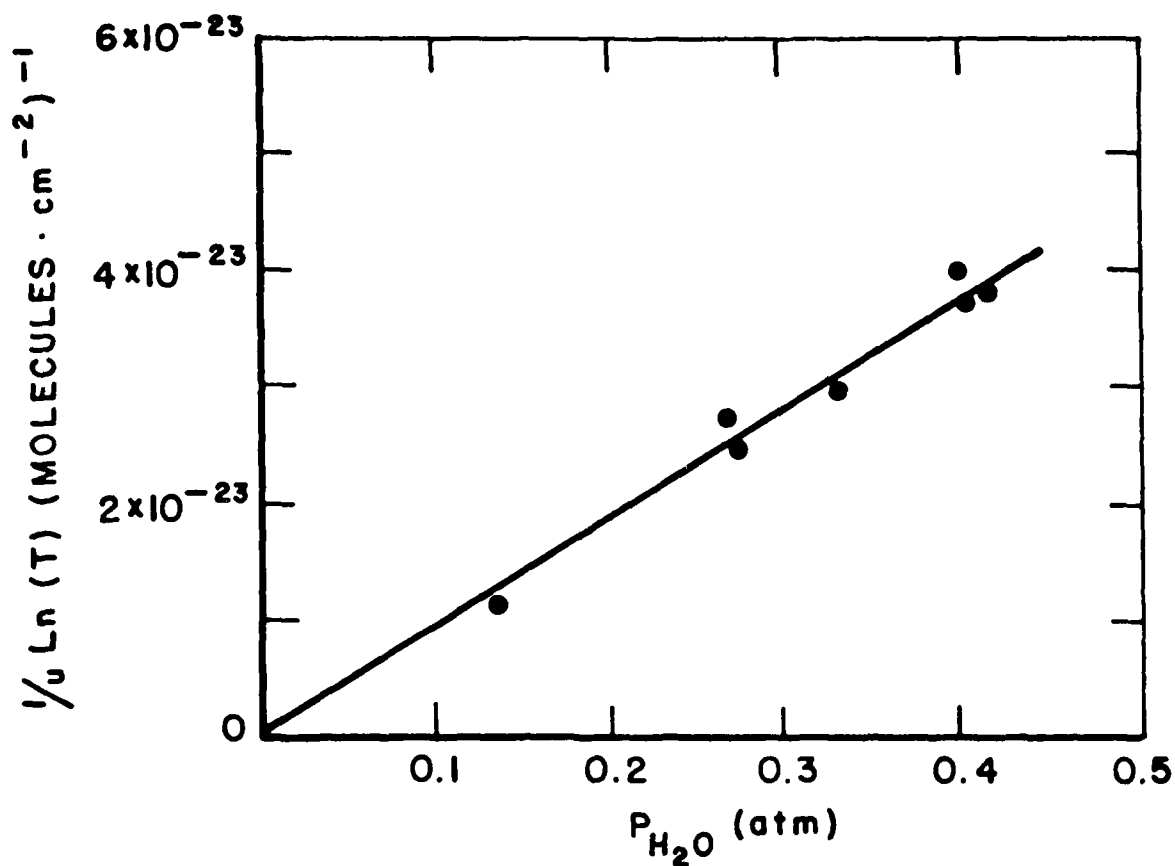


Figure 1. Plot of absorption coefficient $k'(\nu)$ at $\nu = 844.2 \text{ cm}^{-1}$ as defined in Equation (4) as a function of water vapor pressure for a sample of pure water vapor at $T = 387 \text{ K}$. Reproduced from Reference [15].

dimers. Thus, a study of the pressure dependence of the continuum absorption coefficient in the 8 μm to 12 μm region does not constitute positive verification of one absorption mechanism over the other.

In order to discuss the results of previous research on the water vapor continuum, we will develop the details expressed in Equations (1) and (2). The absorption coefficient given in Equation (2) can be compared to the absorption coefficient in Equation (4) by noting that

$$u = w_{\text{H}_2\text{O}} \cdot L \quad (5)$$

where $w_{\text{H}_2\text{O}}$ is the number density of water vapor molecules in units of molecules $\cdot \text{cm}^{-3}$. From Equations (2) and (4)

$$\frac{-1}{L} \ln T(v) = k(v) = w_{\text{H}_2\text{O}} k'(v) . \quad (6)$$

The explicit pressure dependence of $k(v)$, then, is

$$k(v) = w_{\text{H}_2\text{O}} \left[C_s^0(v) P_{\text{H}_2\text{O}} + C_N^0(P - P_{\text{H}_2\text{O}}) \right] . \quad (7)$$

This can be written

$$k(v) = C_s^0(v) w_{\text{H}_2\text{O}} \left[P_{\text{H}_2\text{O}} + \frac{C_N^0}{C_s^0} (P - P_{\text{H}_2\text{O}}) \right] . \quad (8)$$

In these two equations, P is the total pressure. In the past, the assumption has been made that the ratio $C_N^0(v)/C_s^0(v)$ is independent of frequency. Roberts points out that this might not be the case, and perhaps certain provisions should be made to accommodate this in future expressions. For the rest of this development, however, it will be assumed to be independent of frequency. Thus,

$$k(v) = C_s^0(v) w_{H_2O} \left[P_{H_2O} + \gamma (P - P_{H_2O}) \right] . \quad (9)$$

Several workers have measured $C_s^0(v)$ and γ at or near room temperature. Bignell [14] reported a contribution to the continuum absorption coefficient which was linear in water vapor pressure that became equal to the foreign broadened term at a water pressure of about 15 mbar (11.25 torr). From this information, the value of γ which he measured was near 0.015. Values of $C_s^0(v)$ measured by Bignell are shown in Figure 5.

Laser absorption studies performed by our laboratory using the P(20) laser line of CO_2 near $10.4 \mu m$ suggest that γ is much smaller. McCoy, et al., reported their data for air broadened water samples in the form of an equation

$$k(v = 944.2 \text{ cm}^{-1}) = 4.32 \times 10^{-6} (\text{km}^{-1} \text{Torr}^{-2}) P_{H_2O} \left[P + 193 P_{H_2O} \right] . \quad (10)$$

Comparison between this equation and Equation (9) can be made when

$$1/\gamma - 1 = 193 \quad (11-a)$$

$$C_s^0(944.2 \text{ cm}^{-1}) w_{H_2O} = 4.32 \times 10^{-6} (\text{km}^{-1} \text{Torr}^{-2}) P_{H_2O} . \quad (11-b)$$

From Equation (11-a) $\gamma = 0.005$. This is a factor of three lower than the value which was inferred from Bignell's work. The value of $C_s^0(944.2 \text{ cm}^{-1})$ derived from McCoy's equation is

$$\begin{aligned} C_s^0(944.2 \text{ cm}^{-1}) &= \frac{4.32 \times 10^{-6} (760)(700) \times 10^{-5}}{(.005) 2.687 \times 10^{-19}} \frac{296}{273} \\ &= 1.85 \times 10^{-22} \text{ cm}^2 \text{molecule}^{-1} \text{atm}^{-1} . \end{aligned}$$

Burch has not been able to measure γ with any degree of reliability. Roberts performed a linear regression to Burch's data in the 16 μm to 30 μm region and extrapolated his results to the 8 μm to 12 μm region. Results of this extrapolation show a value of γ from Burch's work to be 0.0008.

Values represented here for γ differ by a factor 20. It is clear that there is a large experimental uncertainty about γ . Roberts has suggested that until better measurements are made, the LOWTRAN model should eliminate γ . Further unknowns about γ include its frequency dependence as discussed earlier, and also its temperature dependence.

Several studies of pure water vapor samples have been made in this laboratory. McCoy measured the transmittance at 944.2 cm^{-1} and 1047.1 cm^{-1} through 980 m of water vapor at various partial pressures. The absorption coefficients which he measured at these frequencies were fitted to the equations

$$k(944.2 \text{ cm}^{-1}) = 8.39 \times 10^{-4} p_{\text{H}_2\text{O}}^2 \quad (12-\text{a})$$

$$k(1047.1 \text{ cm}^{-1}) = 6.54 \times 10^{-4} p_{\text{H}_2\text{O}}^2 . \quad (12-\text{b})$$

More recently, F.S. Mills and R.K. Long [19] made measurements of the continuum absorption coefficient in pure water vapor at the P(20) laser line of CO_2 at 944.2 cm^{-1} . The data were fitted to the equation

$$k_{\text{Mills}}(944.2 \text{ cm}^{-1}) = 9.67 \times 10^{-4} p_{\text{H}_2\text{O}}^2 . \quad (13)$$

The value of $C_s^0(944.2 \text{ cm}^{-1})$ obtained from this fit is $2.24 \times 10^{-22} \text{ cm}^2 \text{ molecule}^{-1} \text{ atm}^{-1}$.

The difference between the fit obtained by McCoy and the fit obtained by Mills is approximately 13%. Figure 2 shows the two results.

V.N. Aref'ev, et al., [21] have also studied the transmittance of pure water vapor samples. For these results, a multiple-transversal cell with a base path of 50 m was used to achieve path lengths of 3 km. The CO₂ laser which was used as a source was not stabilized and it oscillated alternately on the P(16), P(20), P(22), and P(24) transitions in the 10.4 μm band.

Results of their work done at 294 K are reproduced in Figure 3. The dashed curve represents the results of McCoy, et al., [18], as expressed in Equation (12-a). Aref'ev chose to fit his data to an expression of the form

$$T = \exp(-(0.031w + 0.029w^2)) \quad (14)$$

where w is the centimeters of precipitable water in the 3 cm path. This can be written for arbitrary path length in terms of the water vapor density a (in gm/m³)

$$T = \exp(-(3.1a + 0.87a^2) \times 10^{-3}L) \quad . \quad (15)$$

The absorption coefficient in the form

$$k = (3.1a + 0.87a^2) \times 10^{-3} \quad (16)$$

with a term which is linear in the absorber amount for pure water samples is not in agreement with the results of McCoy and of Mills and Long in Figure 2. In the units chosen by Burch, this linear term in Equation (16) would become a nonzero intercept to Figure 1.

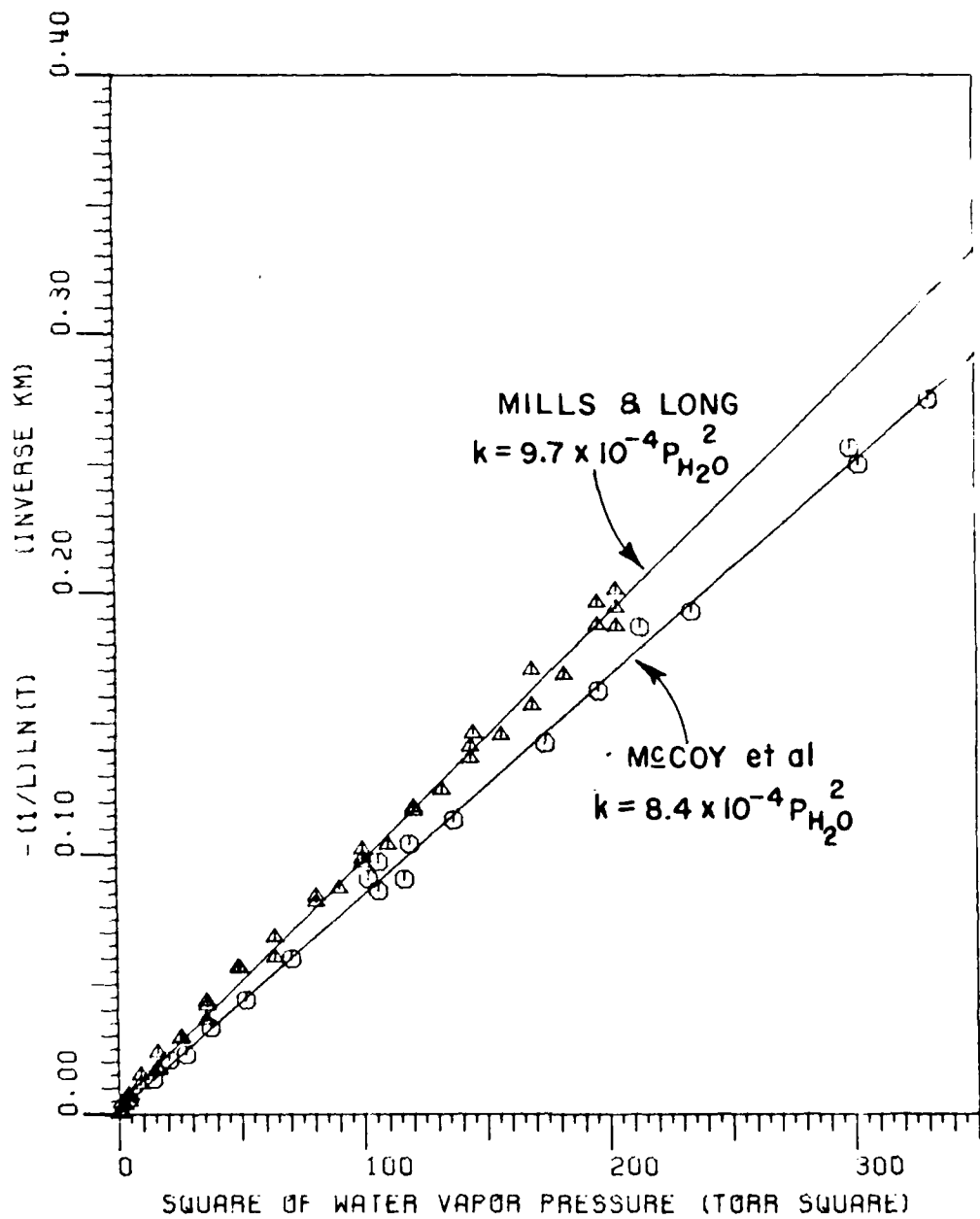


Figure 2. Comparison of the results of McCoy, et al., and the results of Mills and Long for absorption of the P(20) laser line of CO_2 by pure water vapor samples.

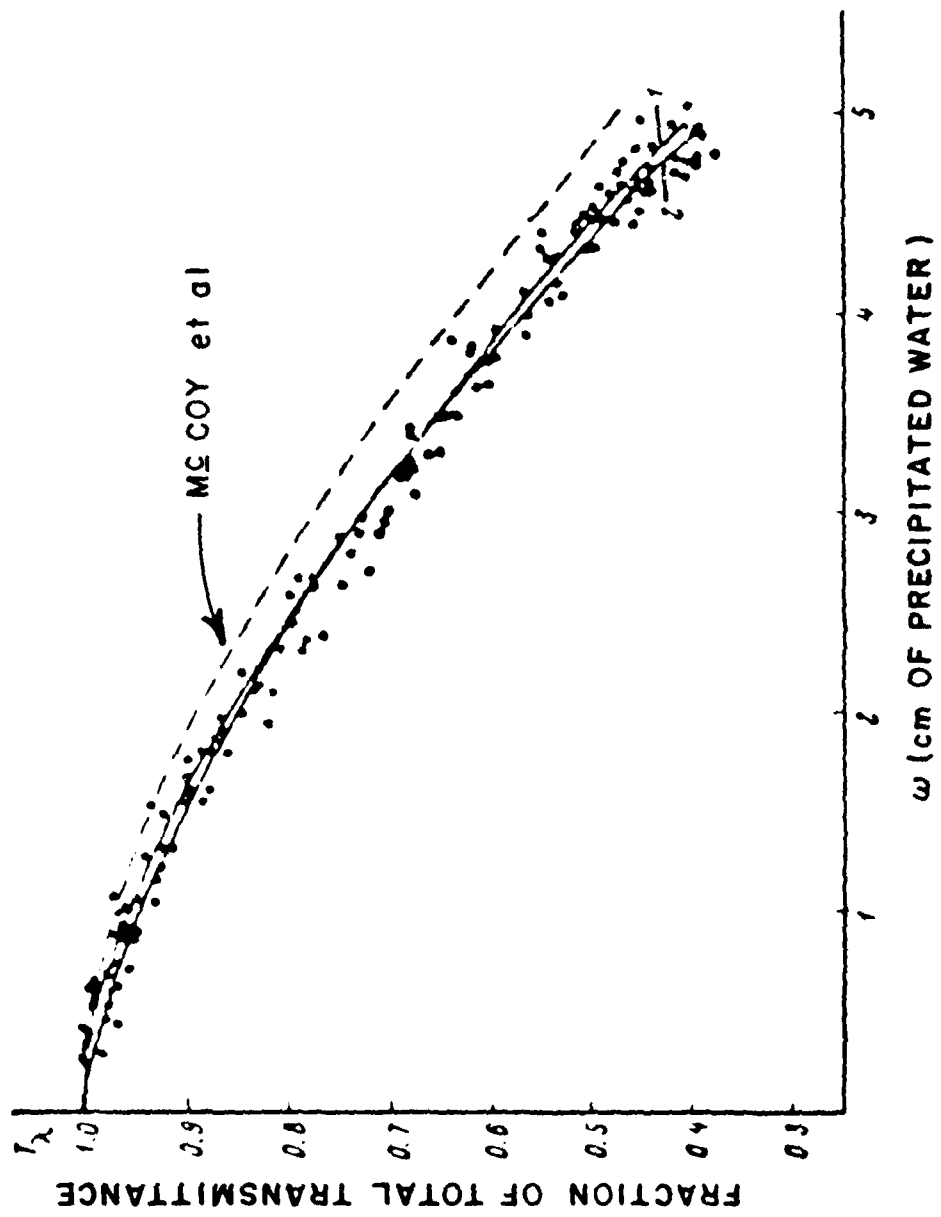


Figure 3. Data reproduced from Reference [20] which show the fraction of total transmittance as a function of precipitable water in a 3 km path. Mc-Coy's data are slightly high which could be due to temperature differences between the two experiments.

In light of this discrepancy, we have examined the data of Figure 3 very carefully. Using a computer graphics technique, we digitized the data of Figure 3 two separate times to create independent data sets. We then ran several curve fit routines on these data sets to determine the necessity of the linear term in Equation (16).

The two independent data sets were fit to a $P_{H_2O}^2$ dependence by converting gm/m^3 to Torr. The conversion used was $1\ gm/m^3 = 1.033\ Torr$ at 294 K. Figures 4 (a) and 4 (b) show plots of $-(1/L)\ln(T)$ in km^{-1} as a function of $P_{H_2O}^2$ for each of the data sets. Allowance was made in the curve fit for the fact that the best straight line might not pass through the origin due to systematic or instrumental errors in the experiment. Results of these fits are shown in Table 1. Also shown are the least square fits to McCoy's data and the data of Mills and Long. The RMS errors of the two data sets from Aref'ev indicate a good fit to the data and we feel that the linear term in Equation (16) is unnecessary.

Comparison of the values of $C_s^0(v)$ taken from various sources is shown in Figure 5. This is a plot of the self-broadening coefficient as a function of frequency in the $8\ \mu m$ to $12\ \mu m$ region. Measurements made at this laboratory on pure water samples, as well as nitrogen broadened water samples, are shown as solid points in the figure. Original data published by Burch in Reference [15] are high in the $8\ \mu m$ region and show a great deal of scatter. Roberts has acquired some recent data by Burch which shows much less scatter. These values are also shown in the plot. Bignell's data were converted from his units of $cm^2\ cm^{-1}$ to the units in Figure 5 by multiplying by $2.99 \times$

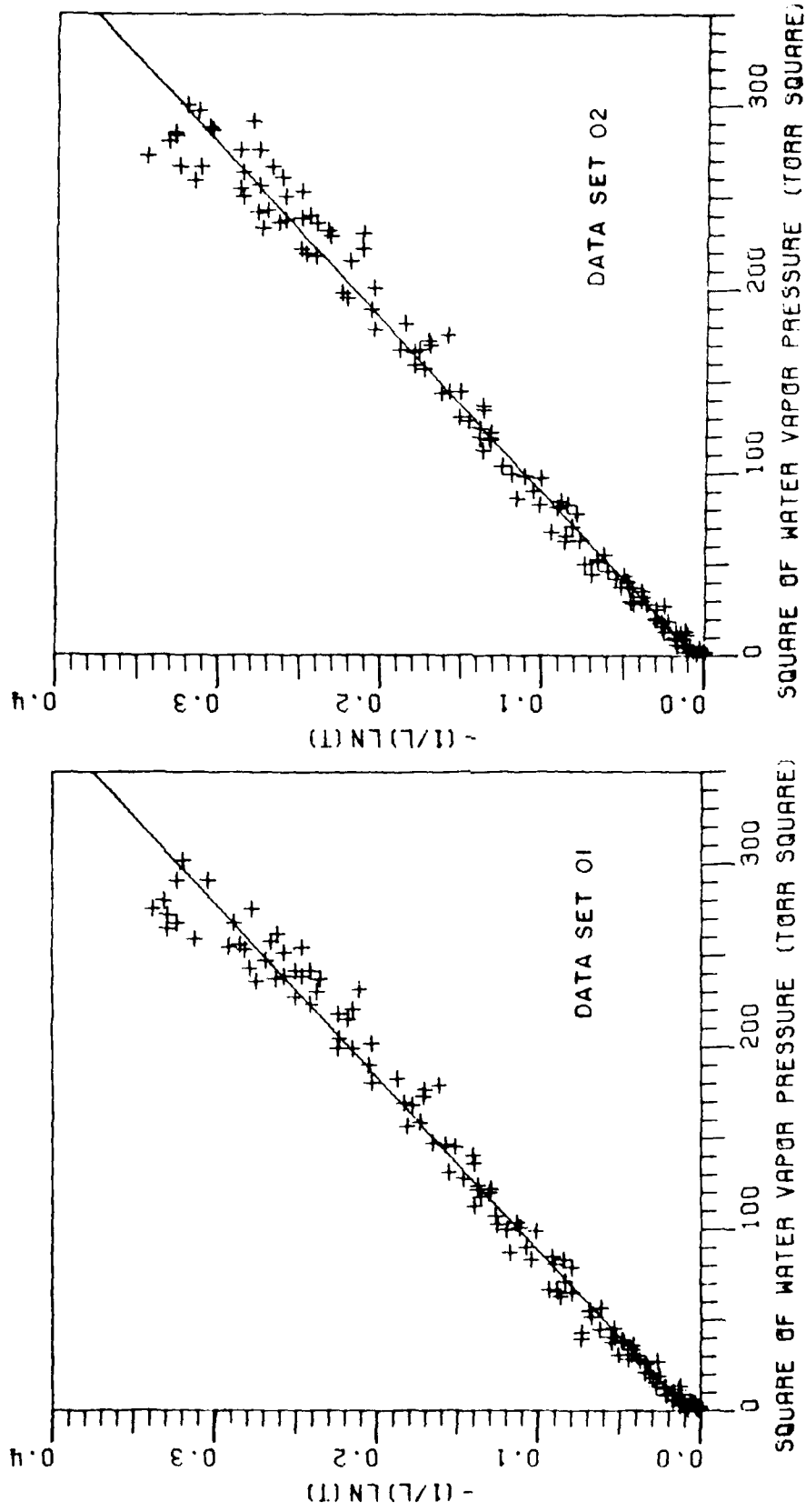


Figure 4 (a-b). Plots of absorption coefficient $k(v)$ as defined by Equation (2) as a function of $P_{H_2O}^2$ for two independent digitizations of the data in Figure 3. Results of the linear least square fits are shown in Table 1.

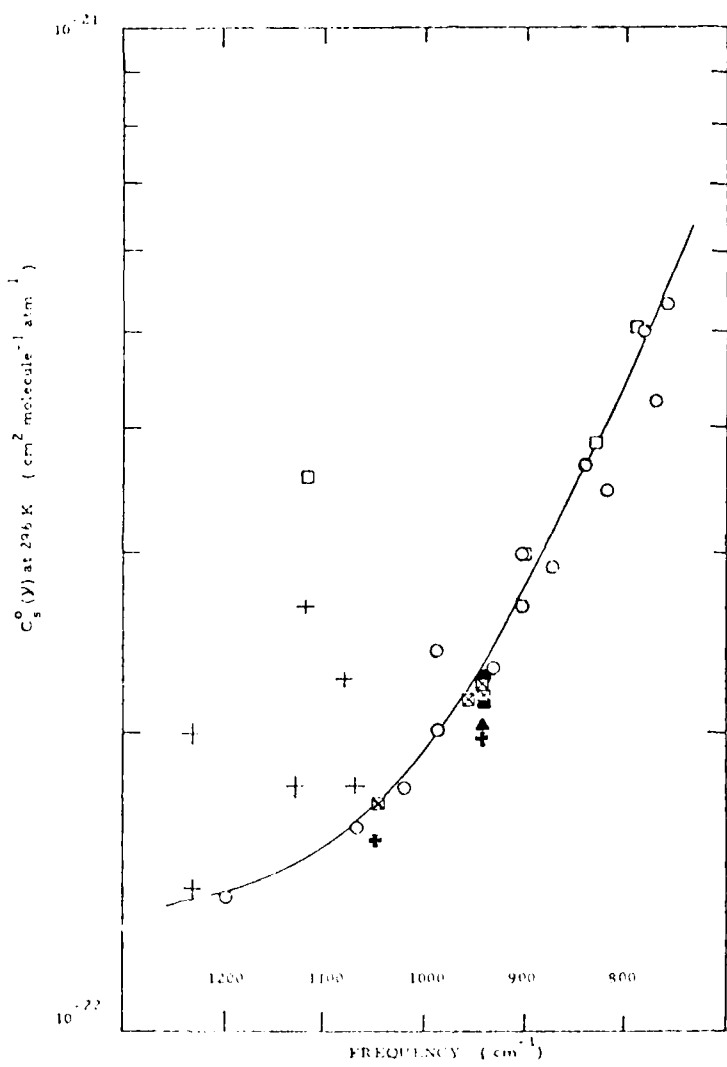


Figure 5. Accumulation of data from several sources on the frequency dependence of the self-broadening coefficient near 296 K in the 8μm to 12μm atmospheric transmission window. Legend:

+ Original Burch data near 8μm	Reference [15]
○ Unpublished Burch data	
□ Bignell	Reference [14]
✖ McCoy, pure H ₂ O samples	Reference [18]
▲ McCoy, air broadened	Reference [18]
■ Mills, Long, pure H ₂ O	Reference [19]
● Mills, Long, nitrogen broadened	Reference [19]
▣ Mills, Long, unpublished	

TABLE 1

LEAST SQUARE FITS OF THE ABSORPTION COEFFICIENTS FROM SEVERAL DATA SETS TO THE FORM $k = a + b P_{H_2O}$

<u>Data Set</u>	<u>Fit</u>	<u>RMS Error</u>
01	$k = (6.19 + 1.06 P_{H_2O}^2) \times 10^{-3}$	1.3×10^{-2}
02	$k = (7.24 + 1.05 P_{H_2O}^2) \times 10^{-3}$	1.3×10^{-2}
McCoy	$k = (1.95 + 0.83 P_{H_2O}^2) \times 10^{-3}$	4.1×10^{-3}
Mills and Long	$k = (4.94 + 0.93 P_{H_2O}^2) \times 10^{-3}$	4.0×10^{-3}

10^{23} .

Roberts has carried out a curve fit to the recent data provided by Burch. His curve

$$C_s^0(v) = a + b \cdot \exp(-\sigma v) \quad (17)$$

is not based on any theoretical model, but it does provide a practical method for calculating the continuum absorption coefficient at any frequency v in the $8 \mu\text{m}$ to $12 \mu\text{m}$ region. Roberts included Burch's data out to $30 \mu\text{m}$, and achieved a coefficient of determination (r^2) of 0.992 with the parameter values of

$$a = 1.25 \times 10^{-22} \text{ cm}^2 \text{ molecule}^{-1} \text{ atm}^{-1}$$

$$b = 1.67 \times 10^{-19} \text{ cm}^2 \text{ molecule}^{-1} \text{ atm}^{-1}$$

$$\sigma = 7.87 \times 10^3 \text{ cm}$$

This fit is shown in the plot.

Temperature Dependence

Data presented in Figure 5 were recorded at a temperature near 296 K. Burch has duplicated these measurements at several temperatures above 296 K. These results are shown in Figure 6. The data at 296 K shown here are the original data which, according to Figure 5, are higher than his recent data in the 8 μm region. From Figure 6, the temperature dependence of $C_s^0(v)$ at several frequencies can be found. We have examined these curves at 850 cm^{-1} , 900 cm^{-1} , and 1000 cm^{-1} . The three data points at each frequency were then fit to an equation of the form

$$C_s^0(v) = a \exp(T_0/T) . \quad (18)$$

An equation of this form is discussed briefly by Roberts, and it has interesting interpretations with respect to the dimer hypothesis.

At 850 cm^{-1} , no correction of the 296 K data was made. At 900 cm^{-1} and 1000 cm^{-1} , two data sets were analyzed at each frequency. The first set included the uncorrected data at 296 K, and the second set included corrected data according to the curve fit in Figure 5. No change of the elevated temperature data was made. The temperature profiles for $C_s^0(v,T)$ at these frequencies are plotted in Figure 7.

Results of the curve fit of Equation (18) are shown in Table 2. The high values for the coefficient of determination (r^2) are due to the fact that only three data points have been used in each fit. The value of a is not expected to be consistent at these different frequencies since it contains the frequency dependence of $C_s^0(v,T)$. To a first approximation, however, the value of T should be independent of

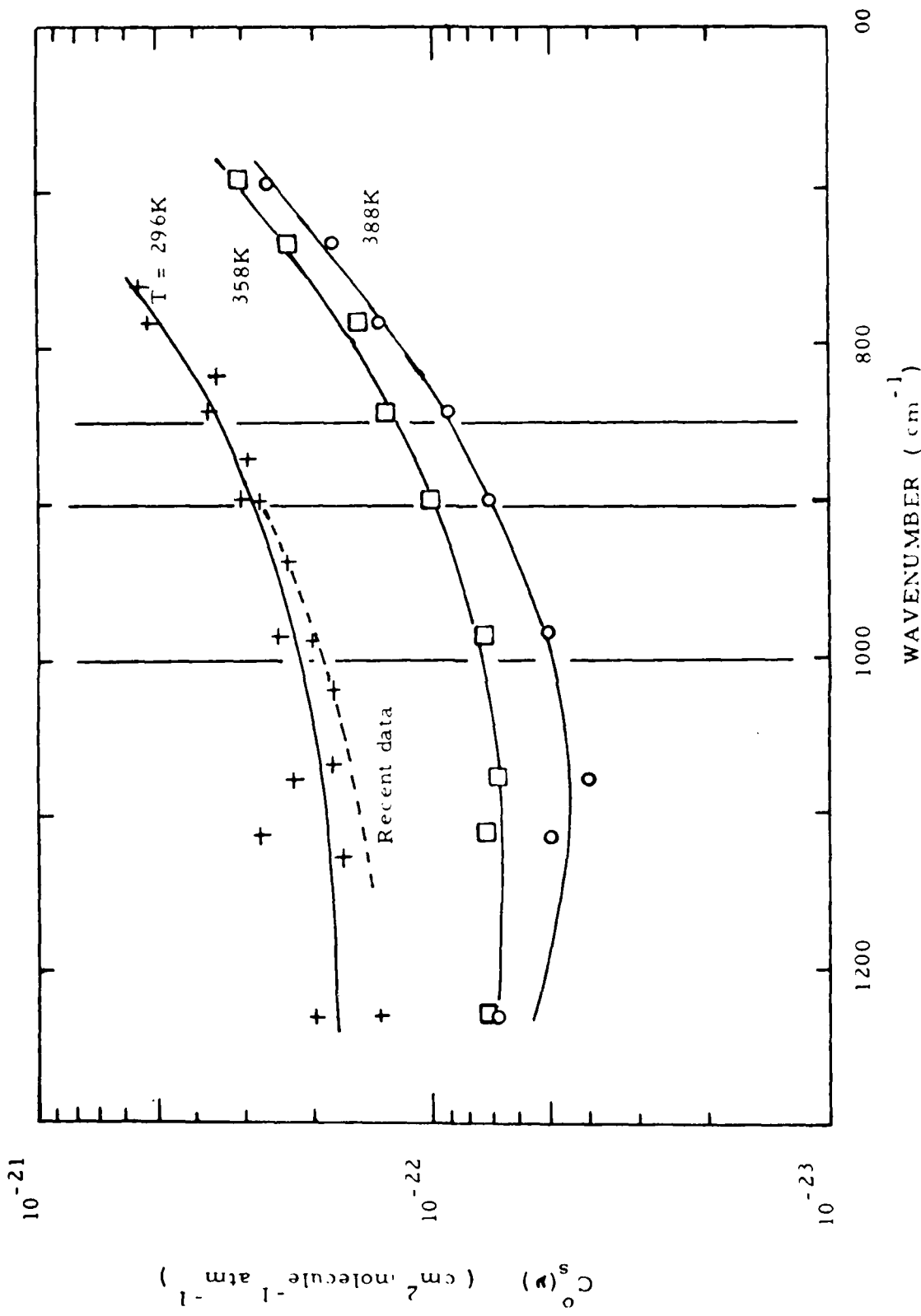


Figure 6. The self-broadening coefficient $C_0^s(v)$ at several temperatures. The dashed line at 296 K represents the curve fit to recent data in Figure 6.

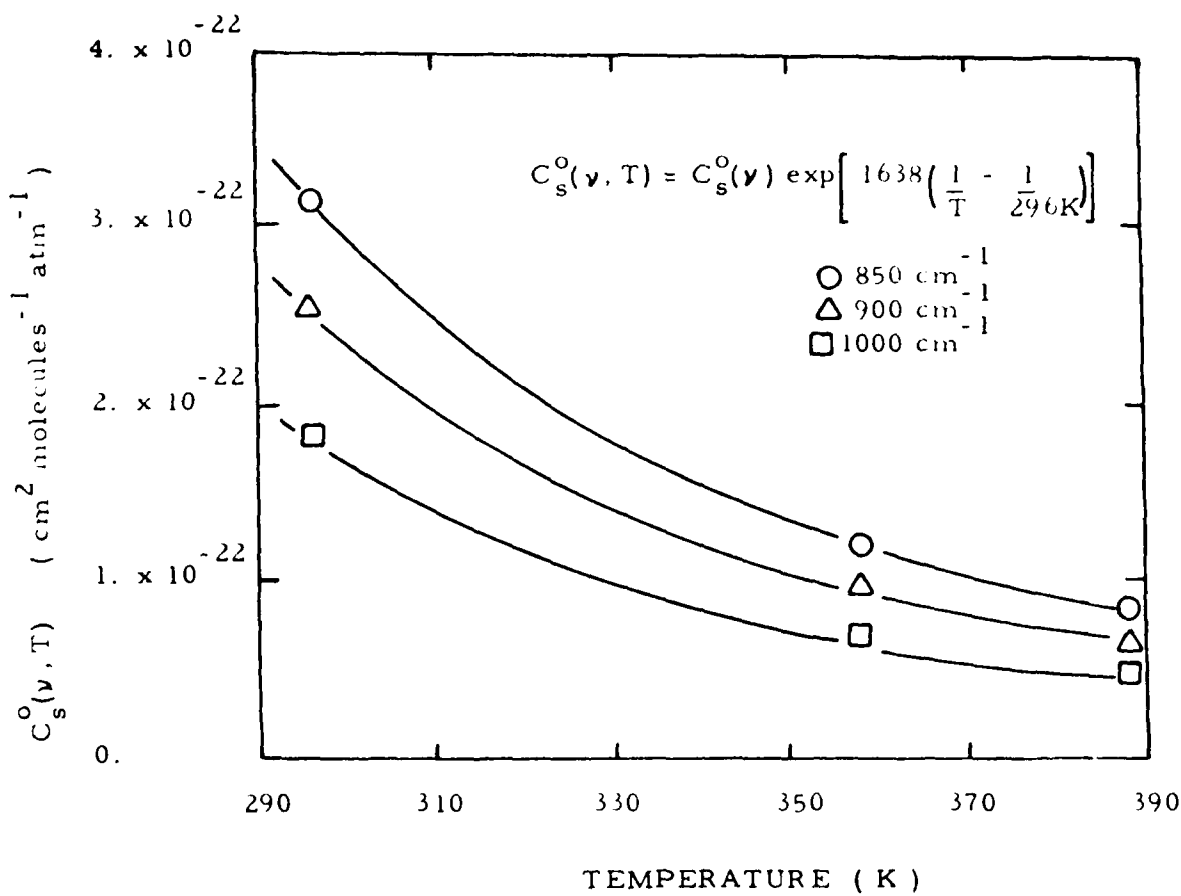


Figure 7. The temperature dependence of the self-broadening coefficient $C_s^0(v)$ at three frequencies. Data are fit to the indicated equation.

TABLE 2
COEFFICIENTS FOR EQUATION (18) DETERMINED FROM A LEAST SQUARE FIT OF BURCH'S DATA
AT SEVERAL FREQUENCIES

	<u>old</u> <u>650 cm⁻¹</u>	<u>new</u> <u>900 cm⁻¹</u>	<u>old</u> <u>1000 cm⁻¹</u>	<u>new</u> <u>1000 cm⁻¹</u>
a	1.265×10^{-24}	8.047×10^{-25}	1.047×10^{-24}	4.755×10^{-25}
T_0	1.635×10^3	1.726×10^3	1.628×10^3	1.792×10^3
r^2	.999	1.000	1.000	.999

frequency in the entire 8 μm to 12 μm region.

If the old data in Table 2 are used, the average value of T_0 is found to be 1718 K. The T_0 values from the more recent data by Burch seem to be much more consistent with the T_0 value at 850 cm, where both old and new data are in agreement. The average value of T_0 derived from the new data is 1638 K. Using this value, an equation which is normalized to room temperature data can be written as:

$$C_s^0(v, T) = C_s^0(v) \exp \left[1638 \text{ K} \left(\frac{1}{T} - \frac{1}{296 \text{ K}} \right) \right]. \quad (19)$$

$C_s^0(v)$ is the self-broadening coefficient at 296 K.

V.N. Aref'ev carried out measurements of the continuum absorption coefficients at the centers of the P(16), P(20), P(22), and P(24) CO_2 laser lines in the 10.4 μm band. As mentioned before, their laser oscillated alternately on each of the lines, and no special steps were taken to separate the results obtained. Measurements were carried out at temperatures of 293 K, 323 K, and 353 K, as reported by Adiks, *et al.*, [22] on pure water samples. Results of this work were reported in the form of an equation

$$k = 1.76 \times 10^{-3} a + 0.42 \times 10^{-6} a^2 \exp \left[\frac{-\Delta H}{RT} \right]. \quad (20)$$

In this equation, a is the amount of water vapor in units of $\text{gm} \cdot \text{m}^{-3}$ and k is in km^{-1} . Since frequency components were not separated, this expression is an average over the four laser lines. In comparing this work with other laser measurements, it is assumed that Equation (20) is valid at the P(20) laser lines position. The value of $-\Delta H/R$ reported was 2273 K.

The presence of a term which is linear in the absorber amount has been questioned earlier in this report. The fact that it is now assumed to be independent of temperature makes this term even more suspect. An equation of the form shown in Equation (20) is not in agreement with Equations (8), (10), and (19). Furthermore, it does not even agree well with Equation (16), as can be seen by using $T = 294$ K in Equation (20) to write

$$k = (1.76a + 0.96a^2) \times 10^{-3} . \quad (21)$$

Other workers have estimated the size of the exponential factor T_0 in Equation (18). Roberts has summarized these results in his report on the water vapor continuum [23]. Rather than reporting the value which Aref'ev and Dianov-Klokov found as 2273 K, Roberts fit their data to an equation of the form given in Equation (16). Results of this fit give $T_0 = 1810$ K. Table 3 summarized values of the exponential constant found by several workers. In all of this work, errors of ± 200 K are not uncommon.

TABLE 3

COMPARISON OF VALUES OF T_0 IN EQUATION (18) DETERMINED FROM
SEVERAL WORKERS

Reference	T_0 (K)
Burch [15] (old data)	1718
Burch (new data)	1638
Aref'ev [22]	2273
Aref'ev*	1810
Bignell [14]	1800
Varanasi, et al., [17]	2000

*Using Aref'ev data and fitting to Equation (19)

A Case for Water Dimer Absorption

Burch found that the water vapor continuum absorption coefficients in the 8 μm to 12 μm region are significantly larger than the calculated values based on extreme wings of strong Lorentz water lines. Figure 8 shows that the discrepancy is a full order of magnitude. The simple Lorentz line shape has the form

$$k(v) = \frac{1}{\pi} \frac{S\alpha}{(v-v_0)^2 + \alpha^2} \quad (22)$$

and the full Lorentz line shape has the form

$$k(v) = \frac{1}{\pi} \frac{v}{v_0} \left[\frac{S\alpha}{(v-v_0)^2 + \alpha^2} - \frac{S\alpha}{(v+v_0)^2 + \alpha^2} \right] \quad (23)$$

where S is the intensity, α is the halfwidth, and v_0 is the center frequency of the absorption line. For infrared frequencies, $v+v_0 \gg \alpha$, and the second term in Equation (23) is negligible.

The fact that the experimentally observed absorption is greater than the calculated absorption is just the opposite from the continuum absorption caused by CO_2 in the 14 μm region. For the CO_2 continuum, the absorption coefficient is smaller than the calculated absorption based on wings of Lorentz lines. The suggestion has been made that the increased absorption for the case of water vapor is due to absorption by $(\text{H}_2\text{O})_2$ dimer molecules [17].

The water dimer molecule is in equilibrium with water vapor through the dissociation-association reactions $(\text{H}_2\text{O})_2 \rightleftharpoons 2 \text{H}_2\text{O}$. The equilibrium constant for these reactions is

$$k_{\text{Eq}} = \frac{P_{\text{H}_2\text{O}}^2}{P_{\text{D}}} \quad (24)$$

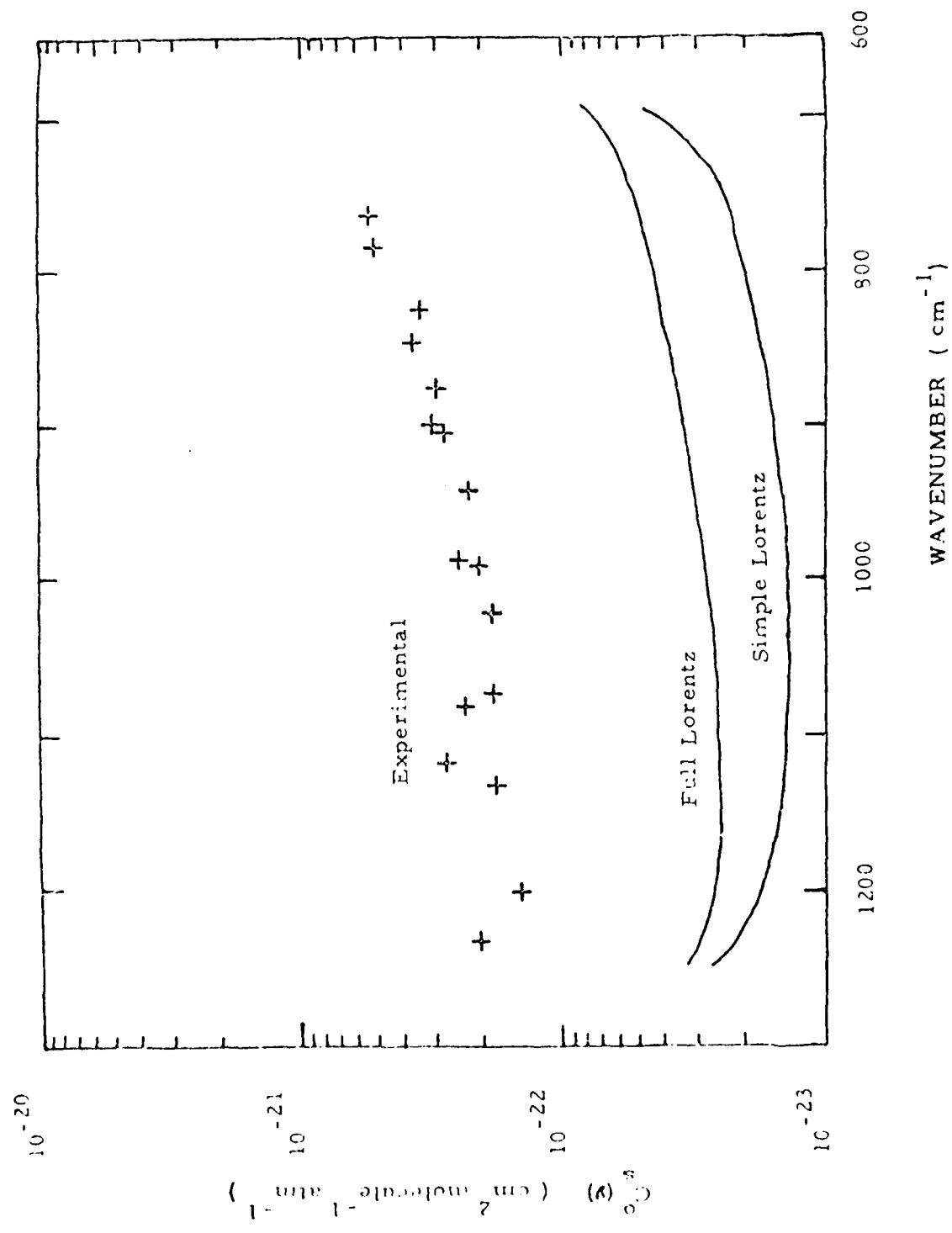


Figure 8. Comparison of experimental values of $C_0^0(v)$ at 296 K with calculated values assuming the continuum absorption is due to the extreme wings of simple Lorentz lines, or of full Lorentz lines. Reproduced from Reference [15].

where the subscript D refers to the dimer.

Energy transmitted by a gas of dimer molecules is expected to follow the usual

$$T_D(v) = \exp(-k_D(v)u_D) \quad (25)$$

where $k_D(v)$ is the absorption coefficient of the dimer gas and u_D is the optical thickness which can be written by Equation (5) as $u_D = w_D \cdot L$.

From Equation (25), $k_D(v)$ can be written as

$$k_D(v) = \frac{-1}{u_D} \ln T_D(v) \quad . \quad (26)$$

If the water dimer is indeed causing the absorption in the 8 μm to 12 μm region, then $k_D(v)$ is the experimentally measured absorption coefficient. However, this coefficient is measured experimentally with respect to the concentration of water vapor (u_{H_2O}), not with respect to dimer concentration. From Equation (24), u_D can be converted to u_{H_2O} .

$$u_D = \frac{1}{k_{Eq}} u_{H_2O} P_{H_2O} \quad . \quad (27)$$

Substitution of this expression into Equation (26) gives

$$k_D(v) = \frac{k_{Eq}}{P_{H_2O}} \frac{-1}{u_{H_2O}} \ln T_D(v) \quad . \quad (28)$$

Rearranging terms gives

$$\frac{-1}{u_{H_2O}} \ln T_D(v) = \frac{k_D(v)}{k_{Eq}} P_{H_2O} \quad . \quad (29)$$

The left hand side of this equation is the expression which would be measured as in Figure 1, assuming the continuum absorption is caused by

water vapor. Ignoring dimer-dimer contributions to $k_D(v)$, this expression is linear in the water vapor pressure. This is the same pressure dependence as Burch used, assuming that the continuum was caused by extreme wings of very strong lines. Therefore, a study of the pressure dependence of continuum absorption in the 8 μm to 12 μm region is not expected to support one absorption mechanism over the other.

The temperature dependence of the continuum absorption has been cited by many as strong evidence for the mechanism of dimer absorption [17, 22]. If dimers are responsible for the absorption, the absorption coefficient should have a temperature dependence of the form $\exp(E/RT)$, where E is the bonding energy of the dimer. Results of temperature studies by several workers show that the temperature dependence of the continuum absorption coefficient can be fitted to an exponential form. Figure 7 demonstrates this fit. Table 3 shows that a reasonable estimate for the constant E/R is approximately 1800 K. On the basis of a hydrogen-hydrogen bond, the bonding energy for the water dimer has been estimated at 3 to 5 kcal/mole [17, 22]. Using R=2 cal/mole⁰K, these bond energies give a value of T_0 between 1500 K and 2500 K.

The agreement between the temperature dependence of the water vapor continuum and the temperature dependence of dimer formation plus the fact that continuum absorption is much stronger than predicted from Lorentz lines can be taken as strong evidence in favor of the dimer absorption mechanism. However, as Burch points out [26], so little is known about the true shapes of the extreme wings of water vapor lines that their contribution cannot be ruled out.

Results such as Equations (9), (17), and (19) are largely empirical and do not depend on a particular absorption mechanism. They generate

curves which are fitted to the data and thus represent algorithms for evaluating the absorption coefficient under specific environmental conditions. As such, these results do not possess any power to predict results of experiments outside the limitations of the variables. Absolute determination of the mechanism of continuum absorption in the 8 μm to 12 μm region would enable predictions of the behavior of this absorption under new circumstances to be made.

One idea which may help to determine the absorption mechanism is to study samples of D₂O instead of H₂O. The isotopic shift in the ν_2 band from 6.3 μm to 8.5 μm would effectively bring the CO₂ laser emission frequencies closer to the band center for a different look at absorption due to the wings of strong lines. A close look at the pressure and temperature dependence of the continuum absorption of D₂O might well shed considerable insight on the continuum absorption of H₂O.

The Water Vapor Continuum in the Region of 4 μm

D. Burch [15] has studied continuum absorption in the 4 μm region using a long path absorption cell and a grating spectrometer. Continuum absorption in this region arises from two effects. One is water vapor absorption which has been attributed to the extreme wings of strong water lines in the bands at 6.3 μm and 2.7 μm . The other is pressure-induced nitrogen absorption.

Burch found the experiment difficult to perform and his accuracy was less than he had anticipated. The major difficulty was due to the fact that the absorption in this region due to the water vapor continuum is close to two orders of magnitude smaller than continuum absorption near 10 μm . As a result, he had to use very high temperatures (up to 428 K),

with water vapor pressures of 100 Torr. This led to problems of water vapor absorption onto the cooler mirrors which reduced reflectivity. Figure 9 is a plot of the self-broadening coefficient $C_s^0(v)$ for water vapor absorption in the region from 2400 cm^{-1} to 2800 cm^{-1} at several different temperatures. The magnitude of the values of $C_s^0(v)$ in this plot should be compared to the magnitude of $C_s^0(v)$ in Figures 5 and 6.

If the temperature dependence of the water vapor continuum absorption in the $4 \mu\text{m}$ region is accurately represented by Equation (18), then plots of $\ln(C_s^0(v))$ as a function of $1/T$ for various frequency positions should be linear. Figure 10 shows such a plot for four selected frequencies. The linear fits to the data are very good, and the slopes are approximately equal, indicating that the T_0 value in this region is not frequency dependent. The lines must be extrapolated outward to find $C_s^0(v)$ at room temperature, since this quantity cannot be measured directly.

Several studies [27, 28] of the propagation of radiation from the deuterium fluoride laser have used the results of Burch. F.S. Mills [27] has stated that, on the basis of his DF laser studies, the extrapolation done by Burch was probably correct. However, Mills recommended that this problem should be studied carefully with the use of a spectrophone.

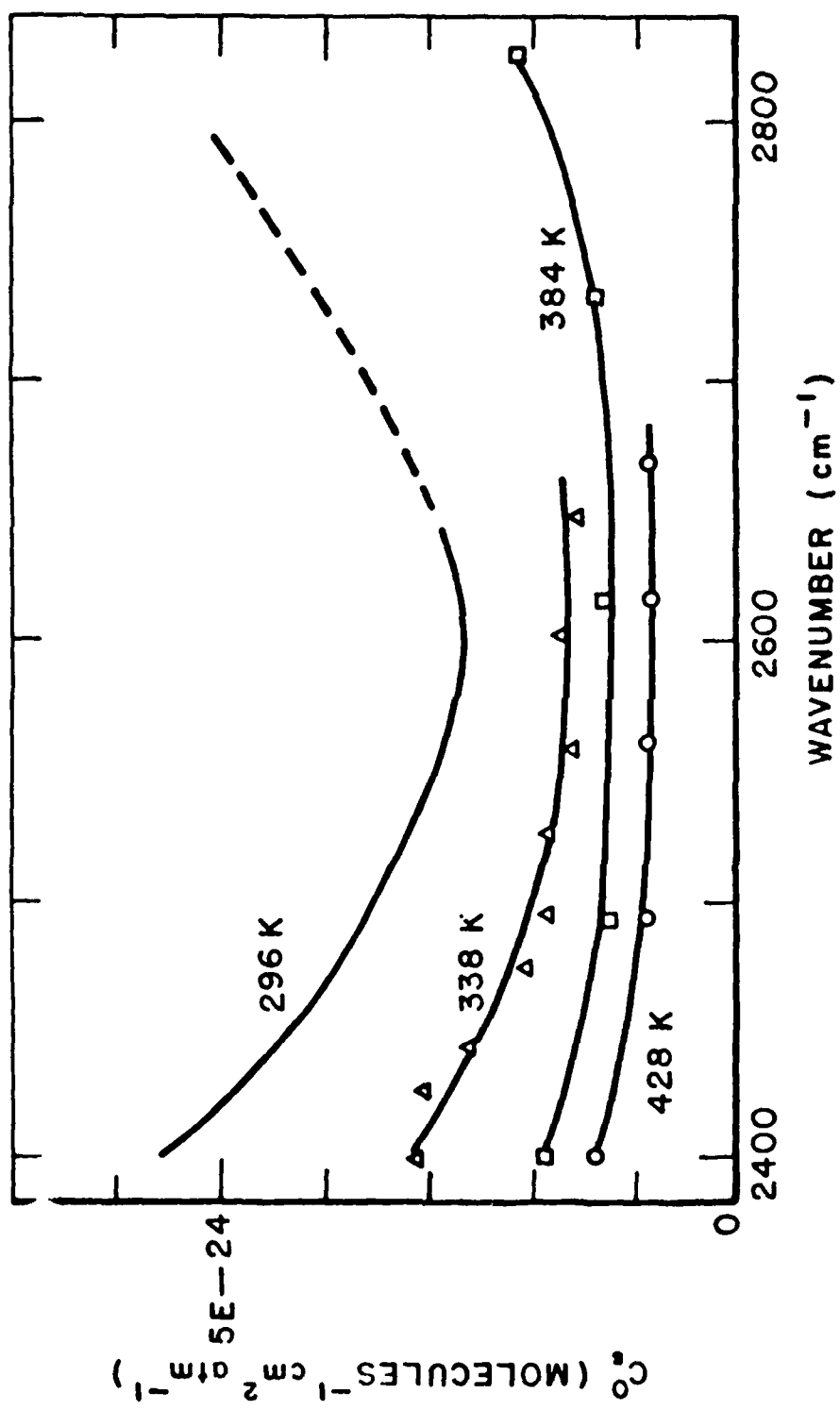


Figure 9. Spectral plots of $C_0^{(\nu)}$ between 2400 cm^{-1} and 2820 cm^{-1} for pure H_2O at four temperatures. The curve at 296 K is constructed with the help of Figure 10. Reproduced from Reference [15].

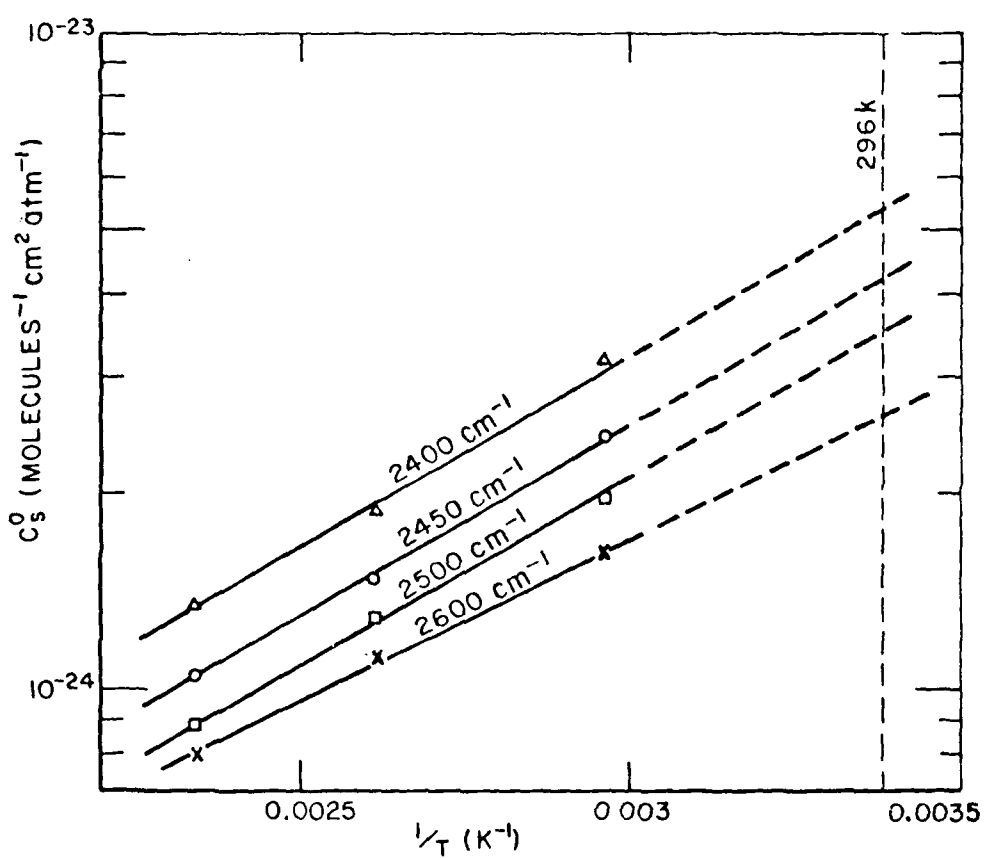


Figure 10. Semi-logarithmic plots of $C_s^0(v)$ versus $1/T$ for four different frequencies. The plots are extrapolated to $T=296 \text{ K}$ to find $C_s^0(v)$ at room temperature.

REFERENCES

- 1 S.P. Langley, Mem. Natl. Acad. Sci. 4, 159 (1888).
- 2 S.P. Langley, Ann. Ap. Obs., Smithsonian Institution, 1, 1 (1900).
- 3 A. Adel, Astrophys. J. 87, 198 (1938), 91, 1 (1940), 93, 506 (1941).
- 4 A. Adel, J. Opt. Soc. America 37 769 (1947).
- 5 M.V. Migeotte, Phys. Rev. 73, 519 (1948).
- 6 M.V. Migeotte, Phys. Rev. 75, 1108 (1949).
- 7 J.H. Shaw, M.L. Oxholm and H.H. Claassen, Astrophys. J. 116, 554 (1952).
- 8 W.M. Elsasser, "Heat Transfer by Infrared Radiation in the Atmosphere", Harvard University Press, Cambridge, Mass. (1942).
- 9 H.W. Yates and J.H. Taylor, "Infrared Transmission of the Atmosphere", NRL Report 5453 (AD 240-88) (1960).
- 10 A. Adel, Astrophys. J. 89, 1 (1939).
- 11 R. Anthony, Phys. Rev. 85, 674 (1952).
- 12 W.T. Roach and R.W. Goody, Quart. J. Roy. Meteorol. Soc. 84, 319 (1958).
- 13 K. Bignell, F. Saiedy, and P.A. Sheppard, J. Opt. Soc. America 53, 466 (1963).
- 14 K.J. Bignell, Quart. J. Roy. Meteorol. Soc. 96, 390 (1970).
- 15 D.E. Burch, Aeronutronic Publication No. U-4784, "Semi-Annual Technical Report", Air Force Cambridge Research Laboratories, Contract No. F19628-69-C-0263, January 1970.
- 16 D.E. Burch, D.A. Gruyvnak, and J.D. Pembroke, Aeronutronic Publication No. U-4897, "Investigation of the Absorption of Infrared Radiation by Atmospheric Gases: Water, Nitrogen, Nitrous Oxide", Air Force Cambridge Research Laboratories, Contract No. F19628-69-C-0263, January 1971.
- 17 P.S. Varanasi, S. Chou, and S.S. Penner, J. Quant. Spectros. Radiat. Transfer 8, 1537 (1968).
- 18 J.H. McCoy, D.B. Rensch, and R.K. Long, Appl. Opt. 8, 1471 (1969).

- 19 F.S. Mills, R.K. Long, and E.K. Damon, "Laser Absorption Studies (First Semi-Annual Report)", Report 784054-2, July 1975, The Ohio State University ElectroScience Laboratory, Department of Electrical Engineering; prepared under Contract No. RADC-TR-75-288 for Rome Air Development Center (OCSE).
- 20 I.I. Ippolitov, Opt. Spektrosc. 27, 246 (1969).
- 21 V.N. Aref'ev, V.I. Dianov-Klokov, V.N. Radionov, and N.I. Sizov, Opt. Spektrosc. 39, 560 (1975).
- 22 T.G. Adiks, V.N. Aref'ev, and V.I. Dianov-Klokov, Jor. J. Quant. Electron. 5, 481 (1975).
- 23 R.E. Roberts, L.M. Biberman and J.E.A. Selby, "Infrared Continuum Absorption by Atmospheric Water Vapor in the 8-12 m Window", Institute for Defense Analysis Science and Technology Division, IDA Log No. HQ76-18059, April 1976.
- 24 J.E.A. Selby and R.A. McClatchey, "Atmospheric Transmittance From 0.25 to 28.5 μm : Computer Code LOWTRAN 3", AFCRL-TR-75-0255, Air Force Cambridge Research Laboratories Environmental Research Papers, No. 513 (1975).
- 25 J.E. Lowder, L.A. Kennedy, K.G.P. Sulzmann, and S.S. Penner, J. Quant. Spectrosc. Radiat. Transfer 10, 17 (1969).
- 26 D.E. Burch, "Radiative Properties of the Atmospheric Windows", presented at the Conference on Atmospheric Radiation sponsored by the American Meteorological Society, Ft. Collins, Colorado, August 1972.
- 27 F.S. Mills, "Absorption of Deuterium Fluoride Laser Radiation by the Atmosphere", Report 784054-3, September 1975, The Ohio State University ElectroScience Laboratory, Department of Electrical Engineering; prepared under Contract No. RADC-TR-75-0029 for Rome Air Development Center (OCSE).
- 28 R.E. Meredith, T.W. Tuer, and D.R. Woods, "Investigation of DF Laser Propagation", Research and Development Technical Report, Atmospheric Sciences Laboratory, ECOM-74-4, December 1974.

SECTION III

THE N₂-BROADENED WATER VAPOR ABSORPTION LINE SHAPE AND
INFRARED CONTINUUM ABSORPTION

Part I: Theoretical Development

INTRODUCTION

Strong absorption bands of water vapor and carbon dioxide separate spectral regions of high infrared transmittance within the lower atmosphere into several spectral windows. It has long been known that attenuation of radiation within these transmittance windows is greater than predicted from calculations of local Lorentzian absorption line contributions and from possible aerosol contributions. The residual absorption in excess of the predicted amount has been called continuum absorption since it is a slowly varying function of frequency. This continuum absorption represents a depression in the spectral background from the 100% transmittance level, and has been linked to water vapor content along the absorbing path.

Continuum absorption in the 8-14 μm region has been the topic of a great deal of study [1-5]. Investigations of its behavior as a function of total atmospheric pressure, partial water vapor pressure, and temperature have been made. Similar measurements have been performed in the 3.5-4 μm region [6,7], although these experiments have been more difficult because the continuum absorption in this region is much weaker than the absorption around 10 μm .

The exact mechanism of water vapor continuum absorption within a transmittance window has not been understood. Originally it was thought to be the result of wings of very strong water vapor lines located in the absorption bands bordering the transmittance window.

However, it was shown [2] that self-broadened Lorentzian absorption line wings were not adequate to model the 10 μm continuum absorption caused by pure water vapor samples. Furthermore, absorption in the wings of Lorentzian lines near 10 μm increases with increasing temperature while experiments show the measured absorption actually decreases with increasing temperature [8,9].

Based on these inadequacies of the Lorentz absorption line wing theory to model the water vapor continuum, other mechanisms for the absorption were sought. Infrared absorption by water dimers [10,11] or by more complex molecular clusters [12] have been proposed as possible attenuation mechanisms. It is argued that water vapor aggregates could have unresolved absorption bands throughout the infrared spectral region and although the fractional concentration of aggregates would be small compared to the concentration of H_2O molecules, the absorption could still be large enough to be detected in the transmittance windows.

Perhaps the most convincing argument in favor of the attenuation being caused by water vapor aggregates is that this mechanism predicts the observed negative temperature dependence. It is argued that since the attenuation is directly proportional to the number of aggregates present, which in turn is proportional to $\exp(-\Delta H/kT)$ where ΔH is the change in enthalpy on aggregate formation and is negative, the resulting attenuation will exhibit a negative temperature dependence. Furthermore, measurements of the temperature dependence of water vapor continuum absorption in the 8-14 μm spectral region are in good agreement with predictions based on hydrogen-hydrogen bond dissociation rates [13].

Of course there is always the possibility that both absorption mechanisms are occurring simultaneously. Measurements of the temperature

dependence of continuum absorption at 1203 cm^{-1} by Montgomery [14] showed that as the temperature of the water vapor sample was increased from room temperature, the absorption reached a minimum. This behavior was interpreted by Montgomery as showing the competitive effects of dimer absorption and far wing absorption. He suggested that initially the measured absorption decreased as the temperature increased because of dimer dissociation. Above 400 K, however, with dimers depleted, far wings of the strong absorption lines of water vapor began to dominate and push the absorption up slowly.

Figure 1 demonstrates that the accumulative effects caused by the overlap of absorption line wings can be significant. Three spectra of the $4.3\text{ }\mu\text{m}$ absorption region of the CO_2 molecule are shown. The background spectrum shows the absorption caused by atmospheric CO_2 in the few meters of path between the infrared source and the entrance to our evacuated, long-path absorption cell. The high-frequency edge of the v_3 band of CO_2 shows an abrupt cut-off of the absorption near 2380 cm^{-1} which is characteristic of the band head.

A spectrum recorded with 80 torr of pure CO_2 in a 300 m path, however, shows that the absorption caused by this band can extend beyond the band head. Ignoring the very weak resonance absorption band structures which become visible at this optical depth, it is clear that a structureless absorption, manifested as a slowly varying depression of the background exists even past 2450 cm^{-1} . Filling the absorption cell to 740 torr with pure CO_2 , as shown in the third spectrum, causes the influence of this absorption band to extend past 2550 cm^{-1} .

This increase in absorption at frequencies above the band head near 2380 cm^{-1} is the result of the accumulation of far wings of the absorption lines of the v_3 band. To model this absorption properly,

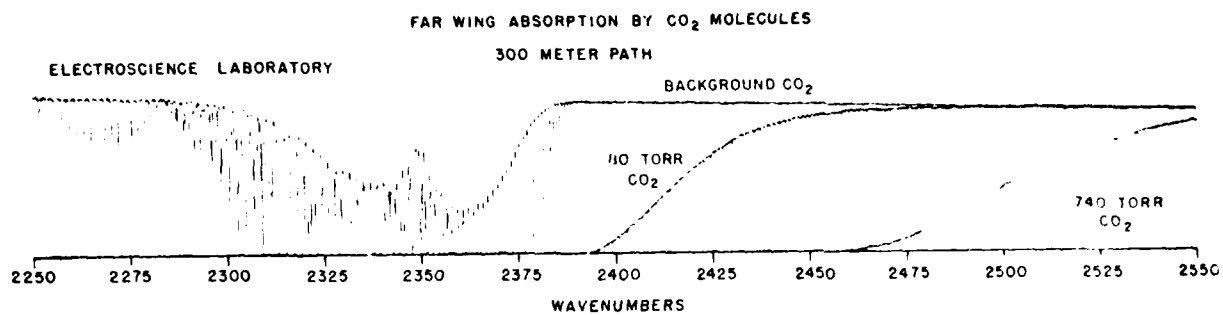


Figure 1. Far wing absorption by CO₂ molecules.

the shape of the absorption line profile for each CO₂ line in the absorption band is needed. Clearly, an incorrect line profile which underemphasizes each contribution to the total absorption in the far wings would result in excess absorption appearing to be present in the measured spectrum.

The spectrum of CO₂ was used to visualize the continuum-like absorption which can be caused by far wings of resonant absorption lines. For the case of water vapor, it is difficult to find clear spectral regions free from local lines in which to observe absorption line wings. Furthermore the physical properties of water vapor prevent the use of reasonably large pressures (near 1 atm, for example) without high temperatures. Thus, it is difficult at times to separate pressure dependent and temperature dependent effects experimentally.

In order to model water vapor continuum absorption, it is necessary to determine the contributions made by the accumulation of the far

wings of pressure-broadened water vapor absorption lines. Only then can the importance of absorption mechanisms based on molecular aggregates be established.

In this study we have begun to investigate the importance of far wing absorption for characterizing the water vapor continuum. An infrared line shape for pressure-broadened water absorption has been derived which is valid under tropospheric conditions. It was found during the study that the traditional assumptions which lead to the Lorentz line shape could not be used when considering the far wings of water vapor absorption lines.

The total, normalized line profile was used to predict the absorption at specific frequencies within the 8-14 μm and 3.5-4 μm transmittance windows. The experimental methods and the results are discussed in detail in another report [15]. In this section we shall discuss the development of the infrared absorption line profile for water vapor molecules.

THEORY

The absorption coefficient, $k(v)$, for attenuation caused by absorption lines can be written

$$k(v) = \sum_i S_i j_i(v - v_{0i}) \quad (1)$$

where S_i is the line strength of the i^{th} absorption line, and $j_i(v - v_{0i})$ is the line shape function of the i^{th} absorption line centered at frequency v_{0i} . It can be assumed that any differences in the line shapes of different water vapor lines can be expressed parametrically

within the same overall function. That is, $j_i(v-v_{oi})$ is better written as $j(v-v_{oi};\beta_i)$ where β_i represents a set of parameters which represent the i^{th} absorption line.

The line shape function is normalized by the requirement

$$\int_0^{\infty} j(v-v_{oi};\beta_i) dv = 1 \quad (2)$$

for all i .

Any description of the absorption coefficient, $k(v)$, then can be divided into a line strength term and a line shape term.

The Hamiltonian

The starting point for the development of the spectral line profile is with the total Hamiltonian describing the molecular system. In this case, the system consists of a number n_a of gas-phase, interacting molecules which can absorb infrared radiation. Also present are other molecules which can interact with the absorbing molecules via collisions. Thus, the Hamiltonian can be written as

$$H_{Tot}(t) = H_{a_1} + H_b + H_p + H_{a_1p}(t) + H_c(t) \quad (3)$$

where H_{a_1} is the Hamiltonian for the absorbing molecule

H_b is the Hamiltonian for the buffer molecules

H_p is the Hamiltonian for the photon field

$H_{a_1p}(t)$ is the interaction Hamiltonian between the absorbing molecule and photon field

$H_c(t)$ is the collision Hamiltonian which describes molecule-molecule interactions.

Time dependent terms are explicitly indicated. The collision Hamiltonian will be written to account for absorber-absorber molecule interactions (spectral self-broadening) and to account for absorber-buffer molecule interactions (spectral foreign-broadening).

H_{a_1} represents the absorbing molecule. The added subscript 1 indicates the specific molecule considered to be doing the absorption while the $n_a - 1$ identical molecules are considered for the moment to be perturbers. The unperturbed Hamiltonian for the absorbing molecule is

$$H_{a_1} = H_{a_{ROT}} + H_{a_{VIB}} + H_{a_{EL}} + H_{a_{TRN}} \quad (4)$$

where

$H_{a_{ROT}}$ describes the rotation energy of the molecule

$H_{a_{VIB}}$ describes the vibrational energy of the molecule

$H_{a_{EL}}$ describes the electronic energy of the molecule

and $H_{a_{TRN}}$ describes the translational energy of the molecule.

The first three terms are fundamental to the study of molecular spectroscopy and to the production of spectral lines. The term $H_{a_{TRN}}$ will not be directly included in this analysis. Motion perturbed line profiles such as the Doppler profile can be derived from the term.

In the total Hamiltonian, the term H_b is a many-particle Hamiltonian. This includes foreign molecules and molecules identical to the absorber.

It can be written

$$H_b = \sum_{j=2}^{n_a} H_{a_j} + \sum_{k=1}^{\kappa} \sum_{m=1}^{n_k} H_{b_{km}}. \quad (5)$$

Here n_a is the number of absorbing molecules, κ represents the number

of types of foreign molecules, and n_k is the number of molecules of the k th type. Each Hamiltonian is structured in the same way as Equation (4); that is the rotational, vibrational, electronic, and translational energies are represented.

H_p is the free space photon Hamiltonian, written as

$$H_p = \sum_{q\sigma} \hbar\omega(\vec{q}) [a_\sigma^\dagger(\vec{q})a_\sigma(\vec{q}) + \frac{1}{2}] \quad (6)$$

where $a_\sigma^\dagger(\vec{q})$ is the photon creation operator and $a_\sigma(\vec{q})$ is the photon annihilation operator for a photon of polarization σ and wave number \vec{q} corresponding to the angular frequency $\omega = \hbar|\vec{q}|$.

The interaction Hamiltonian, $H_{a_1 p}(t)$, between the absorbing molecule and the photon field can be written [16]

$$\begin{aligned} H_{a_1 p}(t) &= \frac{-e}{2mc} [\vec{p} \cdot \vec{A}(\vec{r}, t) + \vec{A}(\vec{r}, t) \cdot \vec{p}] \\ &+ \frac{e^2}{2mc^2} \vec{A}(\vec{r}, t) \cdot \vec{A}(\vec{r}, t) \end{aligned} \quad (7)$$

where \vec{p} is the particle momentum operator, and $\vec{A}(\vec{r}, t)$ is the photon field magnetic vector potential operator, written as

$$\begin{aligned} \vec{A}(\vec{r}, t) &= \left[\frac{2\pi c}{qV} \right]^{\frac{1}{2}} \left\{ a_\sigma(\vec{q}) \vec{v}_\sigma(\vec{q}) \exp(i(\vec{q} \cdot \vec{r} - \omega t)) \right. \\ &\left. + a_\sigma^\dagger(\vec{q}) \vec{v}_\sigma^*(\vec{q}) \exp(-i(\vec{q} \cdot \vec{r} - \omega t)) \right\} \end{aligned} \quad (8)$$

In this expression $\vec{v}_\sigma(\vec{q})$ is a unit vector perpendicular to the free

space photon propagation direction and represents the polarization of the electromagnetic radiation.

To first order, the interaction Hamiltonian becomes

$$H_{a_1 p}(t) = H_{a_1 p}^{ab} \exp(-i\omega t) + H_{a_1 p}^{em} \exp(i\omega t) \quad (9)$$

where the $\vec{A} \cdot \vec{A}$ term has been dropped. The term $H_{a_1 p}^{ab}$ represents the collection of operators and factors which multiply the negative exponential after Equations (7) and (8) have been combined. This term represents the absorption of radiation by the molecule [17]. Similarly, the term $H_{a_1 p}^{em}$ represents the emission of radiation by the molecule.

Finally, $H_c(t)$ represents the intermolecular potential which couples the absorbing molecule to molecules surrounding it. It is the least understood term in the total Hamiltonian, and yet, it is the most important when attempting to understand the nature of resonant line profiles. A general many-body expression can be written as

$$H_c(t) = \sum_{j=2}^{n_a} H_{a_j a_1}(t) + \sum_{k=1}^{\kappa} \sum_{m=1}^{n_k} H_{b_m k a_1}(t) \quad (10)$$

when restricting the discussion to binary collisions only. Again, κ is the number of different foreign gases, and n_k is the number of molecules of the k th gas. Figure 2 illustrates the geometry involved in such an interaction. For electrically neutral molecules (no ionic interaction) with permanent electrostatic potentials, a single Hamiltonian in Equation (10) takes the form [18]

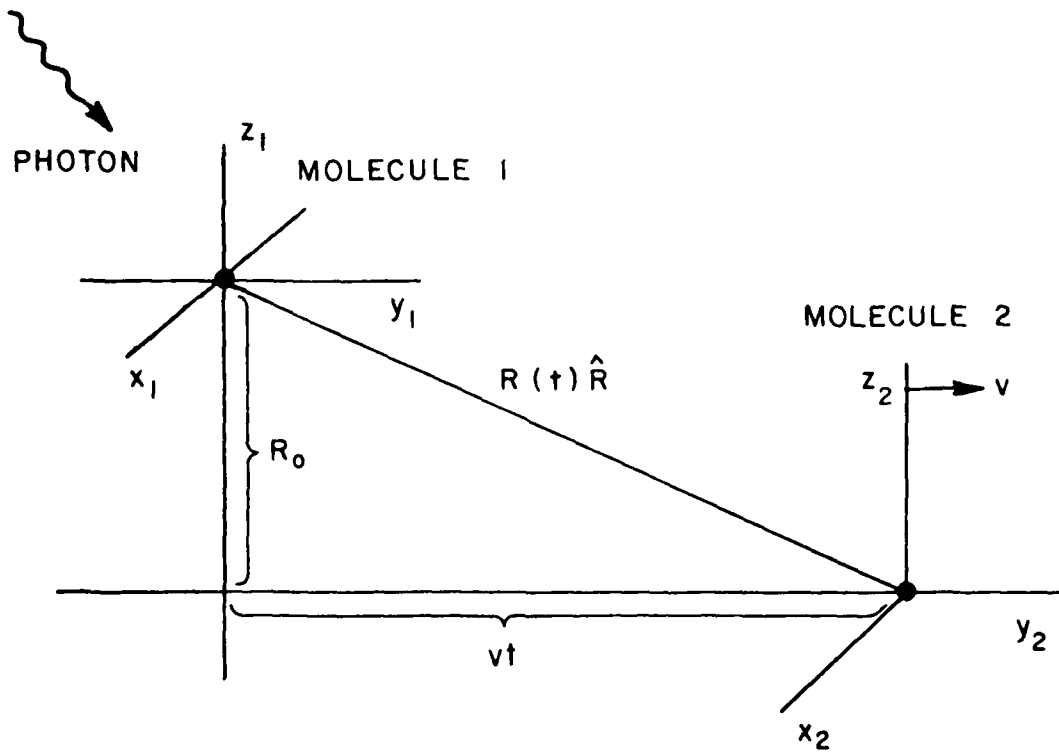


Figure 2. Interaction geometry.

$$H_{b_{mk}a_1}(R(t); \vec{r}_{mk}, \vec{r}_1) = \langle V_{\text{Electrostatic}} + V_{\text{Magnetostatic}} \rangle_{\text{Rot}}$$

$$-V_{\text{Dispersive}} -V_{\text{Inductive}} +V_{\text{repulsive}} \quad (11)$$

As shown in Figure 2, $R(t)$ is the intermolecular distance between the absorber and perturber. The quantities \vec{r}_{mk} and \vec{r}_1 locate the charged particles within the molecular coordinates of the foreign and absorber molecules respectively. The magnetostatic potential function is significantly smaller than the electrostatic potential and this is ignored hereafter.

A brief description of the potential terms is necessary. A multi-pole expansion of the electrostatic potential is

$$V_{\text{Electrostatic}} = \frac{V_{DD}(\vec{r}_{mk}, \vec{r}_1)}{R^3(t)} + \frac{V_{DQ}(\vec{r}_{mk}, \vec{r}_1)}{R^4(t)} + \frac{V_{DO}(\vec{r}_{mk}, \vec{r}_1)}{R^5(t)} + V_{QQ}(\vec{r}_{mk}, \vec{r}_1) + \dots \quad (12)$$

where

$V_{DD}(\vec{r}_{mk}, \vec{r}_1)$ is the dipole-dipole interaction term

$V_{DQ}(\vec{r}_{mk}, \vec{r}_1)$ is the dipole-quadrupole interaction term

$V_{DO}(\vec{r}_{mk}, \vec{r}_1)$ is the dipole-octopole interaction term

and $V_{QQ}(\vec{r}_{mk}, \vec{r}_1)$ is the quadrupole-quadrupole interaction term.

These potentials can be expressed as

$$V_{DD}(\vec{r}_{mk}, \vec{r}_1) = \mu_{mk} u_1 f(\Omega_{mk}, \Omega_1, \vec{r}_{mk}, \vec{r})$$

$$V_{DQ}(\vec{r}_{mk}, \vec{r}_1) = \mu_{mk} \bar{Q}_1 g_1(\Omega_{mk}, \Omega_1, \vec{r}_{mk}, \vec{r}) + \bar{Q}_{mk} u_1 g_2(\Omega_{mk}, \Omega_1, \vec{r}_{mk}, \vec{r})$$

$$V_{DO}(\vec{r}_{mk}, \vec{r}_1) = \mu_{mk} \bar{R}_1 h_1(\Omega_{mk}, \Omega_1, \vec{r}_{mk}, \vec{r}) + \bar{R}_{mk} u_1 h_2(\Omega_{mk}, \Omega_1, \vec{r}_{mk}, \vec{r})$$

$$\text{and } V_{QQ}(\vec{r}_{mk}, \vec{r}_1) = \bar{Q}_{mk} \bar{Q}_1 q(\Omega_{mk}, \Omega_1, \vec{r}_{mk}, \vec{r}).$$

The μ_{mk} is the dipole moment of the m th molecule of the k th type, and u_1 is the dipole moment of the absorber. Employing the same convention with the subscripts, \bar{Q} and \bar{R} represent the mean quadrupole and octopole moments of the molecules, respectively. The terms Ω_{mk} and Ω_1 represent the parameters necessary to establish the orientation of the multipole moment of both the perturber and absorber molecules in a space-fixed coordinate system. These parameters are arguments of expressions f , g , h , and q which determine the angular dependence of the electrostatic interaction potentials.

The molecules are rotating during the collision. The total rotation during interaction will depend on the rotational energy of the molecule and the duration of the collision. The forces produced by the electrostatic potential will attempt to orient the molecules in a minimum potential energy configuration. A weighted average over the rotation is performed in order to account for the ability of the absorber molecule to achieve this preferred orientation. The average is denoted by $\langle \cdot \rangle_{\text{Rot}}$, and is written

$$\langle v_{E1} \rangle_{\text{Rot}} = \frac{\int d\Omega v_{E1} \exp(-v_{E1}/kT) p(\Omega_0, t_d, f_{mk}^R, f_1^R)}{\int d\Omega \exp(-v_{E1}/kT) p(\Omega_0, t_d, f_{mk}^R, f_1^R)}. \quad (13)$$

Here $d\Omega$ is the differential element of solid angle for all possible orientations and $p(\Omega_0, t_d, f_{mk}^R, f_1^R)$ is a pulse function with unit amplitude and a pulse duration which depends explicitly on the initial orientation Ω_0 , the collision duration time t_d , and the rotational frequencies of the perturbing and absorbing molecules f_{mk}^R and f_1^R , respectively.

For collisions with large impact parameters the collision duration time is very small, and

$$\langle v_{E1} \rangle_{\text{Rot}} \approx v_{E1}. \quad (14)$$

For collisions with small impact parameters the electrostatic potentials can be so strong that the interaction can no longer be considered to be a small perturbation to the unperturbed Hamiltonian of the absorber molecule. This occurs during close encounters and during the formation of liquids and solids. The ability of the molecule to rotate is inhibited and the absorber molecule takes a relatively fixed orientation.

At this extreme, the average over orientations breaks down and in fact the formulation of the unperturbed Hamiltanian as Equation (4) is no longer valid.

Other long range electrostatic potentials can be of interest to molecular collision dynamics. The most important of these are induction and dispersion potentials, both of which vary as $R^{-6}(t)$. Induction potentials represent the interaction of a permanent electric multipole of one molecule with an induced multipole of another molecule. The resulting potential is attractive. Dispersion potentials arise from the random motion, within the bounds of the Uncertainty Principle, of electrons about the nuclei generating instantaneous multipoles. A discussion of these potentials is given elsewhere [18] and approximate forms are [19]

$$V_{\text{Inductive}} = - \frac{[\epsilon_1^2 \bar{\alpha}_{mk} + \mu_1^2 \bar{\alpha}_1]}{R^6(t)} \quad (15a)$$

$$V_{\text{Dispersive}} = - \frac{\bar{\alpha} e^2 \langle r^2 \rangle}{2 R^6(t)} \quad (15b)$$

where $\bar{\alpha}$ is the mean electric polarizability of the molecule, and e is the charge on an electron.

The final term in the collision Hamiltonian as written in Equation (11) is $V_{\text{Repulsive}}$. During very close encounters between molecules, repulsive forces such as electron cloud interaction can occur. For this study, such potentials were not explicitly considered.

THE TRANSITION RATE

Following the work of Anderson [20] and of Tsao and Curnutte [21], the rate for a radiation absorption transition from a lower molecular energy level to an upper molecular energy level separated by $E_u - E_l = \hbar\omega_0$ is

$$\frac{\Gamma}{\hbar^2} = \frac{2}{\hbar^2} \operatorname{Re} \left\{ \int_0^\infty d\tau \exp(-i\Delta\omega\tau) \operatorname{Tr} \left[\rho_0 H_{a_1 p}^{ab} S_c^{-1}(\tau) H_{a_1 p}^{ab} S_c(\tau) \right] \right\}, \quad (16)$$

where $S_c(\tau)$ is the time development operator for the collision Hamiltonian at time τ and is written

$$S_c(\tau) = \exp \frac{1}{i\hbar} \int_0^\infty H_c(\tau) d\tau.$$

In Equation (16), ρ_0 is the density matrix generated by the initial states, and $\Delta\omega = \omega - \omega_0$ is the amount of off-resonance between the radiation frequency ω and energy level spacing. This equation can be written in a compact form as

$$\begin{aligned} \frac{\Gamma}{\hbar^2} = & \frac{2}{\hbar^2} \operatorname{Re} \left\{ \int_0^\infty d\tau \exp(-i\Delta\omega\tau) \times \right. \\ & \sum_q \frac{1}{g_q} \rho_q f_q^b b_q T \sum_u \langle a_q J_q^b b_q^* q \rangle \left| H_{a_1 p}^{ab} \right| \left\langle a_u J_u M_u^b b_u^* q \right\rangle - \langle a_u J_u M_u^b b_u^* q \rangle \\ & \left. \left| S_c^{-1}(\tau) H_{a_1 p}^{ab} S_c(\tau) \right| \left\langle a_q J_q^b b_q^* q \right\rangle \right\} \end{aligned} \quad (17)$$

In this expression,

g_ℓ is the degeneracy of the lower level,

$\frac{1}{g_\ell} \rho_{\ell} = \rho_{VibRot}$ is the density matrix over vibrational and rotational states

ρ_p is the density matrix of the photon field

$n_{q\sigma u}$, $n_{q\sigma \ell}$ are the photon numbers when the system is in the upper (final) and lower (initial) states respectively,

and $\rho_{s\ell}^b$ is the density matrix over vibrational and rotational states of the broadening molecule.

The "a" quantum numbers represent all quantum numbers other than J and M necessary to describe the upper and lower levels of the absorbing molecule. The terms s_f^b and s_u^b represent all quantum numbers necessary to describe the lower and upper levels of the broadening molecule.

The summations in Equation (17) are over states and should be written as

$$\sum_{\ell} \rightarrow \sum_{a_{\ell}, J_{\ell}, M_{\ell}} s_{\ell}^b$$

$$q_{\ell}, \sigma_{\ell}$$

where q_{ℓ} is the initial wavenumber state of the photon and σ_{ℓ} is the polarization state of the photon. A similar expansion can be written for the upper, final state.

Abbreviating the notation, let $\ell = a_{\ell} J_{\ell} M_{\ell}$ and $u = a_u J_u M_u$. Realizing that $H_{a_1 p}^{ab}$ is independent of s_f^b and s_u^b , Equation (17) can be written

$$\begin{aligned} \Gamma_{\ell \rightarrow u} = & \frac{2\pi}{\hbar^2} \left[\sum_{\substack{a_1 J_\ell M_\ell \\ a_u J_u M_u}} \rho_\ell \frac{1}{g_\ell} \sum_{q_u, \sigma_u} \sum_{q_\ell, \sigma_\ell} \rho_p \langle n_{q\sigma\ell} | H_{a_1 p}^{ab} | u n_{q\sigma u} \rangle \sum_{s_u^b s_\ell^b} \delta_{s_\ell^b} \delta_{s_u^b} \right. \\ & \times \left. \int_0^\infty d\tau e^{-i\Delta\omega\tau} \langle u s_u^b n_{q\sigma u} | S_c^{-1}(\tau) H_{a_1 p}^{ab} S_c(\tau) | \ell s_\ell^b n_{q\sigma\ell} \rangle \right] \quad (18) \end{aligned}$$

Reducing the sums for nontrivial matrix elements

$$\begin{aligned} \Gamma_{\ell \rightarrow u} = & \frac{2\pi}{\hbar^2} \text{Re} \left[\sum_{\substack{a_1 J_\ell M_\ell \\ a_u J_u M_u}} \rho_\ell \frac{1}{g_\ell} \sum_{q_\ell, \sigma_\ell} \sum_{q_u, \sigma_u} \rho_p \langle n_{q\sigma\ell} | H_{a_1 p}^{ab} | u n_{q\sigma u} \rangle \sum_{s_u^b} \delta_{s_u^b} \right. \\ & \times \left. \frac{1}{\pi} \int_0^\infty d\tau e^{-i\Delta\omega\tau} \langle u s_u^b n_{q\sigma u} | S_c^{-1}(\tau) H_{a_1 p}^{ab} S_c(\tau) | \ell s_\ell^b n_{q\sigma\ell} \rangle \right]. \quad (19) \end{aligned}$$

The subscripts u and ℓ have been dropped from the S^b since the Kronecker- δ in Equation (18) requires $\ell=u$. By inserting unit operators between the time development operators and the interaction Hamiltonian $H_{a_1 p}^{ab}$ the second matrix element expression in Equation (19) becomes

$$\begin{aligned} \langle u s_u^b n_{q\sigma u} | S_c^{-1}(\tau) H_{a_1 p}^{ab} S_c(\tau) | \ell s_\ell^b n_{q\sigma\ell} \rangle = & \\ & \sum_{u' s_u^b} \langle u s_u^b n_{q\sigma u} | S_c^{-1}(\tau) | u' s_u^b n_{q\sigma u}' \rangle \langle u' s_u^b | H_{a_1 p}^{ab} | \ell s_\ell^b n_{q\sigma\ell}' \rangle \\ & n_{q\sigma u}' \\ & s_u^b n_{q\sigma u}' \\ & \times \langle \ell' s_\ell^b | n_{q\sigma\ell}' | S_c(\tau) | \ell s_\ell^b n_{q\sigma\ell} \rangle \quad (20) \end{aligned}$$

Since $S_c(\tau)$ is independent of the photon field, and $H_{a_1 p}^{ab}$ does not operate on states of the broadening molecule, then $s^{b'} = s^{b''}$, $n_{q\sigma\ell} = n_{q\sigma\ell'}$, and $n'_{q\sigma u} = n_{q\sigma u}$.

The adiabatic assumption [21,22] is now made requiring $u = u'$, $s^b = s^{b'}$, and $\ell = \ell'$. By this approximation, the right hand side of Equation (20) becomes

$$\langle us^b | S_c^{-1}(\tau) | us^b \rangle \langle un_{q\sigma u} | H_{a_1 p}^{ab} | \ell n_{q\sigma\ell} \rangle \langle \ell s^b | S_c(\tau) | \ell s^b \rangle. \quad (21)$$

Substituting this result into Equation (19), the transition rate can be written

$$\begin{aligned} \Gamma_{\ell \rightarrow u} &= \frac{2\pi}{\hbar^2} \sum_{a_\ell, j_\ell} \rho_\ell \frac{1}{g_\ell} \sum_{\substack{M_\ell M_u \\ q_\ell \sigma_\ell}} \sum_{q_u \sigma_u} \rho_p |\langle un_{q\sigma u} | H_{a_1 p}^{ab} | \ell n_{q\sigma\ell} \rangle|^2 \frac{Re}{\pi} \int_0^\infty d\tau e^{-i\Delta\omega\tau} \\ &\times \sum_b \rho_{s^b} \langle us^b | S_c^{-1}(\tau) | us^b \rangle \langle \ell s^b | S_c(\tau) | \ell s^b \rangle. \end{aligned} \quad (22)$$

Assuming binary collisions only, the matrix elements of the time development operator $S_c(\tau)$ can be written

$$\begin{aligned} \langle \ell s^b | S_c(\tau) | \ell s^b \rangle &= \langle \ell s^a | S_{ca_1 a} | \ell s^a \rangle^{n_a-1} \langle \ell s^{b_1} | S_{ca_a b_1} | \ell s^{b_1} \rangle^{n_1} \dots \\ &\dots \langle \ell s^{b_k} | S_{ca_1 b_k} | \ell s^{b_k} \rangle^{n_k}. \end{aligned} \quad (23a)$$

$$\begin{aligned} \langle us^b | S_c^{-1}(\tau) | us^b \rangle &= \langle us^a | S_{ca_1 a}^{-1} | us^a \rangle^{n_a-1} \langle us^{b_1} | S_{ca_a b_1}^{-1} | us^{b_1} \rangle^{n_1} \dots \\ &\dots \langle us^{b_k} | S_{ca_1 b_k}^{-1} | us^{b_k} \rangle^{n_k}. \end{aligned} \quad (23b)$$

In these expressions, the terms similar to $S_{ca_1 b_k}$ represent quantities averaged over impact parameters and summed over collisional events.

The sums over broadening states s^b in Equation (22) can be expanded

$$\begin{aligned} \sum_{s^b} \rho_{s^b} & \langle us^b | S_c^{-1}(\tau) | us^b \rangle \langle \ell s^b | S_c(\tau) | \ell s^b \rangle = \\ & \left[\sum_{s^a} \rho_{s^a} \langle \langle us^a | S_{ca_1 a}^{-1}(\tau) | us^a \rangle \langle \ell s^a | S_{ca_1 a}(\tau) | \ell s^a \rangle \rangle_{R_0, v, t_0} \right]^{n_a} \times \\ & \cdots \times \left[\sum_{s^{b_k}} \rho_{s^{b_k}} \langle \langle us^{b_k} | S_{ca_1 b_k}^{-1}(\tau) | us^{b_k} \rangle \langle \ell s^{b_k} | S_{ca_1 b_k}(\tau) | \ell s^{b_k} \rangle \rangle_{R_0, v, t_0} \right]^{n_{b_k}} \end{aligned} \quad (24)$$

The symbol $\langle \rangle_{R_0, v, t_0}$ indicates the average over impact parameters and velocities and a sum over collision events. It is written mathematically for arbitrary A as

$$\langle A \rangle_{R_0, v, t_0} = \frac{1}{V} 8\pi^{1/2} \left(\frac{\pi}{2kT} \right)^{3/2} \int_0^\infty v^3 dv e^{-(\mu^2/kT)} \int_{R_{\text{Min}}}^\infty R_0 dR_0 \left(\sum_{t_b} A, \right) \quad (25)$$

where V is volume, μ is the reduced mass of the binary system, T is temperature and k is the Boltzmann constant. Also, because $n_a \gg 1$ the approximation $n_a - 1 \approx n_a$ was used in Equation (24).

It is convenient at this point to define

$$\begin{aligned} C_{a_1 a}(\tau) &= \sum_{s^a} \rho_{s^a} \langle \langle us^a | S_{ca_1 a}^{-1}(\tau) | us^a \rangle \langle \ell s^a | S_{ca_1 a}(\tau) | \ell s^a \rangle \rangle_{R_0, v, t_0} \\ &\dots \\ &\dots \\ C_{a_1 b_k}(\tau) &= \sum_{s^{b_k}} \rho_{s^{b_k}} \langle \langle us^{b_k} | S_{ca_1 b_k}^{-1}(\tau) | us^{b_k} \rangle \langle \ell s^{b_k} | S_{ca_1 b_k}(\tau) | \ell s^{b_k} \rangle \rangle_{R_0, v, t_0}. \end{aligned} \quad (26)$$

Then

$$\begin{aligned}
 \sum_b \rho_{sb} & \langle us^b | S_c^{-1}(\tau) | us^b \rangle \langle es^b | S_c(\tau) | es^b \rangle \\
 & = C_{a_1 a}^{n_a}(\tau) C_{a_1 b_1}^{n_1}(\tau) \dots C_{a_1 b_k}^{n_k}(\tau) \\
 & = C(\tau)
 \end{aligned} \tag{27}$$

With this notation, the transition rate can be written

$$\begin{aligned}
 \ell \Gamma_u &= \sum_{a_\ell J_\ell} \rho_\ell \left(\frac{2\pi}{\hbar^2} \frac{1}{g_\ell} \sum_{M_u, M_\ell} \sum_{q_\ell, \sigma_\ell} \rho_p |\langle u n_{q\sigma u} | H_{a_1 p}^{ab} | e n_{q\sigma \ell} \rangle|^2 \right. \\
 &\quad \times \left. \left\{ \text{Re} \frac{1}{\pi} \int_0^\infty d\tau e^{-i\Delta\omega\tau} C(\tau) \right\} \right)
 \end{aligned} \tag{28}$$

For no external perturbations except photon interactions $H_c(t)=0$ and $C(\tau)=1$. Then

$$\text{Re} \frac{1}{\pi} \int_0^\infty d\tau e^{-i\Delta\omega\tau} C(\tau) = \delta(\Delta\omega),$$

and the transition rate as expressed in Equation (28) takes the familiar form of Fermi's Golden Rule.

The right hand side of Equation (28) is the product of two terms. The first term is interpreted as the transition strength, while the second term is an off-resonance amplitude correction to the transition strength. This second term then is the frequency profile of the transition, otherwise referred to as the line shape. We write

$$j_c^R(\Delta\omega) = \frac{1}{\pi} \operatorname{Re} \int_0^\infty d\tau \exp(-i\Delta\omega\tau) C(\tau), \quad (29)$$

where the subscript c refers to the collision broadened line shape.

THE CORRELATION FUNCTION

$C(\tau)$ as defined in Equation (27) is interpreted as the autocorrelation function between the state of the molecular system at time $t=0$ and time $t=\tau$. Just as an interferogram produced by a Michelson interferometer is the autocorrelation function of the incident electric field and is symmetric about the zero retardation point, so the function $C(\tau)$ is symmetric about $\tau=0$. Using this symmetry, Equation (29) can be written

$$\begin{aligned} j_c^R(\Delta\omega) &= \frac{\operatorname{Re}}{2\pi} \int_{-\infty}^{\infty} d\tau \exp(-i\omega_0\tau) \exp(i\omega_0\tau) C(\tau) \\ &= \operatorname{Re} \{ \mathcal{F}^{-1}(\exp(i\omega_0\tau) C(\tau)) \} \end{aligned} \quad (30)$$

That is, the line shape function $j_c^R(\Delta\omega)$ and the function $\exp(i\omega_0\tau) C(\tau)$ are related by the Fourier transform. To generalize the concept further, let $j_c^I(\Delta\omega)$ be the Hilbert transform companion to $j_c^R(\Delta\omega)$.

We define

$$j_c(\Delta\omega) = \mathcal{F}^{-1}(\exp(i\omega_0\tau) C(\tau)) = j_c^R(\Delta\omega) + i j_c^I(\Delta\omega). \quad (31)$$

and $j_c^I(\Delta\omega)$ represents refractive index effects caused by the collision processes. Since the goal of this study is a more thorough understanding of the water vapor absorption line shape, the refractive index terms will be ignored and the superscript R suppressed. Thus

$$j_c(\Delta\omega) = \operatorname{Re} \{ \mathcal{F}^{-1}(\exp(i\omega_0\tau) C(\tau)) \}. \quad (32)$$

This equation indicates that a study of the absorption line shape depends on an understanding of the correlation function $C(\tau)$. An intuitive understanding of the relation between the spectral line shape and the correlation function is shown in Figure 3. Long correlation times τ imply that the binary collision perturbation was weak and did not greatly upset the energy levels of the absorber. Thus, appreciable absorption caused by a transition from the lower energy level to the upper energy level will occur at frequencies ω close to the unperturbed center frequency ω_0 . In the spectrum, the absorption line is narrow.

If, however, the correlation time for the energy levels is short, a strong interaction between absorber and perturber molecule occurred. This can cause the absorber molecule to absorb radiation at frequencies ω which are far from ω_0 . The spectral line appears broad.

Of course, in an experiment all ranges of correlation times are experienced by the ensemble of absorber molecules. The total line shape is a composite resulting from the different ranges of correlation functions.

The Lorentz Line Shape

It is reasonable, but not entirely correct, to assume that the correlation function is a monotonically decreasing function of positive τ . That is, the molecular system tends to become less correlated as time proceeds. If this monotonic decay can be written as a simple exponential of the form

$$C(\tau) = \exp(-\alpha\tau) \quad (33)$$

Then from Equation (32), the line shape becomes

$$j_C(\Delta\omega) = \frac{1}{\pi} \frac{d}{\Delta\omega^2 + \alpha^2} \quad (34)$$

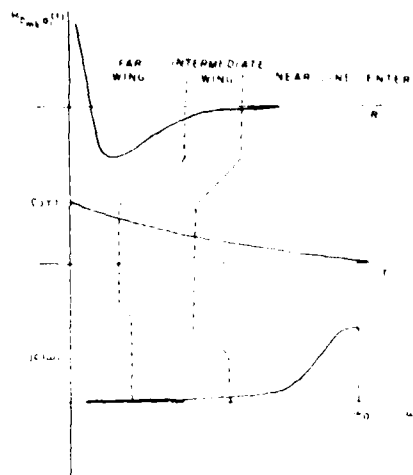


Figure 3. Comparison among the intermolecular potential, the correlation function, and the spectral line shape.

which is the familiar Lorentz line shape with a halfwidth α . The Lorentz line shape is an adequate model for the absorption line profile only when the correlation function can be expressed as an exponentially decaying function. It will be shown later that this assumption can be applied to the water vapor line shape only under certain conditions. For the most part, the profile of water vapor absorption lines is decidedly non-Lorentzian.

Collision Dynamics

For this study, it was decided that the best approach for establishing an absorption line profile was to classify the correlation functions into three general categories corresponding to short, intermediate, and long correlation times. By a previous discussion, this classification divides the absorption line profile into three regimes corresponding to far wing, intermediate, and near line center domains. Figure 4 illustrates the division of the collision dynamics implied by this approach. Trajectories labeled 1 and 2 represent possible collisional

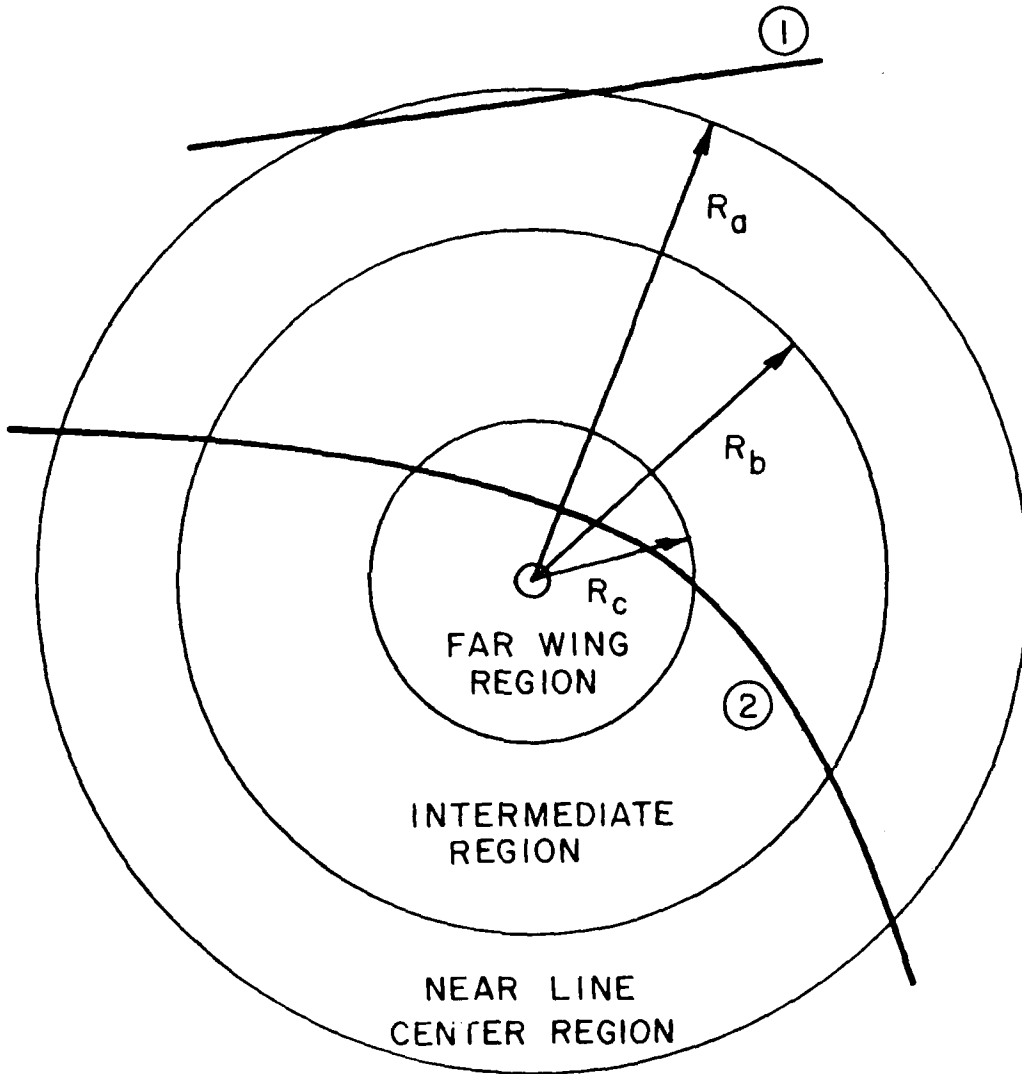


Figure 4. Possible collision trajectories.

paths. Table I lists the general characteristics of collisions in each region. These conditions must be applied to the correlation function in order to extract the proper form of the function to be applied in each region. This division implies

TABLE 1
CHARACTERISTICS OF COLLISION DYNAMICS

$R_F = R_A = R_P$	Very little effect on absorbing projectiles
$R_F < R_A = R_P$	Interrupt broadening near line-center phenomena
1.	short duration of collision
2.	Time between collisions is long compared to duration of collisions
3.	Binary collisions
4.	Total correlation time
$R_F > R_A = R_P$	Intermediate resolution difficult to model
1.	Many body problem
$R_A > R_F = R_P$	Statistical problems - star wings
1.	Binary collision
2.	Duration of collision
3.	short correlation time

$$\begin{aligned}
 j_C(\Delta\omega) &= \text{Re}\{\mathcal{F}^{-1}(\exp(i\omega_0\tau)C_{FW}(\tau)) + \mathcal{F}^{-1}(\exp(i\omega_0\tau)C_{IW}(\tau)) \\
 &\quad + \mathcal{F}^{-1}(\exp(i\omega_0\tau)C_{NLC}(\tau))\} \\
 &= j_{cFW}(\Delta\omega) + j_{cIW}(\Delta\omega) + j_{cNLC}(\Delta\omega). \tag{35}
 \end{aligned}$$

The term $j_{cFW}(\Delta\omega)$ describes the far wing collision line shape and is derived from correlation functions with short correlation times. The contributions to be near-line-center shape, $j_{cNLC}(\Delta\omega)$, come from all collisional processes, but are dominated by correlation functions with long correlation times. The intermediate wing region $j_{cIW}(\Delta\omega)$ represents a transition region where correlation functions with both long and short correlation times compete equally. Rather than solving for the line shape function in this region, boundary conditions that the total line shape function and the derivative of the function must be continuous across the domains will be applied.

Solutions to the near-line-center problem and the far wing problem can be formulated. The intermediate-wing region, however, is not solvable by direct methods.

The collision Hamiltonians for H₂O-H₂O and H₂O-broadener binary interactions become

$$\begin{aligned} H_{aa_1} &= \frac{\mu_1^2 f}{R^3(t)} + \frac{\mu_1 \bar{Q}_1 g_1 + \mu_1 \bar{Q}_1 g_2}{R^4(t)} + \dots \text{Rot} \\ &\quad - \frac{2\mu_1^2 \bar{\alpha}_1 + \frac{1}{2}\bar{\alpha}_1 e^2 \langle r_1^2 \rangle}{R^6(t)} + \dots \end{aligned} \quad (36a)$$

$$H_{ba_1} = \frac{\mu_1 \bar{Q}_2 g}{R^4(t)} + \dots \text{Rot} - \frac{2\mu_1 \bar{\alpha}_2 + \frac{1}{2}\bar{\alpha}_1 e^2 \langle r_2^2 \rangle}{R^6(t)} \quad (36b)$$

The terms have been described earlier and the subscripts 1 and 2 represent water vapor and broadener molecule, respectively.

The short collision times characteristic of interruption broadening in Table I allow the approximation of Equation (14) to be made for the near line center problem. Retaining only the leading terms in each Hamiltonian above is equivalent to assuming that the H₂O-H₂O interaction is a dipole-dipole interaction, while the H₂O-N₂ interaction is a dipole-quadrupole interaction. The limiting case of weak collisions can be modeled with the Hamiltonians.

$$H_{aa_1} = \frac{\mu_1^2 f}{R^3(t)} \quad (37a)$$

$$H_{ba_1} = \frac{\mu_1 \bar{Q}_2}{R^4(t)} g \quad (37b)$$

Strong collisions which contribute to the far wings of absorption lines may or may not require evaluation of the rotational average in Equations (36a) and (36b). The importance of the rotational average can be evaluated by examining the collision time and the rotational time for the molecules. Choosing the broadening molecules to be N_2 , an estimate for the collision duration can be made, based on the average thermal velocities and impact parameters of strong collisions for both H_2O-H_2O and H_2O-N_2 binary collisions. The results show the collision duration to be

$$t_d = \frac{2R_0}{v} \left\{ \begin{array}{ll} 10^{-2} \text{ sec} & H_2O-H_2O \\ 10^{-13}-10^{-12} \text{ sec.} & H_2O-N_2. \end{array} \right.$$

Using a rigid rotor picture of the molecules, typical rotation periods for the N_2 molecule are between 10^{-10} and 10^{-11} sec, while for the H_2O molecule the rotation periods are between 10^{-11} and 10^{-13} sec. These values can be derived from a purely classical view of the molecule using angular momentum values which are derived from representative values of the J quantum number ($J \leq 5$ to 20).

Since the collision times for H_2O-N_2 are for the most part short compared to the rotational period of the N_2 molecule, a "snapshot" view of the interaction can be adopted. That is the N_2 broadener molecule does not rotate significantly during the interaction and therefore the rotational average is not performed. Similar results are derived when considering H_2O-O_2 collisions. However, for H_2O-H_2O collisions,

the colliding molecule can rotate many times during the collision, making the rotational average important. For far wing absorption line shapes, the binary interaction Hamiltonians become

$$H_{aa_1} \approx \frac{\frac{2}{\mu_1^2}}{R^3(t)} f_{Rot} - \frac{2\mu_1^2 \bar{\alpha}_1 + \bar{\alpha}_1 e^2 \langle r_2^2 \rangle}{R^6(t)} \quad (38a)$$

$$H_{ba_1} = \frac{\mu_1 \bar{Q}_2}{R^4(t)} \quad (38b)$$

The average over rotation as defined in Equation (13) can be performed by recognizing the analogy between this and orientation polarizability calculations [23].

$$\langle \frac{\mu_1^2}{R^3(t)} f \rangle_{Rot} = \frac{\mu_1^2}{R^3(t)} - L(x) \quad (39)$$

where $L(x)$ is the Langevin function and $x = 2\mu_1^2/[kT R^3(t)]$, where T is temperature. Figure 5 shows a plot of this function. If x is small, $L(x) \approx x/3$, and the rotational average becomes

$$\langle \frac{\mu_1^2}{R^3(t)} f \rangle_{Rot} = \frac{2\mu_1^4}{3kT} \frac{1}{R^6(t)}, \quad (40)$$

which is similar to results given by Eisenberg and Kauzmann [19].

The next term in the expansion of $L(x)$ is of order x^3 . This produces a term in the Hamiltonian of order $R^{-12}(t)$. Terms of this order become important during very close collisions, but their influence drops rapidly as $R(t)$ increases. For this study, such terms are not being considered.

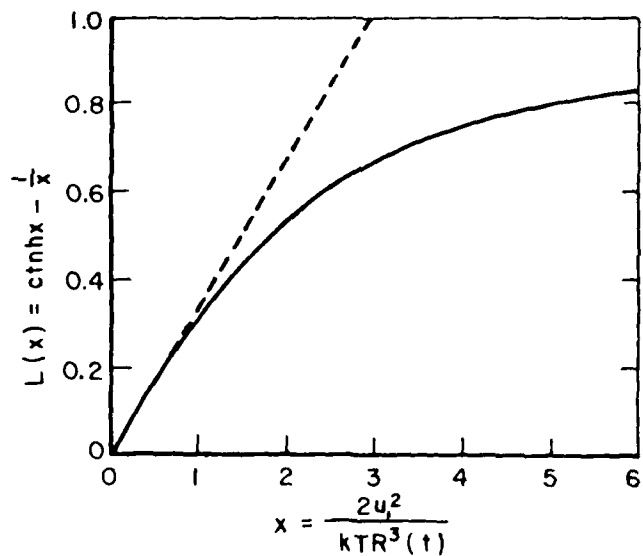


Figure 5. Langevin function.

Thus, from Equation (38a), the self-broadening influence in the far wings of water vapor absorption lines is controlled to first order by a $R^{-6}(t)$ potential. This differs from the self-broadened nature of the near-line-center Hamiltonian which varied as $R^{-3}(t)$ for large $R(t)$. The foreign-broadening potentials for near-line-center and far wing cases both vary as $R^{-4}(t)$.

Interruption Broadening

Table I lists the conditions for interruption or impact broadening.

These conditions can be applied to a general correlation function $C_{a_1 b}(\tau)$ as defined in Equation (26). Because interaction time is brief under this assumption, the correlation function can be re-examined after a small change in time.

$$C_{a_1 b}(\tau + d\tau) = \sum_s \rho_s^b \langle \langle u s^b | S_{ca_1 b}^{-1}(\tau + d\tau) | u s^b \rangle \rangle \langle \langle \ell s^b | S_{ca_1 b}(\tau + d\tau) | \ell s^b \rangle \rangle_{R_0, v, t_0} \quad (41)$$

The time-development operator $S_{ca_1 b}(\tau + d\tau)$ can be written as a time development operator which evolves the system to time τ operated on by a time-development operator which evolves the system from time τ to $\tau + d\tau$. That is

$$S_{ca_1 b}(\tau + d\tau) = S_{ca_1 b}(\tau \rightarrow \tau + d\tau) S_{ca_1 b}(\tau) \quad (42)$$

With this, Equation (41) becomes

$$\begin{aligned} C_{a_1 b}(\tau + d\tau) &= \sum_s \rho_s^b \langle \langle u s^b | S_{ca_1 b}^{-1}(\tau \rightarrow \tau + d\tau) | u s^b \rangle \rangle \langle \langle \ell s^b | S_{ca_1 b}(\tau \rightarrow \tau + d\tau) | \ell s^b \rangle \rangle_{R_0, v, t_0} \\ &\times \langle \langle u s^b | S_{ca_1 b}^{-1}(\tau) | u s^b \rangle \rangle \langle \langle \ell s^b | S_{ca_1 b}(\tau) | \ell s^b \rangle \rangle_{R_0, v, t_0}. \end{aligned} \quad (43)$$

To obtain separate averages, it was assumed that events at time τ and time $\tau+d\tau$ are independent [21]. Within the limits of the impact approximation, the second average is independent of the sum over quantum numbers of the broadening molecule and in fact is equal to the correlation function $C_{a_1 b}(\tau)$ at time τ . Thus, Equation (43) can be written

$$C_{a_1 b}(\tau+d\tau) = C_{a_1 b}(\tau)\phi(\tau+\tau+d\tau) \quad (44)$$

where the function $\phi(\tau+\tau+d\tau)$ simplifies the notation of the remaining terms in Equation (43), and is dependent only on $d\tau$. A solution to Equation (44) can be written

$$C_{a_1 b}(\tau) = C_{a_1 b}(0)\exp(-\gamma_{a_1 b}\tau) \quad (45)$$

where $\gamma_{a_1 b}$ can be shown to be

$$\gamma_{a_1 b} = \left\langle 1 - \sum_s \rho_s b \langle us^b | S_{ca_1 b}^{-1}(\tau+\tau+d\tau) | us^b \rangle \langle ls^b | S_{ca_1 b}(\tau+\tau+d\tau) | ls^b \rangle \right\rangle R_0 v \quad (46)$$

The initial condition $C_{a_1 b}(0) = 1$ can be applied, and the total correlation function for a binary mixture can be written by Equation (27) as

$$\begin{aligned} C(\tau) &= C_{a_1 a}^{n_a}(\tau) C_{a_1 b}^{n_b}(\tau) \\ &= \exp(-n_a \gamma_{a_1 a} \tau) \exp(-n_b \gamma_{a_1 b} \tau) \end{aligned} \quad (47)$$

Since $\gamma_{a_1 a}$ and $\gamma_{a_1 b}$ are quantities averaged by the process described in Equation (25), the $1/V$ factor can be brought out explicitly to write

$$C(\tau) = \exp[-(\rho_a \gamma_{a_1 a} + \rho_b \gamma_{a_1 b})\tau] \quad (48)$$

where ρ_a and ρ_b are the molecular number densities of the absorber and perturber gases respectively. By using this correlation function in Equation (30), the interruption broadened line shape is

$$j_{CNLC}(\Delta\omega) = \frac{1}{\pi} \frac{\alpha^R}{(\Delta\omega + \alpha^I)^2 + (\alpha^R)^2} \quad (49)$$

where α^R is the real part of $\rho_a \gamma_{a_1 a} + \rho_b \gamma_{a_1 b}$ and α^I is the imaginary part of the same function. Thus, the function which describes the near line center profile is the Lorentz line shape. The term α^I represents a line shift caused by the impact approximation collisions, while α^R represents the halfwidth of the absorption time.

The derivation of Equation (49) for the long correlation times implied by the impact approximation did not explicitly depend on the functional forms of the self-broadened and foreign-broadened interaction Hamiltonians written in Equations (37a) and (37b). Instead, these interaction potentials influence the nature of $\gamma_{a_1 a}$ and $\gamma_{a_1 b}$ respectively within the derived line shape.

The pressure dependence of the line width and line shift terms in Equation (49) are already apparent since the molecular number densities ρ_a and ρ_b are proportional to pressure by the ideal gas law.

$$\begin{aligned}\alpha^R &= A_1 p_a + A_2 p_b \\ \alpha^I &= B_1 p_a + B_2 p_b\end{aligned}\quad (50)$$

where A_1 , A_2 , B_1 , and B_2 are constants related to $\gamma_{a_1 a}$ and $\gamma_{a_1 b}$, p_a is the partial pressure of the absorber and p_b is the partial pressure of the broadener.

The temperature dependences of the line width and line shift are more difficult to derive. Here, the explicit forms for the interaction Hamiltonians in Equations (37a) and (37b) become important. A second order perturbation expansion of the $\gamma_{a_1 a}$ and $\gamma_{a_1 b}$ [20,21] yields a temperature dependence of the form

$$\alpha \propto \frac{1}{T} . \quad (51)$$

However, this is not always observed [24,25].

The approach which has been adopted here is the phase shift method [26,27], which consists of only phase modulation of the eigenstates, but to all orders. This approach leads to a temperature dependence for the line width of

$$\alpha \propto \frac{1}{T} \quad (52)$$

for the dipole-dipole interactions modeling self-broadening

$$\alpha = -\frac{1}{T^{0.83}} \quad (53)$$

for dipole-quadrupole or foreign-broadening.

Statistical Broadening

Statistical broadening is characterized by short correlation functions caused by strong binary interactions. These interactions contribute to the far wing absorption of a spectral line profile. No perturbation method can be applied. However, the phase shift contributions are solvable. In addition, corrections will be included to account for energy level shifts. The time-development operator $S_{ca_1b}(\tau)$ can be written

$$S_{ca_1b}(\tau) = \exp(-in(\tau)) \quad (54)$$

where

$$n(\tau) = \frac{1}{\hbar} \int_{t_0}^{t_0 + \tau} dt H_{a_1b}(t) \quad (55)$$

and

$$H_{a_1b}(t) = V_j / (R(t))^{m_j}. \quad (56)$$

The parameter m_j is the power of the exponent in the Hamiltonians of Equations (38a) and (38b). For H_2O-H_2O interactions $m_j=6$, while for H_2O-N_2 or H_2O-O_2 , $m_j = 4$. The correlation function initially written in Equation (26) can now be expressed

$$C_{a_1b}^{n_b}(\tau) = \left[\sum_{s^b} \rho_{s^b} \langle \langle u s^b | \exp(i n(\tau)) | u s^b \rangle \langle \langle l s^b | \exp(-i n(\tau)) | l s^b \rangle \rangle_{R_0, v, t_0} \right]^{n_b} \quad (57)$$

This can be written

$$C_{a_1b}^{n_b}(\tau) = \left[\frac{1 + \rho_b}{s^b} \sum_{s^b} \rho_{s^b} \langle \langle u s^b | \exp(i n(\tau)) | u s^b \rangle \langle \langle l s^b | \exp(-i n(\tau)) | l s^b \rangle \rangle_{R_0, v, t_0}^{-1} \right]^{n_b}$$

where $\langle \langle \dots \rangle \rangle_{R_0, v, t_0} = \frac{1}{V} \langle \langle \dots \rangle \rangle_{R_0, v, t_0}$ and $\rho_b = n_b/V$. The fact that n_b is very large permits the correlation function to be written [28]

$$C_{a_1b}^{n_b}(\tau) = \exp \left[-\rho_b \sum_{s^b} \rho_{s^b} \langle \langle 1 - u s^b | \exp(i n(\tau)) | u s^b \rangle \langle \langle l s^b | \exp(-i n(\tau)) | l s^b \rangle \rangle_{R_0, v, t_0}^{-1} \right] \quad (59)$$

The matrix elements in Equation (59) can be manipulated to yield the form

$$\begin{aligned} & \langle us^b | e^{in} | us^b \rangle \langle \ell s^b | e^{-in} | \ell s^b \rangle \\ & e^{in_u - n_\ell} + e^{in_u} \Omega_\ell + e^{-in_\ell} \Omega_u + \Omega_u \Omega_\ell \end{aligned} \quad (60)$$

where

$$\eta_u = \langle us^b | n | us^b \rangle,$$

$$\eta_\ell = \langle \ell s^b | n | \ell s^b \rangle,$$

$$\begin{aligned} \Omega_u &= \sum_{n=2}^{\infty} \frac{(-i)^n}{n!} \sum'_{\ell' s^b} \langle us^b | n | u' s^b \rangle \dots \langle u^{(n-1)} s^{b(n-1)} | n | us^b \rangle, \\ &\quad \cdot \\ &\quad \cdot \\ &\quad \cdot \\ &\quad \ell^{(n-1)} s^{b(n-1)} \end{aligned}$$

and

$$\begin{aligned} \Omega_\ell &= \sum_{n=2}^{\infty} \frac{(-i)^n}{n!} \sum'_{\ell' s^b} \langle \ell s^b | n | \ell' s^b \rangle \dots \langle \ell^{(n-1)} s^{b(n-1)} | n | \ell s^b \rangle. \\ &\quad \cdot \\ &\quad \cdot \\ &\quad \cdot \\ &\quad \ell^{(n-1)} s^{b(n-1)} \end{aligned}$$

The prime on the summation sign indicates that all the indices can not be equal. The Ω 's are the level shift terms and have no closed form expression. Let,

$$f_b(\tau) = e^{in_u} \Omega_\ell + e^{-in_\ell} \Omega_u + \Omega_u \Omega_\ell. \quad (61)$$

Now the correlation function becomes

$$C_{a_1 b}^{n_b}(\tau) = \exp(-\rho_b \sum_s s^b s^b \langle 1 - e^{i(n_u - n_\ell)} \rangle'_{R_o, v, t_o} + \langle f_b(\tau) \rangle'_{R_o, v, t_o}) \quad (62)$$

The phase shift term $\langle 1 - e^{i(n_u - n_\ell)} \rangle'_{R_o, v, t_o}$ can be solved. The major contribution to the phase term comes in the region $t_o < R_o/v$ [29] where v is the velocity of the colliding molecule. The sum over t_o implied by the bracket in Equation (62) as defined in Equation (25) is converted to an integral which gives its major contribution between $-R_o/v$ and R_o/v . In this region

$$n_x = \frac{\langle x s^b | v_j | x s^b \rangle}{\hbar R_o^{m_j}} \frac{\Gamma(m_j - 1)}{\left[\Gamma\left(\frac{m_j}{2}\right) \right]^2} \left(2^{-m_j}\right)^t \quad m_j - \text{even} \quad (63)$$

where x represents the subscripts ℓ and u . The integral over t_o gives

$$\begin{aligned} \langle 1 - e^{i(n_u - n_\ell)} \rangle'_{R_o, v, t_o} &= \left\langle \int_{-R_o}^{R_o/v} dt_o (1 - e^{i(n_u - n_\ell)}) \right\rangle'_{R_o, v} \\ \text{or} \quad \langle 1 - e^{i(n_u - n_\ell)} \rangle'_{R_o, v, t_o} &= \left\langle \frac{2R_o}{v} (1 - e^{i(n_u - n_\ell)}) \right\rangle'_{R_o, v}. \end{aligned} \quad (64)$$

Evaluating the real and imaginary parts separately we have

$$\begin{aligned} \frac{2R_o}{v} (1 - \cos(n_u - n_\ell))'_{R_o, v} &= \\ \frac{4\pi}{m_j} \left(\frac{\tau}{\hbar}\right)^{3/m_j} (v_{ju} - v_{j\ell})^{3/m_j} \xi_j^{3/m_j} \Gamma\left(-\frac{3}{m_j}\right) \cos \frac{3\pi}{2m_j} &\quad m_j - \text{even} \end{aligned} \quad (65)$$

where

$$v_{ju} = \langle us^b | v_j | us^b \rangle$$

$$v_{jl} = \langle \ell s^b | v_j | \ell s^b \rangle$$

$$\xi_j = \frac{\Gamma(m_j - 1) 2^{s-m_j}}{\left[\Gamma\left(\frac{m_j}{2}\right) \right]^2}$$

Similarly for the line shift term

$$\begin{aligned} & \left\langle \frac{2R_0}{v} \sin(\eta_u - \eta_\ell) \right\rangle_{R_0, v} = \\ & \frac{4\pi}{m_j} \left(\frac{\tau}{\hbar} \right)^{3/m_j} (v_{ju} - v_{jl})^{3/m_j} \xi_j^{3/m_j} \Gamma(-3/m_j) \sin\left(\frac{3\pi}{2m_j}\right) m_j\text{-even} \end{aligned} \quad (66)$$

The general correlation function from Equation (62) can now be written,

$$C_{a_1 b}^{n_b}(\tau) = \exp \left[-\rho_b \sum_s \rho_{sb} \left\{ (\gamma_j + i\varepsilon) \tau^{3/m_j} + \langle f_b(\tau) \rangle_{R_0, v, t_0} \right\} \right] \quad (67)$$

Separating real and imaginary terms in the exponent,

$$\begin{aligned} C_{a_1 b}^{n_b}(\tau) &= \exp \left[-\rho_b \sum_s \rho_{sb} \gamma_j \tau^{3/m_j} + \operatorname{Re}[\langle f_b(\tau) \rangle_{R_0, v, t_0}] \right] \times \\ &\exp \left[-i \left\{ \rho_b \sum_s \rho_{sb} \varepsilon \tau^{3/m_j} - \operatorname{Im}[\langle f_b(\tau) \rangle_{R_0, v, t_0}] \right\} \right]. \end{aligned} \quad (68)$$

When a correlation function of this form is substituted into Equation (32), the expression in the second exponential combines with the ω_0

to produce a line shift term in the final line shape $j_c(\Delta\omega)$. It is the amplitude of the correlation function which yields the line profile

$$|C_{a_1 b}(\tau)| = \exp[-\lambda_{bj} g_{bj}(\tau) \tau^{3/m_j}] \quad (69)$$

where the substitutions

$$\lambda_{bj} = \rho_b \sum_s \rho_b \gamma_j \quad (70a)$$

$$g_{bj}(\tau) = 1 + \frac{\text{Re}[\langle f_b(\tau) \rangle_{R_0, v.t_0}]}{\gamma_j \tau^{3/m_j}} \quad (70b)$$

were made.

The general correlation function for a binary mixture is then

$$C_{FW}(\tau) = \exp[-\lambda_{bj} g_{bj}(\tau) \tau^{3/m_j}] \exp[-\lambda_{ak} g_{ak}(\tau) \tau^{3/m_j}] \quad (71)$$

and the far wing line shape is

$$j_{cFW}(\Delta\omega) = \frac{1}{\pi} \text{Re} \left\{ \int_0^\infty d\tau \exp[-i\Delta\omega\tau] C_{FW}(\tau) \right\} \quad (72)$$

An asymptotic expansion of the exponentials in Equation (71) yields

$$C_{FW}(\tau) = \sum_{s=0}^{\infty} \sum_{t=0}^{\infty} \frac{(-\lambda_{ak} g_{ak}(\lambda) \lambda)^{3/m_k s}}{s!} \frac{(-\lambda_{bj} g_{bj}(\tau) \tau^{3/m_j})^t}{t!} \quad (73)$$

This yields a far wing line shape which is written as

$$j_{CFW}(\Delta\omega) = \frac{1}{\pi} \operatorname{Re} \left\{ \sum_{s=0}^{\infty} \sum_{t=0}^{\infty} \frac{\lambda_{ak}^s}{s!} \frac{\lambda_{bj}^t}{t!} \int_0^{\infty} d\tau [\exp -i\Delta\omega\tau] [-g_{ak}(\tau)\tau^{3/m_k}]^s [-g_{bj}(\tau)\tau^{3/m_j}]^t \right\} \quad (74)$$

Making the substitution $\theta = \Delta\omega\tau$, the far wing line shape becomes

$$j_{CFW}(\Delta\omega) = \frac{1}{\omega} \left\{ \sum_{s=0}^{\infty} \sum_{t=0}^{\infty} \frac{\lambda_{ak}^s}{s!} \frac{\lambda_{bj}^t}{t!} \frac{1}{|\Delta\omega|^{1+3s/m_j + 3t/m_j}} \times \operatorname{Re} \left[\int_0^{\infty} d\theta \exp(-i\theta) \left[-g_{ak}\left(\frac{\theta}{\Delta\omega}\right) \right]^s \left[-g_{bj}\left(\frac{\theta}{\Delta\omega}\right) \right]^t \theta^{3s/m_k + 3t/m_j} \right] \right\} \quad (75)$$

The leading terms in this expression occur for $s=1$, $t=0$ and for $s=0$, $t=1$ since the single term where both s and t are zero is zero. These two leading terms have the physical interpretation of being the self-broadened and foreign-broadened contributions to the far wing line shape. If we retain only these leading terms,

$$j_{CFW}(\Delta\omega) = \frac{1}{\pi} \frac{\lambda_{ak}}{|\Delta\omega|^{1+3/m_k}} \operatorname{Re} \left[\int_0^{\infty} d\theta \exp(-i\theta) \left[-g_{ak}\left(\frac{\theta}{\Delta\omega}\right) \right] \theta^{3/m_k} \right] + \frac{\lambda_{bj}}{|\Delta\omega|^{1+3/m_j}} \operatorname{Re} \left[\int_0^{\infty} d\theta \exp(-i\theta) \left[-g_{bj}\left(\frac{\theta}{\Delta\omega}\right) \right] \theta^{3/m_j} \right] \quad (76)$$

Evaluation of the integrals requires substitution of Equations (61) and (70b). In general, it can be argued that the resulting functions will be different when $m_k \neq m_j$.

The far wing line shape can be written

$$j_{CFW}(\Delta\omega) = \frac{1}{\pi} \left\{ \frac{\lambda_{ak}}{|\Delta\omega|^{1+3/m_k}} T_{m_k}(m_k, \Delta\omega) + \frac{\lambda_{bj}}{|\Delta\omega|^{1+3/m_j}} T_{m_j}(m_j, \Delta\omega) \right\} \quad (77)$$

where $m_k=6$ for self-broadening and $m_j=4$ for foreign-broadening by N_2 or O_2 .

The statistical line shape represented by Equation (77) is similar to the results presented by Fomin and Tvorogov [30]. In their development, the term

$$\frac{1}{|\Delta\omega|^{1+3/m}}$$

is multiplied by an exponential factor which is proportional to

$$\{\exp(-|\Delta\omega|^{\frac{m-1}{m}})\}^{2/3}.$$

For self-broadening, this factor in their line shape becomes $\exp(|\Delta\omega|^{0.56})$, while for foreign-broadening this factor is $\exp(|\Delta\omega|^{0.50})$. These factors are expected to be present in the T -functions of Equation (77).

The p-function

In the previous two sections, interruption broadening and statistical broadening were presented. The total line shape is constructed by combining these two resulting line shapes. We have chosen to do this by the application of band-pass and band-stop filter functions to the two derived line shapes. The total line shape is written

$$j_c(\Delta\nu) = N j_{CNLC}(\Delta\nu)p(\nu) + j_{CFW}(\Delta\nu)(1-p(\nu)) \quad (78)$$

where we have made a change of variable from frequency ω (measured in radian/sec) to frequency ν (measured in cm^{-1}). The normalization constant N assures that Equation (2) is satisfied. The function $p(\nu)$ is a normalized band-pass filter function centered at ν_0 . Guidelines for choosing a suitable p -function are given in Table 2.

Based on these guidelines, the p -function was chosen to be

$$P(\nu) = \begin{cases} \frac{1}{2} + \frac{1}{2} \cos\left(\frac{\pi}{5} |\Delta\nu|\right) & |\Delta\nu| < 5 \text{ cm}^{-1} \\ 0 & |\Delta\nu| \geq 5 \text{ cm}^{-1} \end{cases} \quad (79)$$

which is shown in Figure 6.

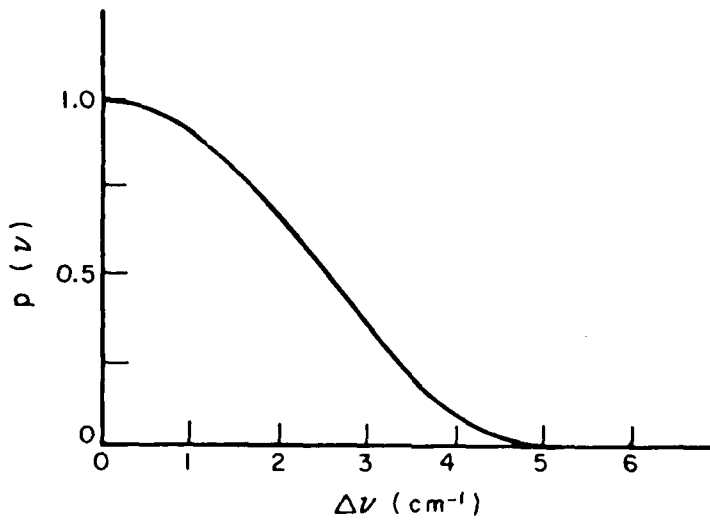


Figure 6. $p(\nu)$ versus $\Delta\nu$

TABLE 2

1. The p-function must be equal to 1 at $\nu = \nu_0$.
2. The p-function must be zero for all ν greater than a cut-off frequency ν_a .
3. The p-function must be a monotonically decreasing function in the region $\nu_0 \leq \nu \leq \nu_a$.
4. The p-function must be symmetric about ν_0 .
5. The derivative of the p-function must be zero at ν_0 and at $\nu = \nu_a$.
6. It is desirable for the total line shape as expressed by Equation (78) to be easily integrated to evaluate the normalization constant N.

The cut-off at 5 cm^{-1} from the line center was chosen so that the p-function would remain essentially unity within several halfwidths of the water vapor line center. This allows interruption broadening to dominate near line center. The stop-band filter function ($1-p(\nu)$) allows the statistical line shape to dominate beyond 5 cm^{-1} (50 to 100 halfwidths from line center).

The region where $p(\nu)$ and $1-p(\nu)$ are approximately equivalent is the intermediate wing region. This method permits a smooth blending of the interruption broadened and statistical broadened line shapes, eliminates the necessity for solving or approximating the interpolation problem.

The choice of the p-function and the exact choice of cut-off frequency are very important to the study of the water vapor

continuum problem in the infrared. The reason for this is that the continuum absorption is theorized here to be caused by the overlap of the far wings of the strong water vapor absorption lines. The intermediate wing region and near-line-center region enter the problem only indirectly in that they must be known to normalize the total line shape function properly. Furthermore, the p-function formalism permits the blending of the different pressure and temperature dependences of the interruption broadened and statistical broadened line shapes as will be seen later [15].

CONCLUDING REMARKS

A total line shape, valid for water vapor absorption lines throughout the infrared has been derived by proper consideration of both impact and statistical collisional processes. Self-broadening is assumed to occur through the electric dipole-dipole interaction, while foreign-broadening is assumed to occur through the electric dipole-quadrupole interaction. Thus, the derived shape is suited for atmospheric (N_2 or O_2) broadening of H_2O absorption lines.

Several approximations were made in the process of deriving a proper infrared line shape for H_2O molecules. Fundamentally, the binary collision approximation and the adiabatic approximation for the energy levels in the absorber molecule restrict the temperature and pressure regimes over which this spectral line shape might be valid.

In the next section, implementation of the total line shape will be discussed, and the ability of this line shape to predict continuum absorption in the 8-12 μm and in the 3-4 μm atmospheric transmittance windows will be discussed.

REFERENCES

- 1 K. Bignell, F. Saiedy, and P.A. Sheppard, J. Opt. Soc. America 53, 466 (1963).
- 2 D.E. Burch, Aeronutronic Publication No. U-4784, "Semi-Annual Technical Report", Air Force Cambridge Research Laboratories, Contract No. F19628-69-C-0263, January 1970.
- 3 J.H. McCoy, D.B. Rensch, and R.K. Long, Appl. Opt. 8, 1471 (1969).
- 4 R.J. Nordstrom, M.E. Thomas, J.C. Peterson, E.K. Damon, and R.K. Long, Appl. Opt. 17, 2724 (1978).
- 5 J.C. Peterson, M.E. Thomas, R.J. Nordstrom, E.K. Damon, and R.K. Long, Appl. Opt. 18, 834 (1979).
- 6 W.R. Watkins, K.O. White, L.R. Bower, B.Z. Sojka, "Pressure Dependence of the Water Vapor Continuum Absorption in the 3.5 to 4.0 Micrometer Region," U.S. Army Electronics Research and Development Command, Report No. ASL-TR-0017, September 1978.
- 7 F.S. Mills, "Absorption of Deuterium Fluoride Laser Radiation by the Atmosphere," Ph.D. Dissertation, The Ohio State University, June 1978.
- 8 J.C. Peterson, "A Study of Water Vapor Absorption at CO₂ Laser Frequencies Using a Differential Spectrophone and White Cell," Ph.D. Dissertation, The Ohio State University, June 1978.
- 9 V.N. Aref'ev and V.I. Dianov-Klokov, Opt. Spectrosc. 42, 488 (1977).
- 10 P.S. Varanasi, S. Chou, and S.S. Penner, J. Quant. Spectrosc. Radiat. Transfer, 8, 1537 (1968).
- 11 Suck, S.H., J.L. Kassner, Jr., and Y. Yamaguchi, Appl. Opt. 18, 2609 (1979).
- 12 H.R. Carlon, "Final Report: Infrared Absorption by Water Clusters," Chemical Systems Laboratory, Report No. ARCSL-TR-79013, March 1979.
- 13 R.E. Roberts, J.A. Selby, and L.M. Biberman, Appl. Opt. 15, 2085, (1976).
- 14 G.P. Montgomery, Jr., Appl. Opt., 17, 2299 (1978).
- 15 M.E. Thomas and R.J. Nordstrom, "A Synergistic Investigation of the Infrared Water Vapor Continuum: Section III," Report 784701-7, April 1981, The Ohio State University ElectroScience Laboratory, Department of Electrical Engineering; prepared under Contract DAAG29-77-C-0010 for U.S. Army Research Office.

- 16 G. Baym, Lectures on Quantum Mechanics, W.A. Benjamin, Inc. (1977).
- 17 Thomas, M.E., "Tropospheric Water Vapor Absorption in the Infrared Window Regions," Report 784701-5, August 1979, The Ohio State University ElectroScience Laboratory, Department of Electrical Engineering; prepared under Contract DAAG-29-77-C-0010 for U.S. Army Research Office.
- 18 H. Mergenau and N.R. Kestner, Theory of Intermolecular Forces, Pergamon Press, (1969).
- 19 D. Eisenberg and W. Kauzmann, The Structure and Properties of Water, Oxford University Press, (1969).
- 20 P.W. Anderson, Phys. Rev. 76, 647, (1949).
- 21 C.J. Tsao and B. Curnette, J. Quant. Spectrosc. Radiat. Transfer 2, 41, (1962).
- 22 M. Barranger, Atomic and Molecular Processes, Academic Press, (1962), D.R. Bates Editor, Chapter 13.
- 23 C. Kittel, Introduction to Solid State Physics, John Wiley and Sons, 4th Edition, (1971).
- 24 E.M. Deutchman and R.F. Calfee, "Two Computer Programs to Produce Theoretical Absorption Spectra of Water Vapor and Carbon Dioxide," AD816 369, April 1967.
- 25 P. Varanasi and F.K. Ko, "Intensity Measurements in the $2 \mu\text{m}$ CO_2 Bands at Low Temperatures," presented at Thirty Third Symposium on Molecular Spectroscopy, The Ohio State University, 1978.
- 26 M. Mizushima, Phys. Rev. 83, 1061, (1951).
- 27 H.M. Foley, Phys. Rev. 69, 616, (1946).
- 28 M. Abramowitz and I.A. Stegun, Handbook of Mathematical Functions, National Bureau of Standards, App. Math Series No. 55.
- 29 C.V. Heer, Statistical Mechanic, Kinetic Theory, and Stochastic Processes. Academic Press, 1972, Chapter 11.
- 30 Fomin, V.V. and Tvorogov, S.D., Appl. Opt. 12, 584 (1973).

Part II: Implementation of the Line Shape

INTRODUCTION

In the preceding paper we developed an expression for the pressure-broadened absorption line shape of H₂O molecules. Only binary collisions were assumed, and both self-broadening and foreign-broadening with N₂ were included. The spectral line shape was developed by first considering the time evolution of the correlation function of the energy levels of the colliding molecules. Collisions were categorized by their severity: weak collisions contributed only to the near-line-center of the spectral profile, while strong collisions contributed to the line shape everywhere including the far wings. The study of H₂O continuum absorption must include a study of the accumulation of these far wings.

Statistical broadening [1] was used in our development to formulate the far wing component to the spectral line shape. Recently, another line shape development used only the impact approximation, modified to account for variations in collision duration [2]. It is not clear at this time whether there is any significant difference in the line shapes produced by these two separate approaches.

In this paper we demonstrate how the spectral line profile, defined by Equations (49), (77), and (78) in the preceding paper, is implemented. Furthermore, comparison between experimental absorption data and the absorption predicted by this line shape is given. We will show that a line shape formulation is adequate to predict all of the behaviors of water vapor continuum absorption over the ranges of pressure and temperature of atmospheric interest. Data will be shown for the 8-14 μm and 3.5-4 μm atmospheric transmission windows.

HISTORICAL PERSPECTIVE

Figure 1 demonstrates the inability of the Lorentz line shape to model the observed pressure dependence of water vapor continuum absorption near 10 μm for H_2O samples pressure broadened to 1 atm with N_2 . The data were recorded using a frequency-stabilized CO_2 laser and a long-path absorption cell described in several references [35]. The curve marked A was generated from data on the AFGL tape [6] using a bound of 20 cm^{-1} . That is, for the calculations at each H_2O partial pressure, only the H_2O absorption lines within a range of $\pm 20 \text{ cm}^{-1}$ from the measurement frequency were assumed to contribute to the absorption at that frequency. All other H_2O absorption lines were assumed to be too far away to make a significant contribution. This bound of 20 cm^{-1} became a standard in early line-by-line calculation programs because it was believed to be a reasonable compromise between spectral representation and computing time.

The curve marked B in Figure 1 was generated by accumulating the contributions of all H_2O absorption lines from 0 to 5000 cm^{-1} . The contributions at the measurement frequency were computed using the Lorentz line shape for all lines listed on the data tape. At low H_2O partial pressures, this line shape overestimates the observed absorption, while at high H_2O partial pressures it underestimates the observed absorption. Despite this failing, the difference between curve A and curve B demonstrates that significant contribution to the total absorption can be found in the accumulation of the far wings of strong absorption lines. The Lorentz profile, however, is not an adequate model for the far wings of lines, so it is not surprising that curve B fails to provide suitable

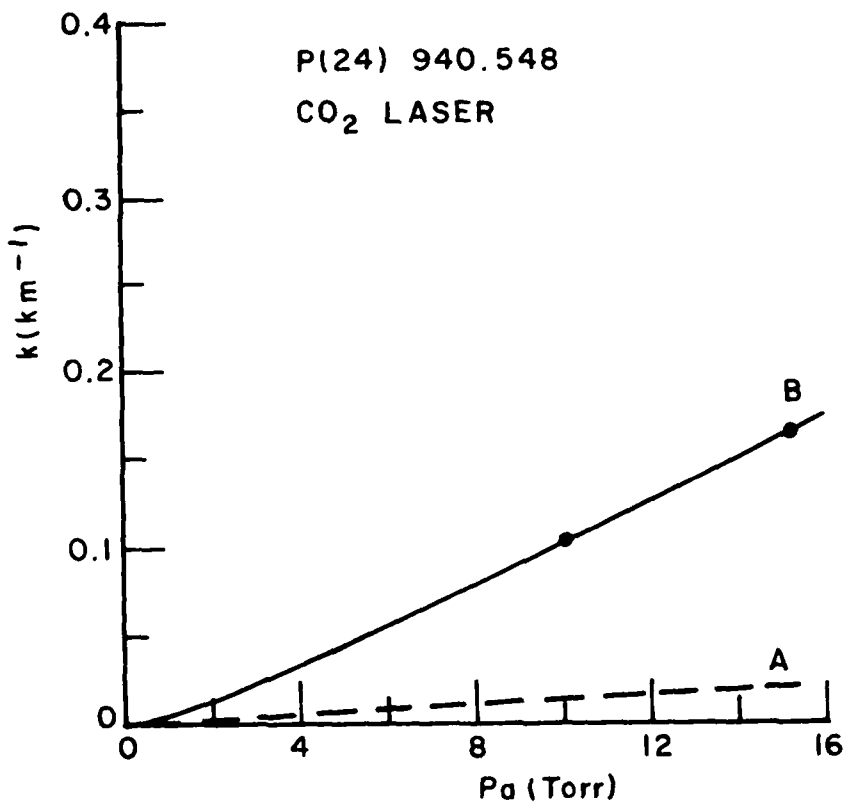


Figure 1. Pressure dependence of water vapor continuum absorption.

agreement with the measured absorption. Motivated by the hope that an accurately derived H₂O absorption line shape would improve the modeling of continuum absorption, we undertook the work presented in this paper and in the previous section.

THE LINE PROFILE

As mentioned in the last section, the absorption coefficient at frequency ν (in cm⁻¹) can be written

$$k(\nu) = \sum_i S_i j(\nu - \nu_{0i}; \beta_i) \quad (1)$$

where S_i is the strength of the i th absorption line and $j(\nu - \nu_{0i}; \beta_i)$ is the shape of the absorption line centered at ν_{0i} and which has a set of shape parameters $\{\beta_i\}$. The major features of the total line shape have been derived in the previous section. It was found that

$$j_C(\Delta\nu) = N \{ j_{CNLC}(\Delta\nu) p(\Delta\nu) + j_{CFW}(\Delta\nu) (1-p(\Delta\nu)) \} \quad (2)$$

where the subscript C denotes that the line shape is collision broadened, and

$$j_{CNLC}(\Delta\nu) = \frac{1}{\pi} \frac{\alpha^R_2}{(\Delta\nu + \alpha^I)^2 + (\alpha^R)^2} \quad (3)$$

$$j_{CFW}(\Delta\nu) = \frac{1}{\pi} \left\{ \begin{array}{l} \frac{\lambda_{ak}}{| \nu |^{1+3/m_k}} T_{m_k}(m_k, \Delta\nu) \\ + \frac{\lambda_{bj}}{|\Delta\nu|^{1+3/m_j}} T_{m_j}(m_j, \Delta\nu) \end{array} \right\} \quad (4)$$

$$p(\Delta v) = \begin{cases} 1/2 + 1/2 \cos \frac{\pi}{5} \Delta v & |\Delta v| < 5 \text{ cm}^{-1} \\ 0 & |\Delta v| \geq 5 \text{ cm}^{-1}. \end{cases} \quad (5)$$

N is the normalization constant. Normalization requires that

$$\int_0^{\infty} j_c(\Delta v) d\Delta v = 1. \quad (6)$$

In order to eliminate the singularities in the far wing line shape functions at $\Delta v=0$, we now adopt the Varanasi formulation [7] which includes an additive term in the denominators of Equation (4). Furthermore, we now set $m_k=6$ and $m_j=4$ as discussed in the previous paper.

$$j_{CFW}(\Delta v) = \frac{1}{\pi} \left\{ \frac{0.3198 \lambda_{a6}}{|\Delta v|^{1.5} + \lambda_{a6}} T_6(m_k=6, \Delta v) + \frac{0.4334 \lambda_{b4}}{|\Delta v|^{1.75} + (\lambda_{b4})^{7/3}} T_4(m_j=4, \Delta v) \right\} \quad (7)$$

This modification of the line shape function does not significantly alter the value of the function when Δv is very large. It only assures that this function is well-behaved at line center for normalization purposes. Furthermore, in our formulation the p -function is turning off the far wing line shape near $\Delta v=0$, so any constant value of $j_{CFW}(\Delta v)$ at $\Delta v=0$ artificially introduced by this modification is given a weighting of zero.

The multiplicative constants which appear in Equation (7) are aids in normalization introduced by the Varanasi formulation. An evaluation of λ_{a6} and λ_{b4} in far wing data ($\Delta v \gg \lambda_{a6}, \lambda_{b4}$) would simply be scaled by

these constants.

Now, the functions T_6 ($m_k=6, \Delta\nu$) and T_4 ($m_j=4, \Delta\nu$) must be discussed.

As mentioned in the previous section, Fomin and Tvorogov [8] derived a term of the form

$$\exp\left\{-\left[\frac{G|\Delta\nu|^{\frac{m-1}{m}}}{T}\right]^{2/3}\right\}$$

where G is a constant and T is the temperature. An exponential decay of some form is expected in the far wings of absorption lines as discussed by Clough and coworkers [2]. For self-broadening ($m=6$) the above term is proportional to $\exp(-|\Delta\nu|^{0.56})$, and for foreign-broadening this term is proportional to $\exp(-|\Delta\nu|^{0.50})$.

We have adopted a simplification of this term. We have set

$$T_6(m_k=6, \Delta\nu) = \exp(-G_{a6}|\Delta\nu|^{0.5}) \quad (8a)$$

and

$$T_4(m_j=4, \Delta\nu) = \exp(-G_{b4}|\Delta\nu|^{0.5}). \quad (8b)$$

We have given the same frequency dependence to both the self-broadened and foreign-broadened terms in order to facilitate the normalization process. The origin of these terms is the level shift contribution which was not fully incorporated in our phase shift approach. Such terms are difficult to derive by perturbation methods since, by definition, in the far wings of infrared absorption lines the perturbation energy ($\Delta\nu$) is no longer small compared to the unperturbed energy levels of the absorbing molecule.

The G parameters above are written

$$G_{a6} = g_a(v) \left(\frac{296}{T} \right)^{\gamma_a(v)} \quad (9a)$$

and

$$G_{b4} = g_b(v) \left(\frac{296}{T} \right)^{\gamma_b(v)} \quad (9b)$$

where the parameters $g_a(v)$, $g_b(v)$, $\gamma_a(v)$, and $\gamma_b(v)$ depend on the vibrational quantum numbers. In particular, it can be anticipated that the parameters might be slightly different for the pure rotational band ($v=0$) where various rotational levels are more easily accessible through thermal energy than in the case for the vibrational energy levels. Thus we might expect one set of parameters to describe the shape of lines in the rotational band and another set of parameters to describe the shape of absorption lines of the vibrational bands.

Equation (7) is then written

$$j_{CFW}(\Delta v) = \frac{1}{\pi} \left\{ \frac{0.3198 \lambda_{a6}}{|\Delta v|^{1.5 + \lambda_{ab}^3}} \exp(-G_{a6}\sqrt{|\Delta v|}) + \frac{0.4334 \lambda_{b4}}{|\Delta v|^{1.75 + \lambda_{b4}^{7/3}}} \exp(-G_{b4}\sqrt{|\Delta v|}) \right\} \quad (10)$$

The temperature and pressure dependences of λ_{ab} and λ_{b4} can be extracted by examining the inputs to Equation (70a) in the previous paper.

$$\lambda_{bj} = \rho_b \sum_s \rho_b \gamma_j \quad (11)$$

where the terms have been defined previously. For self-broadening, this can be written

$$\lambda_{a6} = \frac{p_a}{kT} \sum_s p_b \frac{4\pi}{6} \frac{1}{\hbar} (v_{6u}(T) - v_{6l}(T))^{1/2} \xi_6^{1/2} \Gamma(-\frac{1}{2}) \cos(\frac{\pi}{4})$$

(12)

The potential for self-broadening is seen in Equation (40) of the previous paper to be proportional to $1/T$. Therefore we can write

$$\lambda_{a6} = A1(v) \left(\frac{296}{T}\right)^{1.5} p_a$$

(13)

where p_a is the absorber pressure and $A1(v)$ is a parameter which should have some dependence on the vibrational quantum numbers, and 296 is the reference temperature.

The foreign-broadening parameter can be written

$$\lambda_{b4} = \frac{p_b}{kT} \sum_s p_b \frac{4\pi}{4} \left(\frac{1}{\hbar} (v_{4u} - v_{4l})\right)^{3/4} \xi_4^{3/4} \Gamma(-\frac{3}{4}) \cos(\frac{3\pi}{8})$$

(14)

which can be written simply as

$$\lambda_{b4} = A2(v, J) \left(\frac{296}{T}\right) p_b$$

(15)

where p_b is the broadener pressure and $A2(v, J)$ is a parameter which depends on the vibrational quantum number and on the rotational quantum number J . Because of the statistical averaging over rotations, the H_2O - H_2O potential matrix elements for strong collisions are independent of angle and not a function of the rotation quantum number J . For N_2-H_2O ,

however, the interaction times are shorter than the rotational times; thus, no averaging over rotations is performed. Thus, $A_2(v, J)$ will be a function of the J quantum number. This J dependence can be expressed in terms of the J dependence of the near-line-center halfwidth α_0 [9]

$$A_2(v, J) = A_2(v) \left(\frac{\alpha_0}{0.07} \right)^{1.125} \quad (16)$$

where α_0 is the near-line-center halfwidth, and 0.07 represents a mean value of α_0 for pressure broadened water vapor lines in the mid-infrared.

The pressure and temperature dependence of the halfwidth α was taken as

$$\alpha = \alpha_0 \left(\frac{296}{T} \right)^{0.83} \left\{ B \left(\frac{296}{T} \right)^{0.17} p_a + p_b \right\} \quad (17)$$

where p_a is the absorber pressure and p_b is the broadener pressure. B is the self-to-foreign broadening ratio which is typically set to 5. The self-broadened component of the halfwidth has a temperature dependence of $1/T$, while the foreign-broadened component has a temperature dependence of $1/T^{0.83}$ as discussed in the previous section.

In order to write the absorption coefficient, the line strength is needed.

$$S = S_0 \frac{T_0}{T} \frac{p}{p_0} \left(\frac{T_0}{T} \right)^{1.5} \exp \left[E_l \left(\frac{T-T_0}{kTT_0} \right) \left\{ \frac{1-\exp(-hv_0/kT)}{1-\exp(-hv_0/kT_0)} \right\} \right] \left\{ S_{COR} \right\} \quad (11)$$

The term written as S_{COR} is a correction to the line strength term which takes account of the fact that for shifted energy levels the Boltzmann population distribution is not calculated from the energy level separation hv_0 , but rather from the total energy separation $hv_0 + \Delta E$. The correction is important for the rotational band where different rotational levels are populated at room temperature. The correction is far less important

for the vibrational bands. The term S_{COR} can be shown [9] to take the form

$$\left\{ S_{COR} \right\} = \begin{cases} \frac{v}{v_0} \frac{(1-\exp(-hc v/kT))}{(1-\exp(-hc v_0/kT))} & \text{near line center} \\ \frac{(1-\exp(-hc v/kT))}{(1-\exp(-hc v_0/kT))} & \text{far wing.} \end{cases} \quad (12a)$$

Since these terms are frequency dependent, we can include them in the line shape term. These terms only affect absorption lines below approximately 1000 cm^{-1} . Now the total line shape can be written

$$S_{\ell u} = S_{\ell u}^0 \frac{T_0 p_a}{T p_{ao}} \left(\frac{T_0}{T} \right)^{1.5} e^{E_\ell \frac{T-T_0}{kT T_0}} \frac{(1-e^{-hc v_0/kT})}{(1-e^{-hc v_0/kT_0})}$$

$$j_{cNLC}(v) = \frac{1}{\pi} \frac{v}{v_0} \frac{(1-e^{-hc/kT})}{(1-e^{-v_0 hc/kT})} \frac{\alpha^r}{((\Delta v)^2 + (\alpha^r)^2)}$$

$$j_{cFW}(v) = \frac{1}{\pi} \frac{(1-e^{-hc/kT})}{(1-e^{-v_0 hc/kT})} \left[\frac{.3198 \lambda_{a6} e^{-G_{a6} \sqrt{\Delta v}}}{|\Delta v|^{1.5 + \lambda_{a6}^3}} + \frac{.4334 \lambda_{b4} e^{-G_{b4} \sqrt{\Delta v}}}{|\Delta v|^{1.75 + \lambda_{b4}^{7/3}}} \right]$$

where

$$\lambda_{a6} = A1(v) \left(\frac{296}{T} \right)^{1.5} p_{H_2O}, \quad \lambda_{b4} = A2(v) \left(\frac{\alpha_0}{0.07} \right)^{1.125} \left(\frac{296}{T} \right) p_{N_2}$$

$$\alpha = \alpha_0 \left(\frac{296}{T} \right)^{0.83} \left\{ B \left(\frac{296}{T} \right)^{0.17} p_{H_2O} + p_{N_2} \right\}$$

$$G_{a6} = g_a(v) \left(\frac{296}{T} \right)^{\gamma_a(v)}, \quad G_{b4} = g_b(v) \left(\frac{296}{T} \right)^{\gamma_b(v)}$$

AD-A101 669

OHIO STATE UNIV COLUMBUS ELECTROSCIENCE LAB
A SYNERGISTIC INVESTIGATION OF THE INFRARED WATER VAPOR CONTINUUM—ETC(U)
APR 81 R J NORDSTORM, M E THOMAS, E K DAMON DAAG29-77-C-0010
UNCLASSIFIED ESL-784701-7 ARO-14702-5-GS NL

2 OF 2
AP A
0101869

F/6 4/1

END
DATE
FILED
8-81
DTIC

As mentioned earlier, the near-line-center profile and the far wing profile were blended through the intermediate wing region by the use of the p-function.

$$k(v) = \sum_i s_i \{ j_{CNLC}(v-v_{o_i}; \beta_i) p(\Delta v) + \\ j_{CFW}(v-v_{o_i}; \beta_i) (1-p(\Delta v)) \} \quad (14)$$

The normalization constant for each line is determined by imposing Equation (6) on each line.

COMPARISON WITH EXPERIMENT

A computer program was written which incorporated this line shape in a line-by-line calculation of absorption in the infrared.

Before calculations of the contribution of far wings to H₂O continuum absorption could be made, the various parameters had to be evaluated. This was done by fitting predicted absorption coefficients to measured absorption coefficients in spectral regions where line absorption clearly dominates. It must be mentioned here that absorption data in the window regions where continuum can be measured was not used in this evaluation of the parameters. The regions chosen for the parameter evaluation were located in the absorption bands where absorption coefficient on the order of 100 km⁻¹ are typical. Since continuum absorption is on the order of 0.1 km⁻¹ in the window regions, any possible residual continuum absorption in the regions where the line parameters were evaluated would have been a small fraction of the total absorption.

Data provided by Burch [10] were used to evaluate the parameters which define the rotational band. Data recorded with a CO laser at our

laboratory [9] were used to evaluate parameters of the v_2 vibrational band near 6.6 μm , and HF laser measurements made by White et al [11] were used to estimate the parameters in the v_1 , v_3 spectral region near 3 μm . In all cases it was clear that insufficient temperature data existed to make an accurate estimate of certain temperature controlling parameters such as $\gamma_a(v)$ and $\gamma_b(v)$. For these parameters it was decided to vary them only slightly if necessary from the value 0.67 given by Fomin and Tvorogov [8].

No attempt at a least square analysis was made since the data do not yet possess the accuracy and completeness to make such an analysis meaningful. Table 1 lists the resulting parameters for each H_2O absorption band. As can be seen, the largest deviation between parameter values occurs between the rotational band and the rest of the absorption bands. Although this trend was anticipated, no physical significance should be placed on the small differences which appear to exist between the parameter values for these bands. Again it is important to emphasize that absorption data in the window regions were not used in the evaluation of these parameters.

Once the parameters were estimated, we used the total line shape to calculate the absorption at CO_2 laser frequencies in the 10 μm atmospheric transmission window. Figure 2 shows the results of the calculation at room temperature for the pressure dependence of the absorption coefficient at one of the laser lines. A bound of 1000 cm^{-1} was used, although we found that increasing this made no significant difference to the calculated absorption coefficient. The predicted absorption is in very good agreement with the measured absorption at all pressures. It should be pointed out that the curvature in the data (seen as a p^2 depend-

TABLE 1
THE FAR WING PARAMETERS

A_1 (Rotational) = 2.35	G_a (Rotational) = 0.065	γ_a (Rotational) = 0.67
A_2 (Rotational) = 0.18	G_b (Rotational) = 0.115	γ_b (Rotational) = 0.67
A_1 (v_2) = 1.73	G_a (v_2) = 0.07	γ_a (v_2) = 0.67
A_2 (v_2) = 0.153	G_b (v_2) = 0.084	γ_b (v_2) = 0.67
A_1 (v_1, v_3) = 1.95	G_a (v_1, v_3) = 0.045	γ_a (v_1, v_3) = 0.67
A_2 (v_1, v_3) = 0.165	G_b (v_1, v_3) = 0.088	γ_b (v_1, v_3) = 0.67

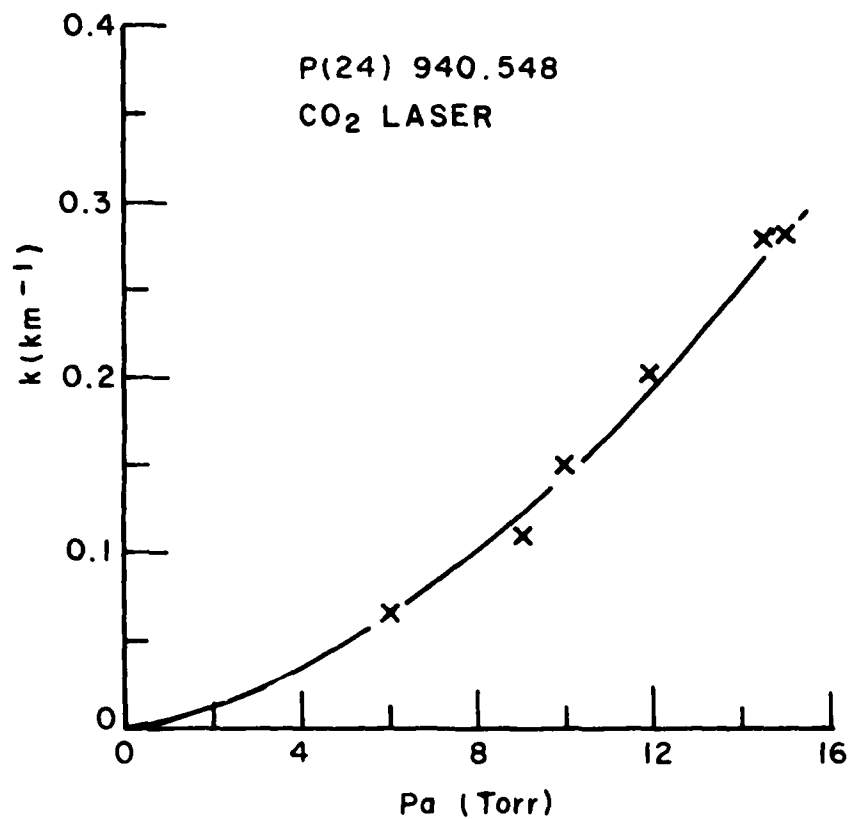


Figure 2. Room temperature modelling of water vapor pressure dependence.

ence) is well modelled by this line shape theory. This is a manifestation of the increased importance of H₂O-H₂O interactions over H₂O-N₂ interactions for strong collisions as developed in the previous paper. Using the Lorentz profile as in Figure 1 the curvature in the data was not well modelled.

Our results in modelling the overall continuum absorption throughout the 8-14 μm atmospheric window can be seen in Figure 3. Measurements of the self-broadened coefficient C_s made by Burch [12] were compared to predictions calculated with various classic line shape formalisms. Using our line shape formalism, a very good fit to the data was achieved.

We have also applied the line shape theory to the 3.5-4 μm transmission window. DF laser measurements made by White et al [13] did not confirm earlier spectroscopic measurements made by Burch [14]. White's measurements were consistently higher than the absorption values reported by Burch, and the curvature as a function of frequency in White's data throughout this region was much greater than seen by Burch.

Figure 4 shows the results of our calculations in the 3.5-4 μm region. The squares are the total absorption calculated using water vapor absorption lines and a partial pressure of 15 torr in an environment of 745 torr N₂. This spectral region contains many absorption lines of the HDO molecule. Burch was careful to avoid regions close to the centers of these absorption lines when he made his measurements. We can accomplish this in our calculations by subtracting the local line contribution within a few wavenumbers. The triangles show the residual continuum absorption predicted by our line shape calculation. The agreement with Burch's data is quite good.

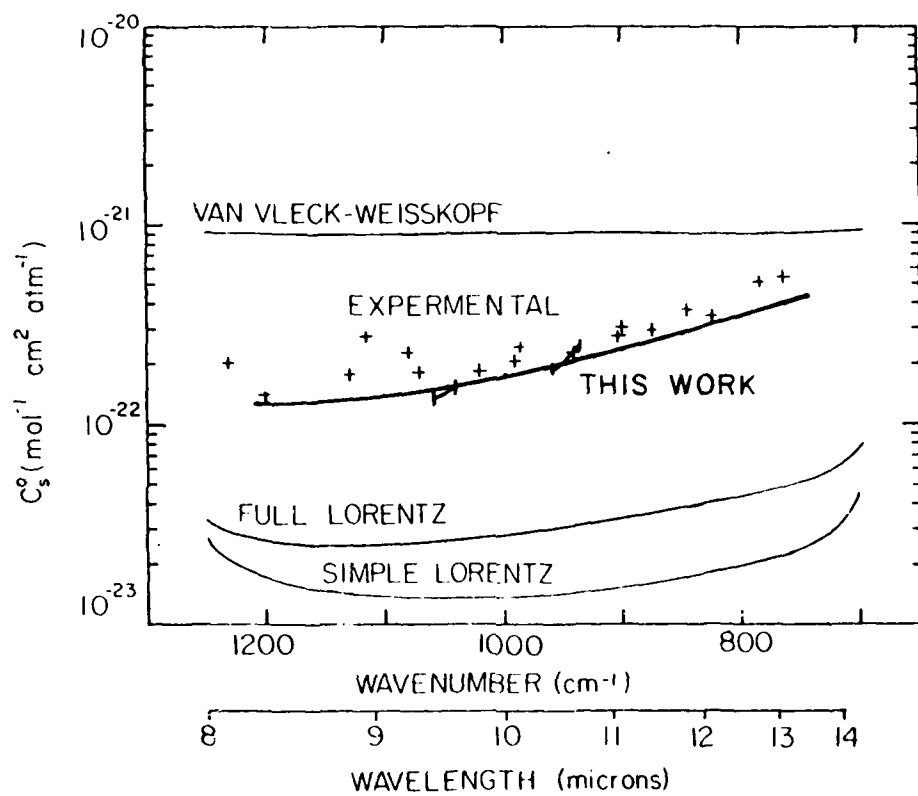


Figure 3. Experimental results in the 8 to 14 μm region.

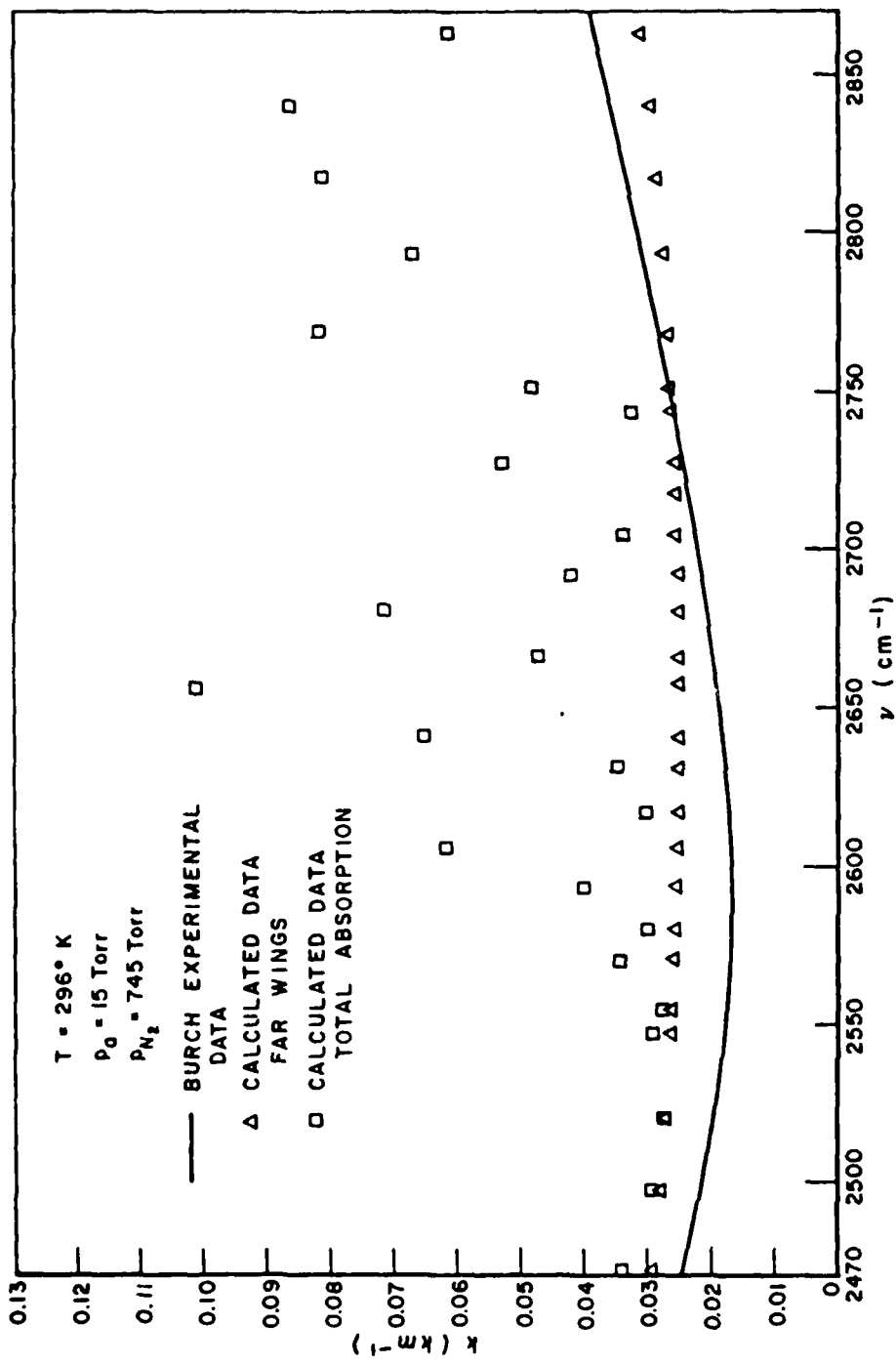


Figure 4 : Comparison of experimental and theoretical frequency-dependence of the absorption coefficient from 2470 cm^{-1} to 2870 cm^{-1} .

Modelling the temperature dependence is much more difficult because a precise understanding of intermolecular interactions does not exist (particularly for the rotational band) and accurate temperature data do not exist for all of the absorption bands of H_2O in the infrared. With the values of the line shape parameters listed in Table I, we calculated the absorption coefficient at the P(20) CO_2 laser line at 944.1945 cm^{-1} . Data which exist [3,15] on the absorption in this region indicate a strong, negative temperature dependence. For this study, values of γ_a and γ_b were fixed to 0.67. Improved data in all spectral regions is necessary before refinement of these parameters can be made.

Figure 5 shows the results of our modelling of the temperature dependence. A negative temperature dependence is predicted from our line shape model. Previously, the negative temperature dependence of the absorption was taken as strong evidence of dimer absorption.

An adequate line shape model for atmospheric H_2O is important not only for modelling the continuum absorption, but also for calculating the effects of overlap between H_2O absorption line features and weak absorptions from a possible trace gas in the atmosphere. Recently, Menyuk et al. [16] used the differential absorption lidar technique to detect trace amounts of NO in the atmosphere. Interference from strong absorption lines of H_2O were not adequately compensated for by two separate programs provided by AFGL. We were asked to calculate the absorption coefficient of pressure-broadened water vapor at their measurement frequencies. Using the results which we provided to them, they recomputed the effects of H_2O interference in their experiment and found much better agreement with their experimental results.

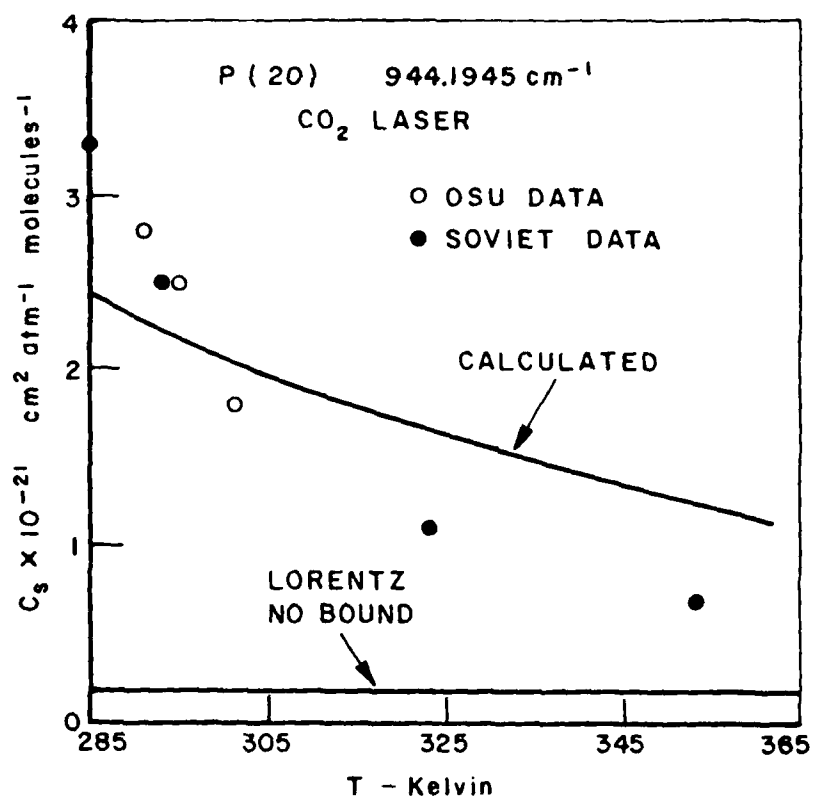


Figure 5. Comparison of experimental and theoretical temperature dependence of C_s at 944.1945 cm⁻¹.

CONCLUSIONS

In these two papers we have developed and discussed the shape of pressure-broadened H₂O absorption lines in the infrared spectral region. The water vapor continuum in both the 8-14 μm and in the 3.5-4 μm atmospheric windows is quite well modelled by this absorption line shape. The success of the modelling extends to a prediction of the negative temperature dependence observed near 10 μm.

REFERENCES

- 1 R.G. Breene, The Shift and Shape of Spectral Lines, Pergamon Press, 1961.
- 2 S.A. Clough, F.X. Kneizys, R. Davies, R. Gamache, and R. Tipping, "Theoretical Line Shape for H₂O Vapor: Application to the Continuum", in Atmospheric Water Vapor edited by Adarsh Deepak, T.D. Wilkerson, and L.H. Ruhnke, Academic Press, 1980.
- 3 J.C. Peterson, "A Study of Water Vapor Absorption at CO₂ Laser Frequencies Using a Differential Spectrophotometer and White Cell," Ph.D. Dissertation, The Ohio State University, June 1978.
- 4 R.J. Nordstrom, M.E. Thomas, J.C. Peterson, E.K. Damon, and R.K. Long, Appl. Opt. 17, 2724 (1978).
- 5 J.C. Peterson, M.E. Thomas, R.J. Nordstrom, E.K. Damon, and R.K. Long, Appl. Opt. 18, 834 (1979).
- 6 McClatchey, R.A., Benedict, W.S., Clough, S.A., Burch, D.E., Calfee, R.F., Fox, K., Rothman, L.S., and Garing, J.S., U.S. Air Force Research Laboratories, AFCRL-TR-73-0096, Bedford, Massachusetts (1973).
- 7 Varanasi, P., Chou, S., and Penner, S.S., J. Quant. Spectroc. Radiat. Transfer, 8, 1537 (1968).
- 8 Fomin, V.V. and Tvorogov, S.D., Appl. Opt. 12, 584 (1973).
- 9 Thomas, M.E., "Tropospheric Water Vapor Absorption in the Infrared Window Regions," Report 784701-5, August 1979, The Ohio State University ElectroScience Laboratory, Department of Electrical Engineering; prepared under Contract DAAG-29-77-C-0010 for U.S. Army Research Office.
- 10 D.A. Gryvnak and D.E. Burch, "Infrared Absorption by CO₂ and H₂O," Aeronutronic Publication U-6417, Air Force Geophysics Laboratories, Contract F19628-76-C-0302, (May 1978).
- 11 W.R. Watkins, R.L. Spellacy, K.O. White, B.Z. Sojka and L.R. Bower, Appl. Opt. 18, 1582 (1979).
- 12 Burch, D.E., Aeronutronic Publication No. U-4784, Semi-Annual Technical Report, AFCRL Contract No. F19628-69-C-0263, U.S. Air Force (1970).
- 13 White, K.O., Watkins, W.R., Bruce, C.W., Meridith, R.E., and Smith, F.F., Appl. Opt. 17, 2711, (1978).

- 14 D.E. Burch, D.A. Gruyvnak, and J.D. Pembrook, Aeronutronic Publication No. U-4897, "Investigation of the Absorption of Infrared Radiation by Atmospheric Gases: Water, Nitrogen, Nitrous Oxide," Air Force Cambridge Research Laboratories, Contract No. F19628-69-C-0263, January 1971.
- 15 V.N. Aref'ev and V.I. Dianov-Klokov, Opt. Spectrosc. 42, 488 (1977).
- 16 N. Menyuk, D.K. Killinger, and W.E. DeFeo, Appl. Opt. 19, 3282 (1980).

SECTION IV

FOURIER TRANSFORM SPECTRA OF H₂O SAMPLES

We have collected two sets of high-resolution absorption spectra of H₂O samples. The first set consists of four spectra of pure H₂O samples. These spectra were recorded at 0.04 cm⁻¹ resolution using an absorption path length of 821 meters in a temperature-controllable White cell equipped with a double-pass optical scheme. The four spectra were recorded at the different temperatures and H₂O pressures indicated in Table 1. For all four of these spectra the spectral regions near absorption band centers are totally opaque. The purpose for collecting the spectra was the observation of H₂O absorption line positions in the atmospheric transmittance window regions. The spectral coverage of these Fourier transform spectra extends from 850 cm⁻¹ to 5000 cm⁻¹. The natural D/H ratio exists in the H₂O samples used.

The second set of data consists of four spectra which demonstrate the pressure-broadening of a single water vapor amount by nitrogen. These spectra were all recorded at room temperature. Varying amounts of N₂ were added to the H₂O sample. The resolution of the spectra is 0.04 cm⁻¹ even though the pressure-broadened lines are much wider than this resolution. Table 2 summarizes the experimental conditions. The path length for these spectra was also 821 meters.

An atlas of pure H₂O absorption lines and an atlas of pressure-broadened H₂O absorption lines are being prepared. These compilations will contain the H₂O absorption lines which lie in the atmospheric transmittance windows. Figures 1a and 1b show a typical page of the atlas and the line directory table, respectively. The experimental conditions are

TABLE 1

EXPERIMENTAL CONDITIONS FOR PURE H₂O SPECTRA
(PATH LENGTH = 821 METERS)

T (°K)	H ₂ O Pressure (Torr)	ω pr-cm
284.4	5	.42
295.3	10	.80
307.1	20	1.54
320.2	40	2.96

TABLE 2

EXPERIMENTAL CONDITIONS FOR NITROGEN BROADENED H₂O SPECTRA
(PATH LENGTH = 821 METERS)

T (°K)	Total Pressure (Torr)	H ₂ O Pressure (Torr)	ω pr-cm
295.3	10	10	.8
295.3	100	10	.8
295.3	300	10	.8
295.3	750	10	.8

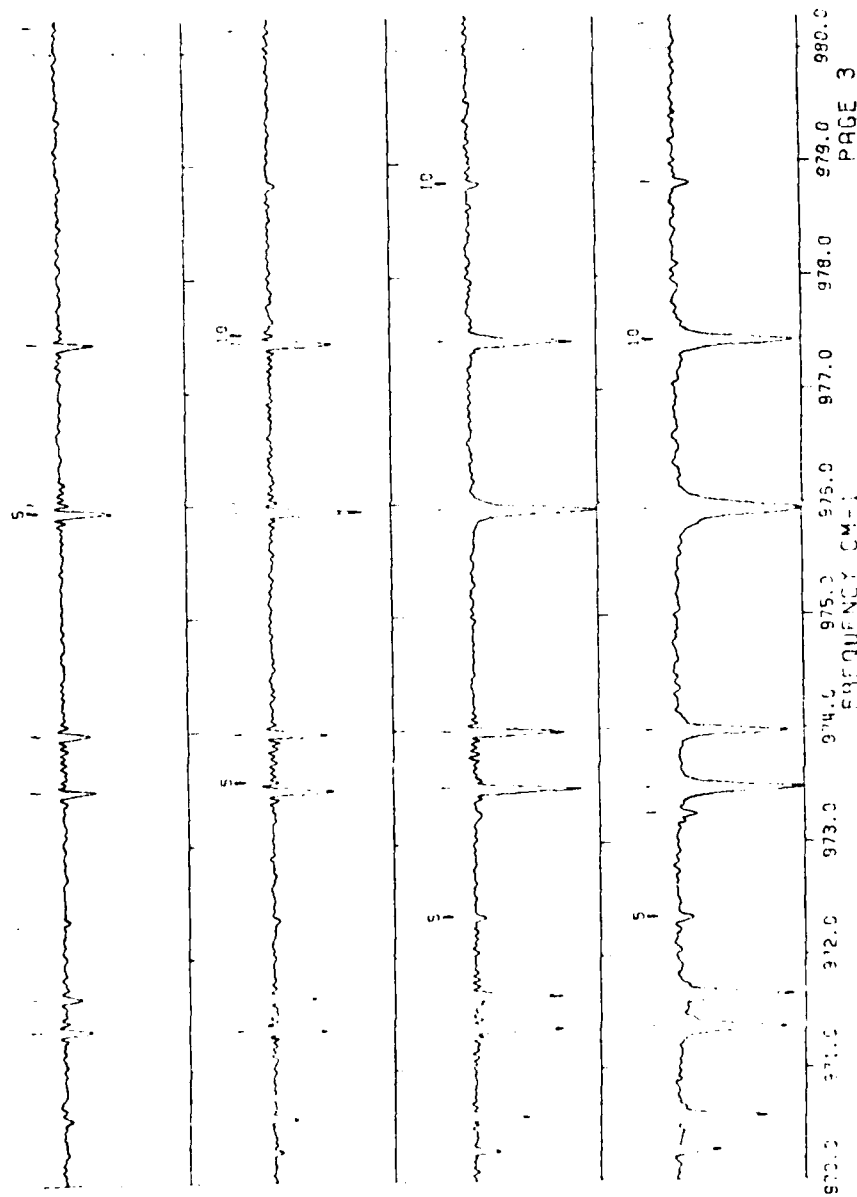


Figure 1. a. HgCdTe
Pure H₂O
970-980 cm⁻¹.

970.0 972.5 973.0 974.5 975.0 975.5 977.0 978.0 979.0 980.0
WAVENUMBER CM⁻¹
ABSORBANCE
PAGE 3



Figure 1. b. HgCdTe
Pure H_2O
 $970-980\text{ cm}^{-1}$.

given in Table 1 with the 5 Torr spectrum at the top of the page. Figures 2a and 2b show a sample from the $2250\text{-}2260\text{ cm}^{-1}$ region, as well as pure H₂O samples as described in Table 1. Figures 3a, 3b, 4a, and 4b show the same regions from the pressure-broadened data set as described in Table 2. The region from 850 to 5000 cm^{-1} is covered in each of these compilations at 10 cm^{-1} per page. Regions near absorption band centers where the large density of strong lines causes total absorption are not plotted. Nevertheless, each atlas of absorption spectra contains over 300 pages. Thus, it is not feasible to include such compilations in this report. Instead, we simply report the availability of these data sets.

An accurate line finding routine has been employed to locate and catalog most of the absorption lines in the spectra. Each atlas is accompanied by a line listing which gives the position (in cm^{-1}) of each absorption line located and numbered by the line finding routine. The frequency accuracy is estimated to be about $\pm 0.003\text{ cm}^{-1}$.

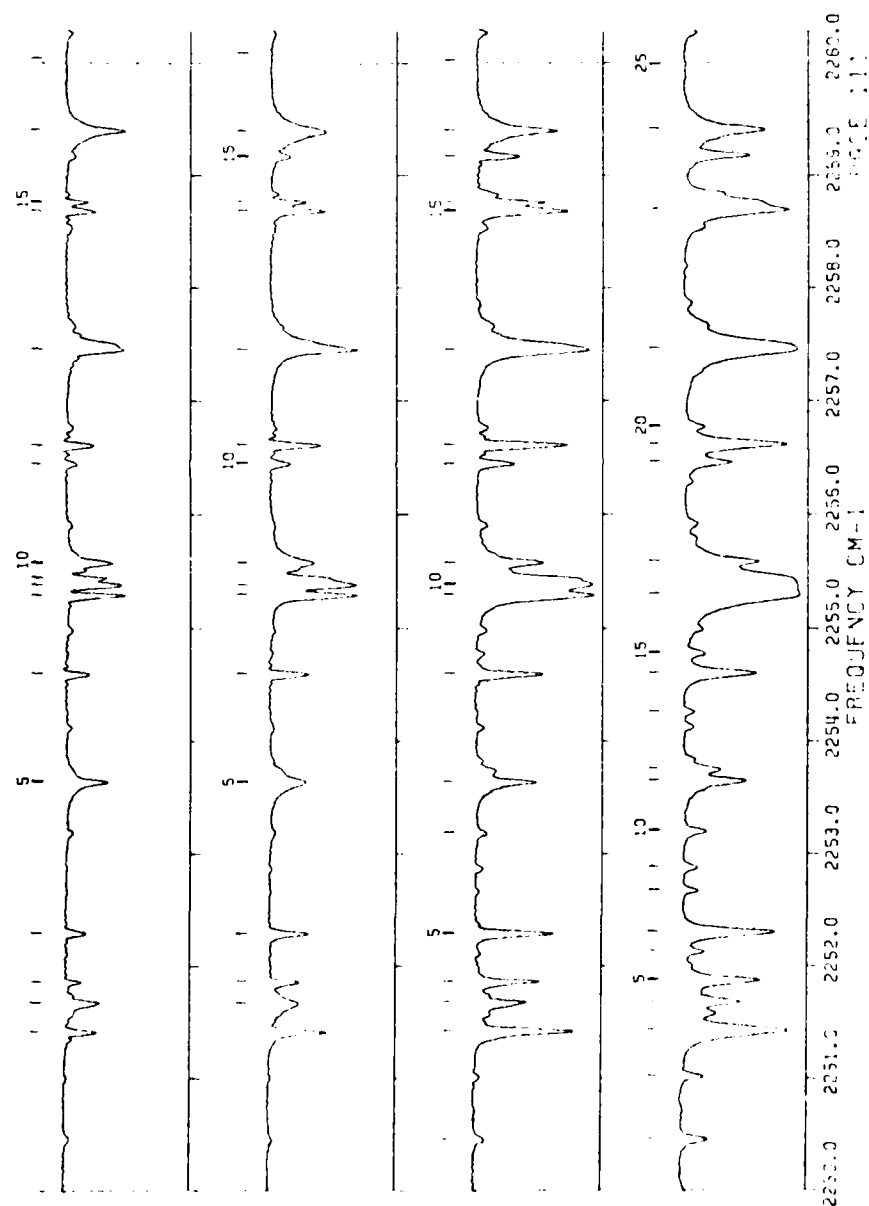


Figure 2. a. InSb
Pure H_2O .

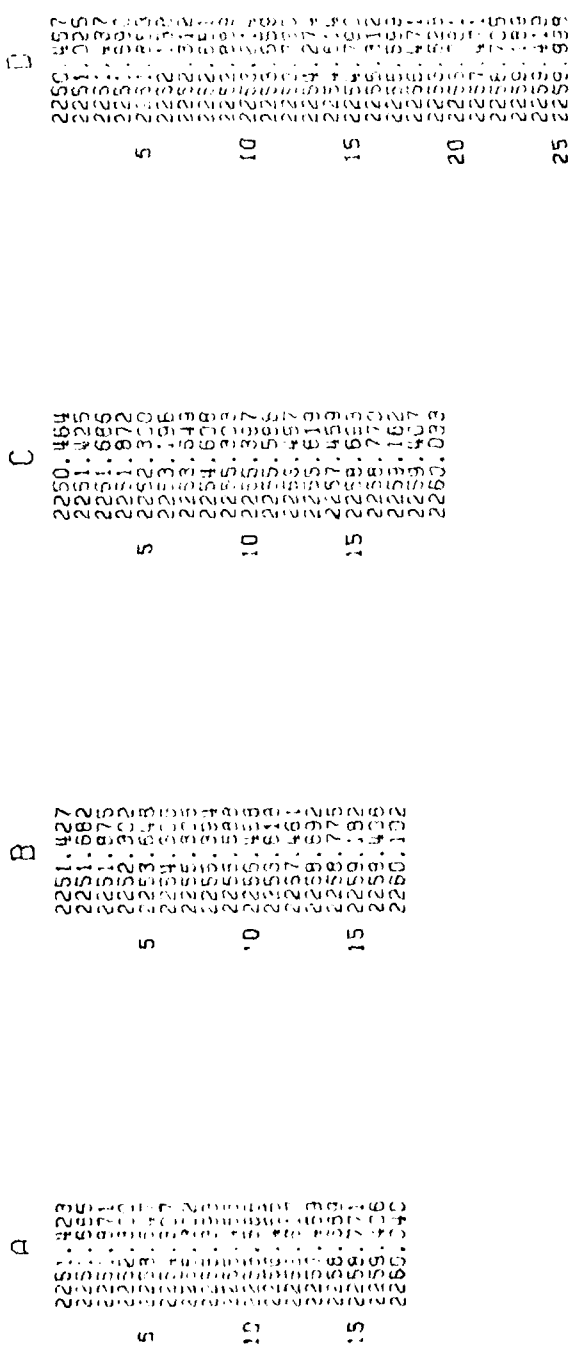


Figure 2. b. InSb
Pure H₂O.

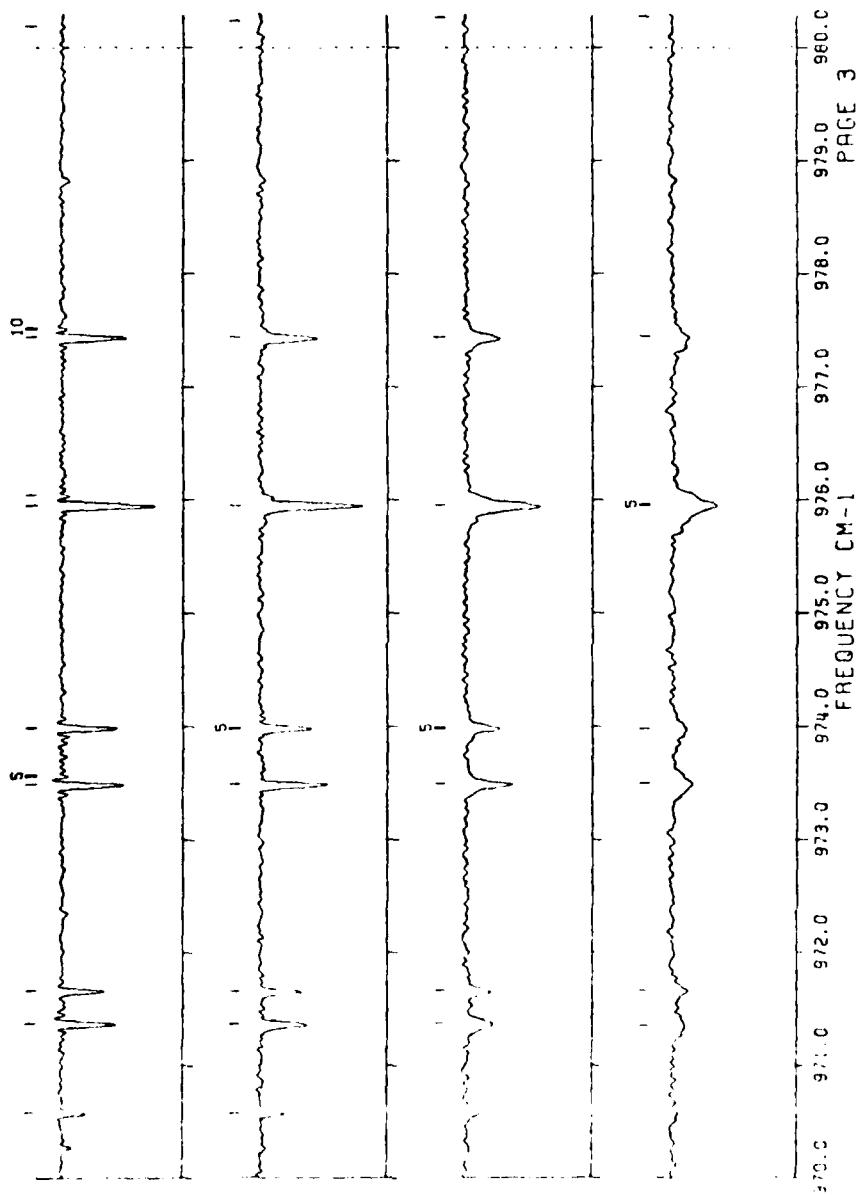


Figure 3. a. HgCdTe
970-980 cm⁻¹
Pressure-broadened.

		970.586
		971.373
		971.667
		973.499
		973.992
		975.954
		977.442
		980.236
		980.270
		971.353
		971.567
		973.507
		973.988
		975.959
		977.449
		980.275
	C	970.586
	C	971.373
	C	971.667
	C	973.499
	C	973.992
	C	975.954
	C	977.442
	C	980.236
	B	970.582
	B	971.373
	B	971.667
	B	973.499
	B	973.992
	B	975.954
	B	977.442
	B	980.236
	A	970.584
	A	971.372
	A	971.666
	A	973.495
	A	973.991
	A	975.953
	A	977.445
	A	980.196

Figure 3. b. HgCdTe
 $970\text{-}980\text{ cm}^{-1}$
 pressure-broadened.

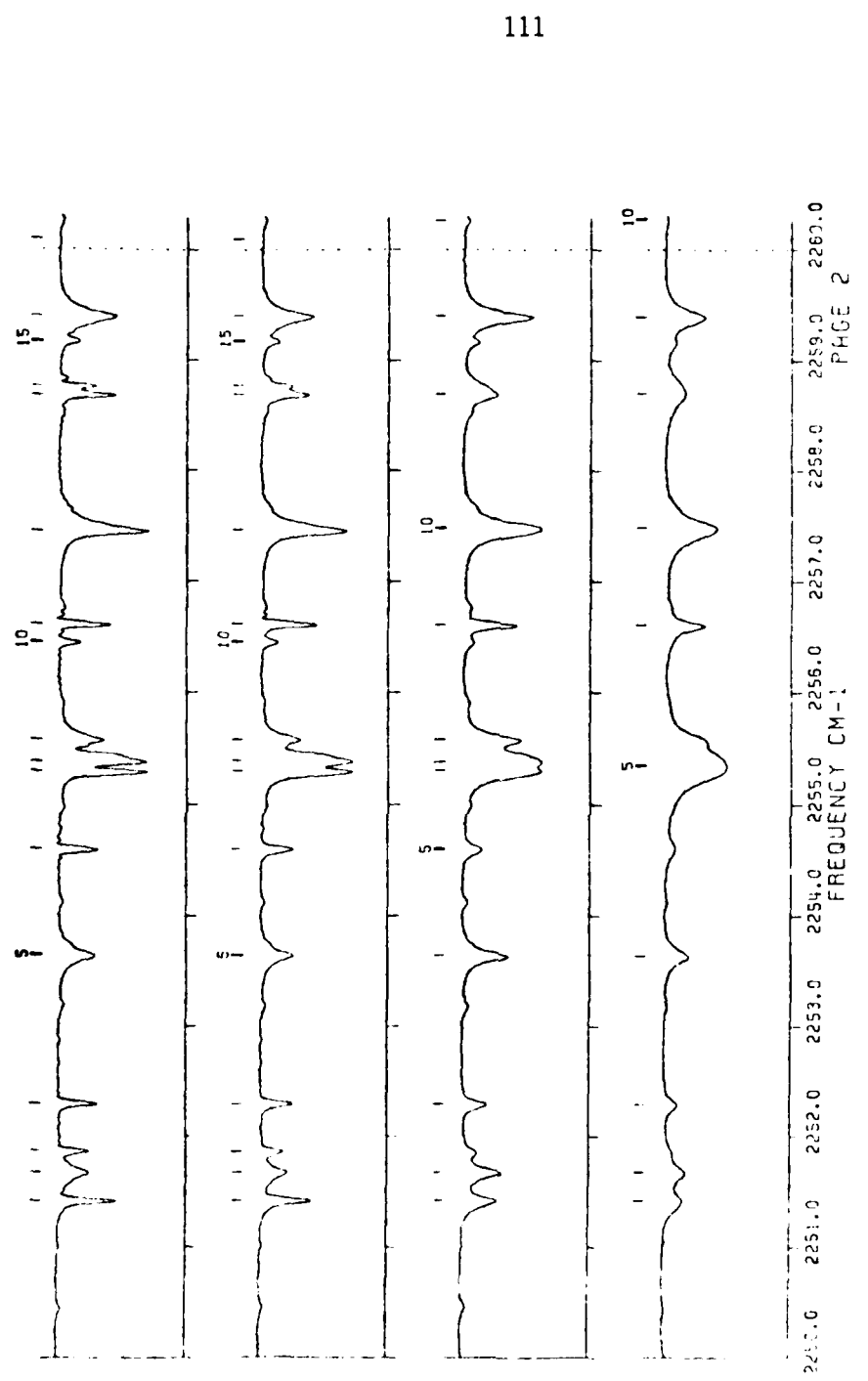


Figure 4. a. InSb
 $2250\text{-}2260\text{ cm}^{-1}$
 Pressure-broadened.

11?

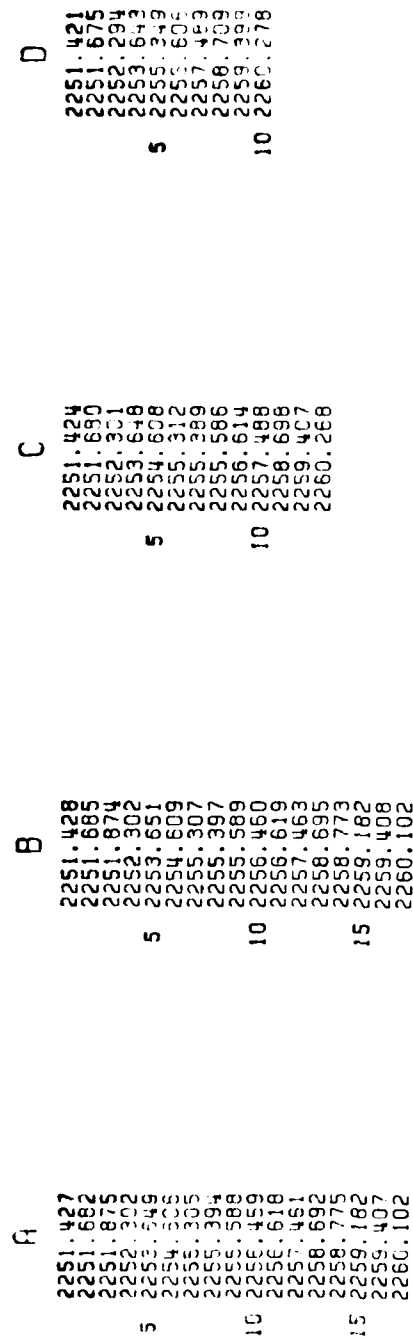


Figure 4. b. InSb
2250-2260 cm^{-1}
pressure-broadened.

